THE DEVELOPMENT OF AN ELASTOMERIC SCAFFOLD FOR SMALL DIAMETER BLOOD VESSEL TISSUE ENGINEERING

by

Bernadette Gillian Ilagan

A thesis submitted to the Department of Chemical Engineering

In conformity with the requirements for

the degree of Master of Science (Engineering)

Queen's University

Kingston, Ontario, Canada

(November, 2007)

Library and Archives Canada

Published Heritage Branch

395 Wellington Street
Ottawa ON K1A 0N4
Canada

Bibliothèque et Archives Canada

Direction du Patrimoine de l'édition

395, rue Wellington
Ottawa ON K1A 0N4
Canada

Your file Votre référence
ISBN: 978-0-494-36995-1
Our file Notre référence
ISBN: 978-0-494-36995-1

Abstract

In coronary artery bypass surgery the autologous saphenous vein is the most commonly used vascular graft. However, in a growing number of patients this vein is not available due to disease or availability. To date, there are no commercially available vascular grafts to replace the autologous saphenous vein. Nevertheless, it is widely accepted that a successful small diameter blood vessel alternative will be found using a tissue engineering approach. A photo-cross-linked biodegradable elastomer of acrylated star-poly(ε-caprolactone-co-D,L-lactide) (ASCP) has recently been developed. The elastomer possesses many desirable properties, such as manufacturability and mechanical properties, making it an interesting scaffolding material candidate for this application.

To test the feasibility of the ASCP elastomer as a scaffolding material, a porous scaffold with 90% porosity was constructed using paraffin microbeads combined with an emulsion of ASCP prepolymer and water. Native arterial mechanical properties were matched with an 1800 Da ASCP elastomeric scaffold (ELAS 1800) having 85% porosity. *In vitro* degradation of scaffolds prepared with two different ASCP M_n (1800 and 4500 Da) was investigated for 8 weeks. Bulk hydrolysis was the mode of degradation regardless of configuration, with the porous scaffold degrading slower than the nonporous control. In addition, the ELAS 4500 scaffold also degraded faster than the ELAS 1800 scaffold with the same porosity.

In order to promote the cellular response to this potential vascular scaffold, the surface of the elastomer was modified to enhance bovine coronary artery smooth muscle cell (SMC) attachment and proliferation. Base etching the surface was not as effective as adding a small peptide sequence Gly-Arg-Gly-Asp-Ser (GRGDS) known to

enhance cell adhesion. The surface modifications did not change SMC phenotype as all surfaces expressed the contractile marker proteins smooth muscle α-actin and h-caldesmon. The SMCs also expressed these marker proteins when seeded on porous scaffolds.

Finally, it was possible to integrate the porous scaffold into a biomimetic blood vessel design. With this initial testing, it appears that the ASCP elastomer is a feasible scaffolding material for small diameter blood vessel tissue engineering. Nevertheless, more detailed testing of mechanical properties and cell behaviour must be conducted to ascertain that the ASCP elastomer and the proposed biomimetic blood vessel design can be appropriate replacements for the autologous saphenous vein.

Acknowledgements

I would like to thank my ever supportive family and friends who have helped me persevere to make this goal a reality. In particular, I would like to thank Neal Miran for always providing a shoulder to lean on. I would also like to thank my supervisor, Dr. Brian Amsden and my co-workers, for all their helpful advice and guidance. A special thanks goes to Charlie Cooney for the SEM images, Ron Murrary for the ATR-FTIR analysis, John DaCosta for the paraffin sections, Dr. Hugh Horton and Geoffrey Nelson for the AFM images and Tony Papanicolaou for help with the fluorescent microscope.

Table of Contents

List of Figures

List of Tables

List of Abbreviations

ACl	Acryloyl chloride
AFM	Atomic force microscopy
ASCP	Photo-cross-linked star-poly(ε-caprolactone-co-D,L-lactide)
ATR-FTIR	Attenuated total reflection Fourier-transform infrared spectroscopy
AV	Arteriovenous
BCASMC	Bovine coronary artery smooth muscle cells
CABG	Coronary artery bypass graft
CAD	Computer-aided design
CL	ε-caprolactone
d_6-DMSO	Dimethyl sulfoxide D-6
Dacron	Polyethylene terephtalate fibre
DAPI	4,6-diamidino-2-phenylindole
DCM	Dichloromethane
DLLA	D,L-lactide
DMAP	4-dimethylaminopyridine
DMPA	2,2-dimethoxy-2-phenyl-acetophenone
DSC	Differential scanning calorimetry
EC	Endothelial cell
ECM	Extracellular matrix
EDC	1-Ethyl-3-[3-dimethylaminopropyl]carbodiimide hydrochloride
ELAS 1800	Elastomers made with ASCP of M_n 1800 Da
EPC	Endothelial progenitor cells
ePTFE	Expanded polytetrafluoroethylene
ES	Electrostatic spinning
GAG	Glycosaminoglycans
GMA	Glycidyl methacrylate
GRGDS	Gly-Arg-Gly-Asp-Ser
HBSS	Hank's buffered salt solution
NHS	*N*-hydroxysuccinimide
NMR	Nuclear magnetic resonance
PAD	Peripheral artery disease

PBS	Dulbecco's phosphate buffered saline
PCI	Percutaneous coronary interventions
PCL/DLLA	linear poly(ε-caprolactone-co-DL-lactide)
PEG	Poly(ethylene glycol)
PEGDA	PEG-diacrylate
PEUU	Poly(ester urethane)urea
PGA	Poly(glycolic acid)
PLCL	Poly(lactide-co-
PLGA	Poly(lactic-*co*-glycolic acid)
PLLA	Poly-L-lactide
PU	Polyurethane
PVA	Polyvinyl alcohol
REDV	Arg-Glu-Asp-Val
RGD	Arg-Gly-Asp
RP	Rapid prototyping
RPDS	Arg-Phe-Asp-Ser
SCP	Star-poly(ε-caprolactone-co-D.L-lactide)
SEM	Scanning electron microscopy
SFF	Solid free form fabrication
SMC	Smooth muscle cell
SMP	Smooth muscle progenitor cells
TCPS	Tissue cultured polystyrene
TEA	Triethylamine
T_g	Glass transition temperature
THF	Tetrahydrofuran

Chapter 1
Introduction

1.1 Cardiovascular Disease

Cardiovascular disease is the leading cause of death in the developed world and the third leading cause of death in the developing world [1]. In 2002, cardiovascular disease accounted for approximately 75 000 deaths in Canada and was estimated to cost the Canadian economy over $18 billion a year [2]. Of all deaths associated with cardiovascular disease, 54% were due to coronary artery disease.

In coronary artery disease the coronary arteries become narrowed or blocked with atherosclerotic plaque causing decreased blood supply to the heart. Often, patients develop angina and are at a greater risk for heart attacks. Depending on the severity of arterial narrowing, medications and lifestyle modifications may be prescribed to prevent progression. When the coronary atherosclerosis limits blood flow in the coronary arteries, percutaneous coronary interventions (PCI) such as coronary angioplasty and intracoronary stents are generally used. However, in about 10% of patients there are multiple atherosclerotic plaques along the left main coronary artery or in all three major coronary arteries. In such cases, a coronary artery bypass graft (CABG) must be used (Figure 1). CABG is also the preferred method in the presence of diabetes and/or heart failure [3]. In 2003, an estimated 467 000 coronary artery bypass graft procedures were performed in the United States alone. In many instances, two CABGs were performed per patient [4]. The bypass graft is typically the autologous saphenous vein, radial artery, or internal mammary artery, with the latter staying open for many more years than the

vein graft. Nevertheless, in 10 to 40 per cent of patients these blood vessels are not available due to trauma, disease such as varicose veins, or previous surgery [5].

Cardiovascular disease not only causes narrowing of the coronary arteries but can cause narrowing in all blood vessels. Increasingly, vascular grafts are needed to treat peripheral artery disease (PAD). In PAD blockages can restrict blood circulation in the arteries leading to the kidneys, stomach, arms, legs and feet. According to the American Heart Association, approximately 20 per cent of adults older than 70 have PAD [4]. Similar to coronary artery disease, the bypass graft most commonly used to treat PAD is the saphenous vein. They are also used as arteriovenous (AV) fistulas for end-stage renal failure. Although, autologous native vessels are advantageous because of their immune acceptance and quick harvest time, availability is very problematic. With such profound statistics and an aging population, there is an urgent need for alternative resources to replace the autologous small diameter vascular graft.

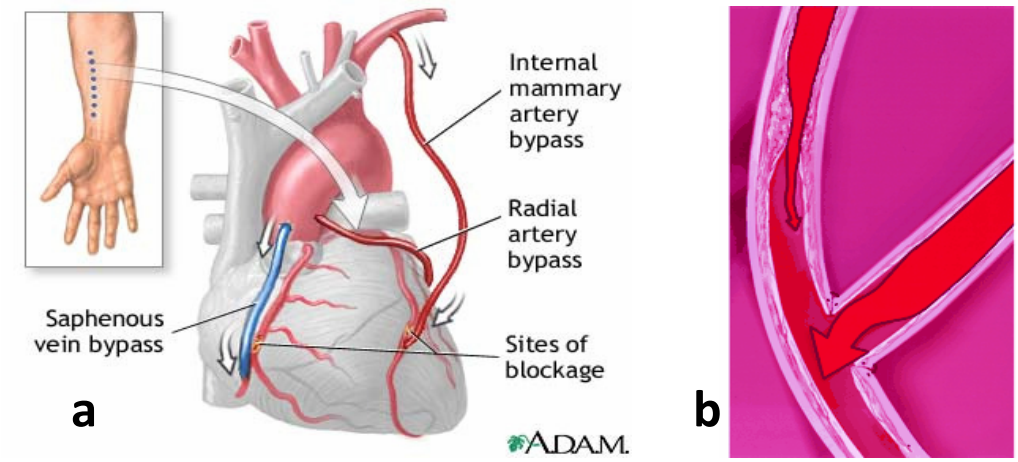

Figure 1: Coronary artery bypass grafts (a) Types of autologous bypass grafts used in CABG surgery (reproduced without permission from: http://www.nlm.nih.gov/medlineplus/ency/article/007115.htm, accessed September 2006) (b) Grafts provide an alternative path for blood to flow from the aorta to heart muscle (reproduced without permission from: Circulation. 2002;106:e187)

1.2 Tissue Engineering as an Alternative

Over 50 years of intense research into alternatives for small diameter vascular grafts has yielded limited success. Nevertheless, advances in tissue engineering approaches have produced promising results and are regarded as optimal alternatives. As the interdisciplinary field between biomedical sciences and engineering, the goal of tissue engineering is to use living cells or to attract endogenous cells to aid, improve or maintain tissue function [6]. In the general paradigm of tissue engineering (Figure 2a), differentiated or undifferentiated cells are seeded on to a biodegradable scaffold and then this construct is matured *in vitro*, usually in a bioreactor. While in the bioreactor, cells proliferate and synthesize extracellular matrix (ECM) products to form new tissue. As new tissue is being formed, the scaffold is degraded so that at the end of the maturation phase, only tissue is present. The construct is then implanted as a prosthesis and *in vivo* remodeling restores normal structure and function. Incomplete paradigms as illustrated in Figure 2b are also possible.

This thesis contributes to the search for an alternative to the autologous small diameter vascular graft by applying tissue engineering concepts. The proposed approach is to develop a biodegradable elastomeric scaffold to be populated by vascular smooth muscle cells (SMCs). The work presented in this thesis is an initial step towards an implantable graft, with the scaffold/cell construct eventually integrated into a complete blood vessel design.

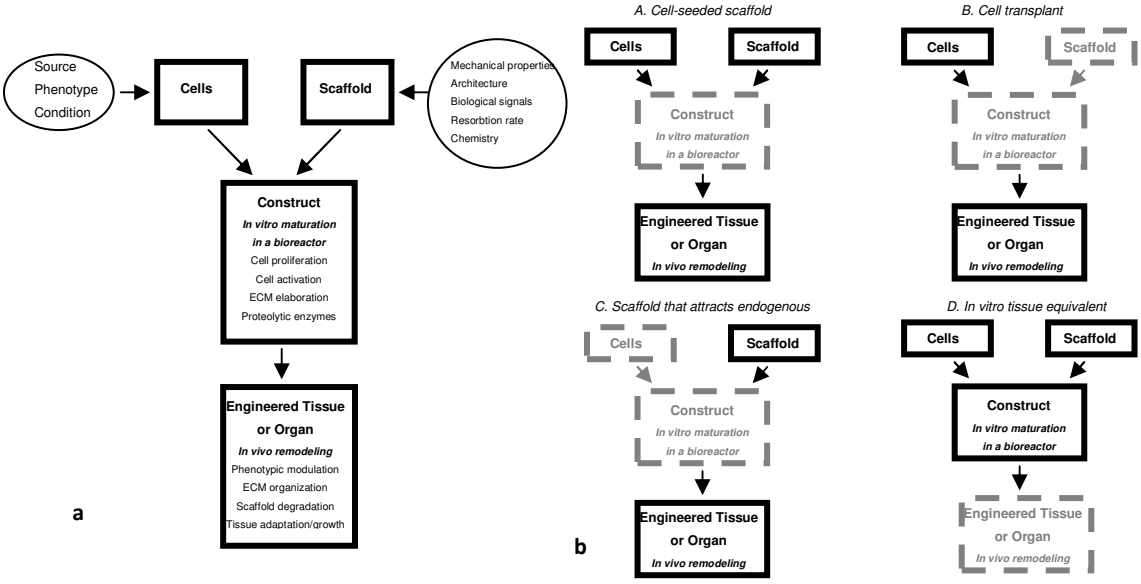

Figure 2: General paradigm of tissue engineering (a) and possible incomplete paradigms (b) (reproduced without permission from [7])

1.3 The Anatomy of Arteries

Blood vessels consist of one to three concentric layers depending on size (Figure 3). Medium arteries such as the coronary and popliteal arteries have all three layers. Beginning from the lumen is the tunica intima. All vessels have an intima which consists of a monolayer of endothelial cells (ECs) and an underlying basal lamina to keep the endothelium together and provide a barrier between blood borne molecules and media. The basal lamina is composed of microfibrils of type IV collagen (diameter ~ 5 nm), the adhesion molecules fibronectin and laminin and smooth muscle cells, although other cells such as lymphocytes, macrophages, mast cells and other inflammatory cells from the blood are sometimes present [8,9]. The endothelium layer is completely renewed every 2-3 years and renewal occurs without the denudation of the basal lamina. New cells grow around and under senescent cells to recover the basal lamina and

reconstitute the endothelial layer integrity. The endothelium provides a smooth, nonthrombogenic surface and is also biologically active [8], playing a critical role in the physiology of vascular functions such as vasoconstriction and vasorelaxation.

Separating the intima from the tunica media is the internal elastic lamina which consists of a layer of elastic fibres, 70-100 nm thick. Fenestrae are present in this elastic layer allowing the communication between endothelial cells and the underlying SMCs. SMCs are the only cell type in the medial layer and they are embedded in elastin, various types of collagen (I,III,V, etc) and other matrix components including proteoglycans. The elastin content is greater in blood vessels closer to the heart and those farther away contain lower amounts of matrix components. Nevertheless, the wall thickness follows Laplace's law such that circumferential wall stress is on the order of 100 kPa, regardless of vessel location. SMCs are responsible for regulating blood flow by constriction and dilation as well as for synthesizing matrix proteins [10,11].

The outermost layer is the tunica adventitia and is comprised mainly of fibroblasts and axially oriented type I collagen. The adventitia provides rigidity and aids in maintaining the shape of blood vessels. The tunica adventitia also contains some elastic fibers, nerves and its own small vasculature, the vasa vasorum. Fibroblasts regulate the matrix, particularly the collagen content.

Blood vessels are innervated most often by sympathetic adrenergic nerves and in some cases, such as in the coronary arteries, by parasympathetic cholinergic nerves. These nerves regulate vascular tone and blood pressure. Sympathetic nerves release norepinephrine which cause SMC contraction and vasoconstriction. Parasympathetic nerves release acetylcholine which bind to SMC and EC receptors. When acetylcholine

binds to EC receptors in conjunction with nitric oxide, a vasodilation effect occurs. Conversely, when acetylcholine binds to SMC receptors, in the absence of nitric oxide, SMC contraction occurs [8].

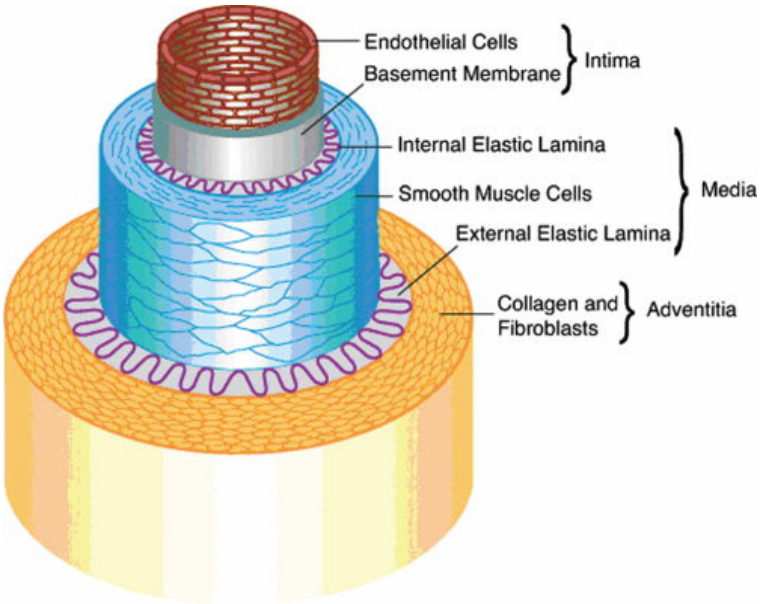

Figure 3: Artery anatomy (reproduced without permission from [12])

1.4 Mechanics of the Blood Vessel

It is assumed that the blood vessel wall is incompressible, such that it remains isovolumetric upon pressurization. All vessels are cylindrical and although the arterial wall is composed of many parts, mechanically it is a homogeneous material. There is little delay or phase lag between change in pressure and diameter; thus, the vessel behaves largely as an elastic body with little viscosity [13].

Under pressure, blood vessels distend in the circumferential and longitudinal directions (tension), while simultaneously undergoing radial thinning (compression) of the wall. These deformations are orthogonal since they occur along three mutually

perpendicular directions with little or no twist or torsion of the vessel. Nevertheless, the radial compression component can be disregarded because the radius-to-wall thickness ratio is approximately 10:1, resulting in a very small (5-10%) relative stress compared to the circumferential and longitudinal directions [13]. Blood vessels are not isotropic (identical in all directions) although the carotid artery approaches isotropy at typical arterial pressures.

The wall of an artery behaves differently based on the intra-arterial pressure. In very low intra-arterial pressures (< 75 mmHg) the arterial wall acts as a vessel of pure elastin. As such, it obeys Hooke's law and acts as an elastic material. In very high intra-arterial pressures (> 200 mmHg) the wall is very stiff and behaves as a tube of pure collagen. At physiological conditions (75-200 mmHg) the elastic behaviour of the arterial wall becomes increasingly non-linear [14].

Although, collagen always has a greater quantity of the two main ECM components in the medial layer, it is elastin that bears the load in all three orthogonal directions with collagen almost solely bearing load in the circumferential direction. Studies on dog blood vessels found that only 8% of the collagen in the carotid and 25 % of the collagen in the renal iliac, mesenteric and coronary artery are load bearing [15]. These studies assumed that elastin and collagen lay parallel with virtually no connections between them. Similarly, when comparing elastic modulus of the vessel wall compared to elastin and collagen, the vessel elastic modulus is closer to that of elastin (0.1-0.6 MPa) versus collagen (1.0-10 MPa) at approximately 0.45 MPa . Collagen instead plays a critical role in maintaining arterial integrity. Degradation of collagen causes pressurized vessels to dilate aneurysmally and rupture, while rupture did not occur when elastin was degraded [16]. The other components in the medial layer, such as glycosaminoglycans (GAGs),

have little effect on mechanical properties, but have been hypothesized to act as wall sensors of shear stress [13].

1.5 Cell Types in the Blood Vessel Wall

1.5.1 Endothelial Cells

Existing as a single, continuous layer of cells, the vascular endothelium is the structural and functional interface between the bloodstream and the blood vessel wall. Endothelial cells (ECs) produce various vasoactive molecules to dilate or constrict the vessel, growth factors, as well as factors that regulate the clotting process. ECs can also modify blood-borne substances for transport into the blood vessel wall (e.g. lipids). Many of the functions of the endothelium are controlled by blood flow-induced shear stress [8,17]. Although, ECs are an important component for proper function of the blood vessel wall, the focus of this thesis is on a scaffold to reproduce a similar tunica media to be populated by SMCs. For more details on the biology of ECs, there are many reviews that provide comprehensive information on the topic [8,17,18].

1.5.2 Smooth Muscle Cells

The primary cells in the tunica media, SMCs have a fundamental function of contraction. By continually contracting and relaxing, SMCs alter the luminal diameter of blood vessels and in turn maintain an appropriate blood pressure. In the normal adult SMCs are arranged in a helical pattern with the majority of force generated exerted in the circumferential direction. SMCs exist as two different phenotypes: contractile and non-proliferating, and proliferating and synthetic [8]. The shift between phenotypes (contractile to synthetic or vice versa), referred to as phenotypic modulation, can be

characterized by examining morphology, expression levels of SMC marker genes, proliferation rates, and migration properties (Figure 4).

SMCs in the contractile phenotype express cytoskeletal marker proteins such as α – actin, myosin, caldesmon, and calponin (Table 1 and Figure 4). They also contract in response to chemical and mechanical stimuli. Nevertheless, between different vessels and within the same vessel there are a diverse number of SMC phenotypes that span the continuum between synthetic and contractile phenotypes (Figure 5).

SMCs are also responsible for maintaining the media through vessel remodeling during physiological conditions such as pregnancy, exercise and after vascular injury [10]. Under these conditions, SMCs synthesize large amounts of ECM materials and have high proliferation and migration rates. Consequently, a high SMC proliferation rate is a characteristic of atherosclerosis.

Differences between SMC phenotypes

Morphologically, contractile SMCs are elongated, spindle-shaped cells. Synthetic SMCs are less elongated and have a cobblestone morphology, which is referred to as epithelioid or rhomboid [19]. They also contain a high number of rough endoplasmic reticulum, Golgi apparatus, and ribosomes, which are organelles involved in protein synthesis. In contractile SMCs, these organelles are replaced by contractile filaments, as illustrated in Figure 6. In terms of proliferative rates, synthetic SMCs generally exhibit higher growth rates and migratory activity [20].

SMCs in culture

It is well recognized that *in vitro*, SMCs behave differently than their *in vivo* counterparts. Primary cultures are known to undergo phenotypic modulation from the

contractile phenotype to the synthetic phenotype. As well, the synthetic phenotype is maintained after subsequent passages [21]. Nevertheless, there are several factors which influence this behaviour.

SMCs have been shown to maintain their contractile phenotype when densely seeded such that a confluent monolayer is formed in the first 2 days. Seeding SMCs with other cell types such as fibroblasts, epithelial or a confluent monolayer of endothelial cells can also maintain phenotype. Serum concentration has a direct influence on the proliferative response of subcultured arterial SMCs. There is minimal growth at 0-0.5% serum. Between 1 and 2.5% there is a significant increase, and at 5, 10 and 20% serum, cells grow logarithmically for increasing periods of time and to higher final cell densities [19].

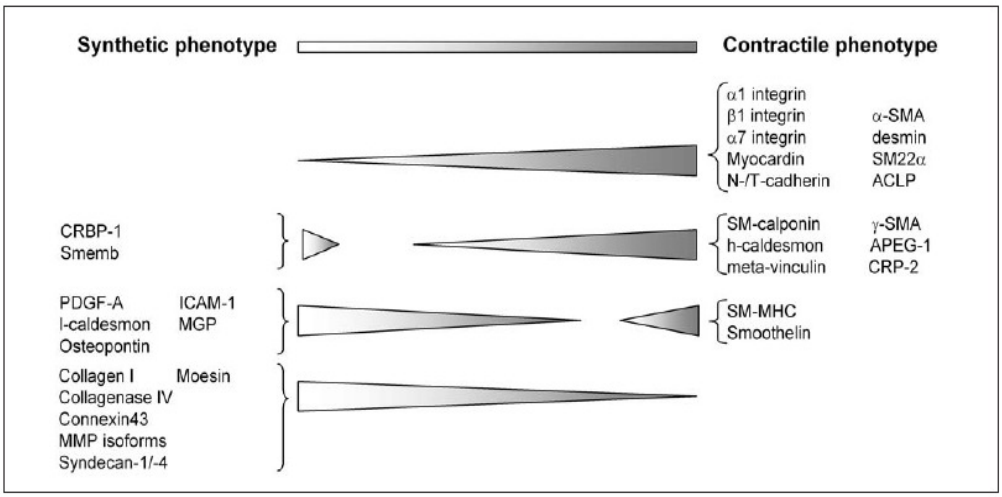

Figure 4: Expression levels of SMC marker genes between phenotypes.
(reproduced without permission from [11])

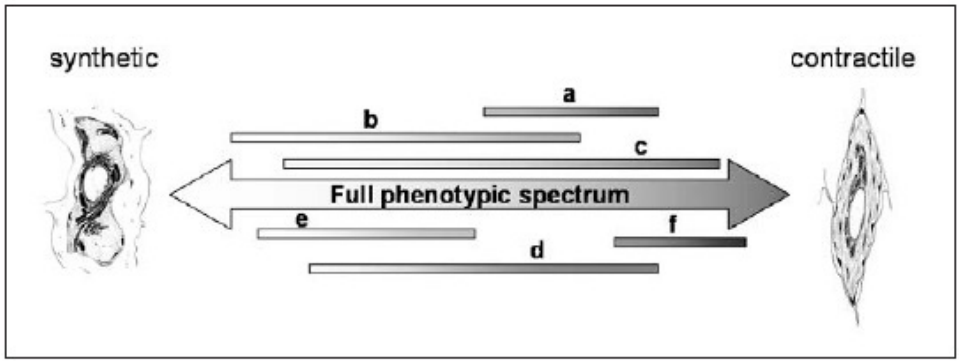

Figure 5: Diversity in SMC phenotypic spectrum. Letters represent different populations of SMCs and their limited spectrum coverage (reproduced without permission from [11]).

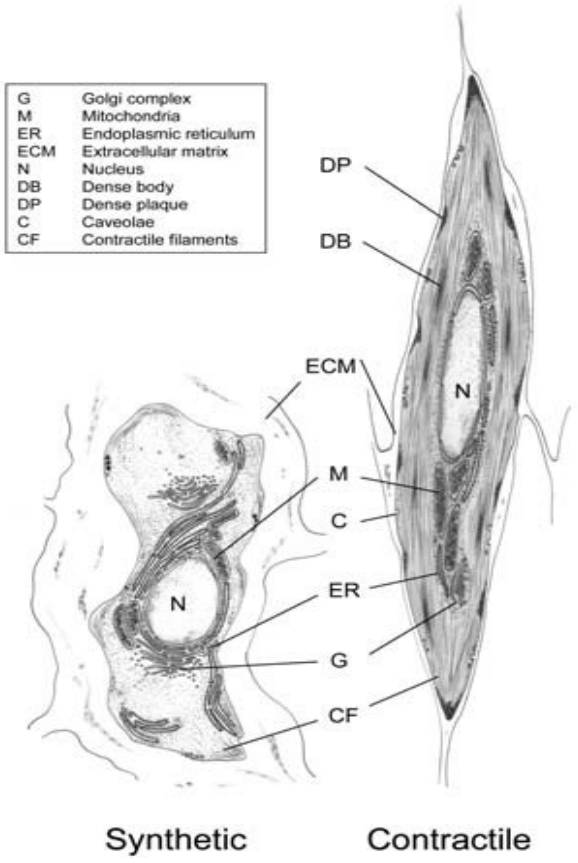

Figure 6: Anatomy of synthetic and contractile SMCs (reproduced without permission from [11])

Table 1: SMC contractility marker proteins (reproduced without permission from [11])

Marker protein	Phenotype specificity (c = contractile s = synthetic)	Subcellular localisation	Function
α- smooth muscle actin	c>s	Contractile filaments	Contraction
Smooth muscle-myosin heavy chain	SM1 c >s SM2 c	Contractile filaments	Contraction
SM22α	c>s	Actin-associated	Regulation contraction
SM-calponin	c>s	Actin-associated/cytoskeleton	Regulation contraction/signal transduction
H-caldesmon	c	Actin-associated	Regulation contraction
Smoothelin	c	Actin-associated	Regulation contraction
Telokin	c>s	Cytoplasmic/membrane	Regulation contraction
Meta-vinculin	c>s	Cytoskeleton	Anchoring cell-ECM
Desmin	c>s	Cytoskeleton	Structural mechanical integrity
CRBP-1	s>c	Cytoplasm	Retinoid transport and metabolism
Smemb	s>c	Contractile filaments	Contraction

1.6 Complications With Small Diameter Blood Vessel Substitutes

The development of a small diameter blood vessel graft (<6 mm) for use in coronary artery bypass surgery or PAD has turned out to be more of a quest for the 'holy grail' for those in cardiovascular research. It has been over fifty years since Vinyon N was introduced as the first synthetic arterial graft [22]. To date, there are no small diameter grafts (<6 mm) approved for clinical use in coronary artery bypass surgery, and grafts used in treating PAD have had limited success. Large diameter arteries (e.g. the aorta) are routinely treated with synthetic grafts such as expanded polytetrafluoroethylene (ePTFE) and Dacron (polyethylene terephthalate fibre). Grafts in small diameter

applications made with similar materials encountered numerous problems, possibly due to the difference in arterial flow regimes and resistances [23].

Unlike large diameter grafts, the long term patency, or being obstruction free of either blood clots or adherent cells, of synthetic grafts made from ePTFE and Dacron are drastically lower than those of autologous blood vessel sources (4 year patency: ePTFE 21% and saphenous vein 70%) [24]. These graft materials are only limited to high-flow/low-resistance conditions because of poor elasticity, low compliance and thrombogenicity [25]. From Table 2, it is evident that ePTFE and Dacron do not have similar mechanical properties as that of the coronary artery or collagen and elastin. Also, the lack of biological functional responses necessary for adaptation and functional responses may not be important in these conditions [26].

Failure of small diameter grafts can occur both in the early and chronic or long term phase of implantation. Early phase failure is mainly due to thrombosis. Chronic phase failure is due to intimal hyperplasia, which is characterized as uncontrollable smooth muscle growth and in turn excessive tissue ingrowth particularly at the anastomosed site (sutured ends). This results in stenosis-induced thrombus formation and occlusion. This growth has been linked to a compensation of an inappropriate mechanical environment [26].

Table 2: Mechanical properties of different scaffold materials and artery components.

Material	**Dacron** [27]	**ePTFE** [27]	**Polyurethanes** [27]	**Coronary Artery** [28]	**Collagen** [17]	**Elastin** [17]	**Smooth Muscle Cell**[17]
Tensile strength	170-180 MPa	14.0 MPa	20-90 MPa	1.40-11.14 MPa	--	--	--
Tensile Modulus	14 000 MPa	0.5 GPa	5-1150 MPa	--	1-10 MPa	0.1-0.6 MPa	0.01-0.25 MPa

1.7 Thrombogenicity and Hydrophobicity

Thrombus formation occurs as part of the foreign body reaction. Proteins that initiate the coagulation pathways are more readily adsorbed onto hydrophobic surfaces [29]. Although, this process occurs in both large and small diameter grafts, it is problematic in small diameter grafts because of their smaller surface areas.

Healthy arteries are non-thrombogenic due to the endothelial layer. An intact and quiescent endothelium proactively inhibits thrombosis. ECs have many mechanisms to prevent thrombosis, as illustrated in Figure 7.

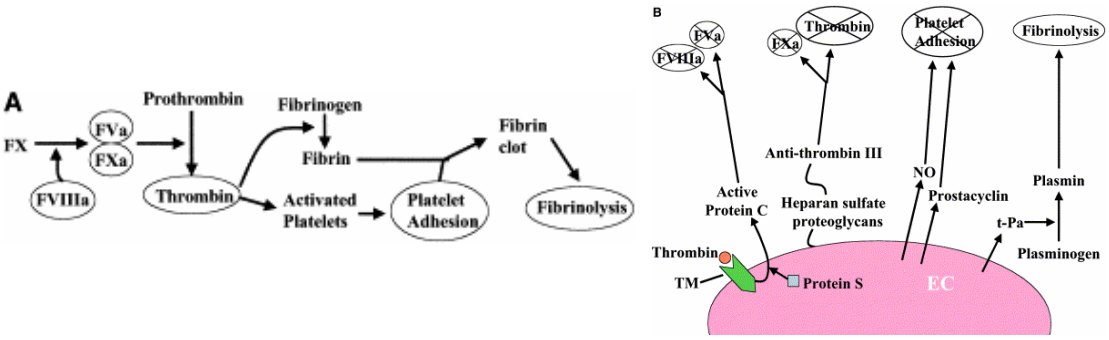

Figure 7: (A)Thrombus pathway (B) EC antithrombogenic signaling (reproduced without permission **from** [30])

Although the saphenous vein is currently the gold standard in bypass surgery, long term patency is significantly less than grafted arteries. Internal thoracic arteries had a patency of 90% versus 57% for the saphenous vein after 10 years [31]. Intimal thickening (hyperplasia) and subsequent luminal narrowing is the major cause of failure for not only Dacron and ePTFE small diameter grafts, but also saphenous vein grafts.

The likely reason for the poor response of vein grafts is that the vein is designed for a low pressure system and does not have the same mechanical properties as arteries.

1.8 Compliance

Compliance is a measure of distensibility and stiffness, as described in equations 1 and 2. It measures the ability of a vessel to expand passively under pressure and take up a certain volume of blood during systole, and to shrink passively during diastole discharging volume of blood smoothly along diastole.

$$C = \frac{\Delta V}{\Delta P} \tag{1}$$

where C = compliance
ΔV = instantaneous change in volume
ΔP = instantaneous change in pressure

$$Stiffness = \frac{1}{compliance} \tag{2}$$

A mismatch of compliance between the host artery and graft induces hemodynamic consequences such as increased resistance, decreased distal perfusion, disturbed flow, turbulence and low shear stress rates [32]. Similar to Table 2, Figure 8 shows that the compliance of the artery is very different from Dacron and ePTFE. Thus, enormous improvements in mechanical properties must be made before a successful vascular graft can be realized.

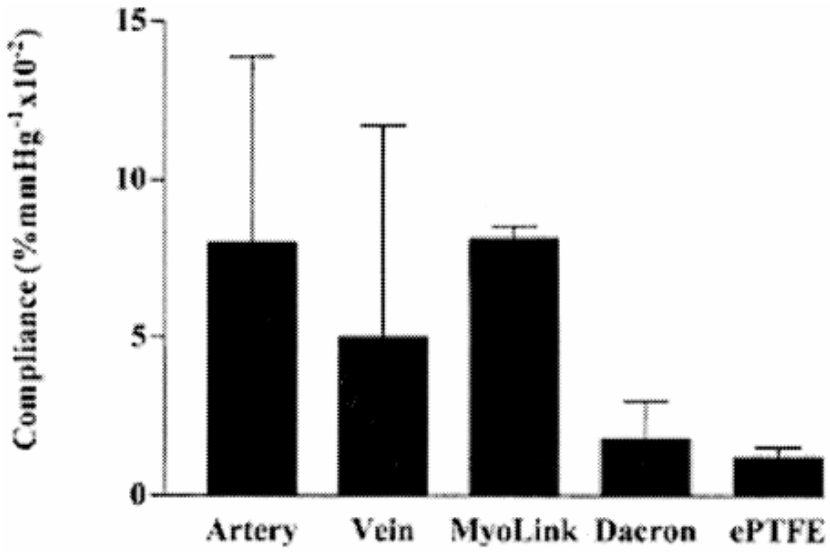

Figure 8: Radial compliance values of arteries, veins, and artificial vascular prostheses (reproduced without permission from [27])

Chapter 2
Literature Review

The ideal vascular graft would be biocompatible, non-thrombogenic, have adequate mechanical strength as well as be compliant and be easy to process and store. Additionally, it would be economical and have localized drug delivery capabilities. Nevertheless, there are no commercially available products that have all these properties.

Current technologies such as ePTFE and Dacron grafts are permanent grafts. Because of the persistent presence of the graft, there will always be a foreign body reaction and no room for remodeling by the native tissue. Nevertheless, technologies that will likely be commercially available in the near future that will improve on this design will be polyurethanes that are stable and provide adequate integration with host tissue so as to not provoke a foreign body response or induce thrombosis. These grafts will still be permanent, but will have mechanical properties closer to those of arteries. As seen in Figure 8, MyoLink, a polyurethane vascular graft from CardioTech International Inc. has a compliance matching those of arteries. However, for small diameter vascular grafts to be a successfully viable and sustainable solution, they must provide optimal integration and have the capacity to remodel. It is widely believed that tissue engineering will provide the means to accomplish this end.

2.1 Tissue Engineering and Vascular Grafts

All facets of tissue engineering are being aggressively investigated (Table 3). Since the first tissue-engineered vessel produced by Weinberg and Bell [33] , numerous

researchers have explored naturally derived [34-36] and denuded cellular materials [37] as well as grafts made completely from cells [38] as possible scaffolds. Nevertheless, such approaches have been plagued by poor mechanical properties and long processing times.

Synthetic polymeric materials have also been considered and are advantageous due to excellent industrial-scale replication as well as the ability to control properties of biochemical and mechanical properties from the point of manufacture. One disadvantage is the lack of cell attachment factors that are present in naturally-derived scaffolds. This chapter will highlight current strategies for small vessel tissue engineering using synthetic polymeric materials.

Table 3: Small-Diameter Blood Vessel Tissue Engineering Fabrication Methods

Method	Advantages	Disadvantages	References
Decellularized tissue	• Rapid cell infiltration • Site-specific remodeling and regeneration	• Reduced ultimate tensile strength and compliance • Xenografts: aneurysm formation, infection and thrombosis • Limited availability	[39,40]
Cell sheets	High burst strengths	• Lack of compliance • Complicated procedure and time consuming (>8weeks)	[38,40]
Biodegradable scaffold from polymers	• Manufacturing: easily reproducible and scale-up • Flexibility to alter physical properties	• Lack of cell adhesion sites • Possible foreign-body reaction	[40,41]

2.1.1 Biodegradable Scaffolds

The arterial wall is composed of dynamic parts that adapt to the conditions of the surrounding environment. As such, the scaffold material should be temporary to accommodate the incoming tissue ingrowth. Polyesters have been widely investigated because of their ease of degradation by hydrolysis of ester linkages, in some cases the degradation products can be resorbed through the metabolic pathways, and the potential to tailor the structure to alter degradation rates [42].

Various biomaterials have been proposed as vascular graft materials such as hyaluronic acid [43], copolymers of poly(glycolic acid)(PGA) [44,45] and polyhydroxyalkanoate [46], poly(lactic-*co*-glycolic acid) (PLGA) [47,48], poly-L-lactide (PLLA), copolymers of polyurethanes (PU) [27,49], collagen [33,40,50], poly(lactide-co-ε-caprolactone) (PLCL)[48,51], chitosan[52], poly citrate diol [53] and many others. The most investigated materials are PGA, PLLA, PU and collagen. Nevertheless, from Table 4 it is obvious that even with the vast research from the past 50 years an ideal graft has yet to materialize.

Table 4: Most investigated materials for small diameter blood vessel tissue engineering

Material	Reason for use	Advantages	Disadvantages	References
Collagen	Major component in media	• low antigenicity, inflammatory and cytotoxic responses • possesses desirable biological and hematological properties • can be remodeled by the host and integrated into existing tissues	• difficult to handle • low mechanical properties (need Dacron mesh sleeve cuff) • long maturation time (need bioreactor to generate additional strength)	[33,40,50]
Polyurethanes	Elastic properties	• elastic mechanical properties • thermoplastic – easy to manufacture	• enzymatic degradation, not stable • possible toxic degradation products • mechanical properties • high Tg • need cell adhesion sites	[27,49]
PLGA	Most popular biodegradable polymer in devices approved by FDA	• degradation products harmless • biocompatible	• crystalline • mechanical properties (too high) • need cell adhesion sites • short degradation time	[47,48]

2.1.2 Elastomeric materials

Many of the above mentioned materials are not crosslinked and not elastic. Elastin, the main component in the arterial wall that contributes to its inherent elastic behavior is a crosslinked polymer. As such, better mechanical properties may be found with crosslinked elastic polymers similar to elastin. Ameer *et al.* have developed biodegradable poly(diol citrate) elastomers with good mechanical properties. The elastomers were constructed into tubes, with the bulk of the mechanical properties coming from the nonporous lumen and not the porous scaffold [53]. In the native artery, it is the media that provides the mechanical properties. Thus, the poly(diol citrate) tubes may not provide the proper mechanical environment for SMCs or ECs to function and integrate properly.

Similarly, Stankus *et al.* developed a biodegradable, elastomeric poly(ester urethane)urea (PEUU) scaffold by electrospinning [54]. VSMCs were incorporated into the scaffold by concurrently electrospraying the VSMCs and electrospinning the scaffold. This technique did not decrease cell viability and high cell densities were obtained after perfusion culture. Nevertheless, mechanical properties could be improved. Both initial modulus (1.7 ± 0.2 MPa) and tensile strength (6.5 ± 1.6 MPa) were in the range of native arteries (Table 7) for scaffolds with SMCs, however, the breaking strain was much higher than native artery values (850 ± 200 %). As with the previous example, these scaffolds may not provide the proper mechanical environment for SMCs to function properly.

2.1.3 Tissue Engineering Approach

For many of the above biodegradable materials (collagen, PEUU), SMCs are seeded on the scaffolds and matured in bioreactors. This is very typical of the *in vitro* tissue engineering approach (Figure 2). Nevertheless, this process is labour-intensive and maturation may take upwards to 8 weeks for completion [40]. Thus, this approach is limited to elective procedures.

In many instances, a vascular graft is needed on a much shorter timeline. Coronary bypass surgeries are frequently done within 24 hours of a heart attack [55]. Thus, an off-the-shelf solution is ideal. The *in vivo* tissue engineering approach (Figure 2b), whether it be cell-seeded scaffold or a scaffold that attracts endogenous cells, may be better suited for this application. In this approach, the implanted scaffold would meet most, if not all, of the features of an ideal vascular graft prior to implantation. This includes being biocompatible, with minimal thromboreactivity, and suitable mechanical properties for normal function until remodeling takes place [56].

Previous work in *in vivo* tissue engineering has focused on decellularized biological scaffolds [39,40]. Nevertheless, there is a growing body of work that suggests that use of synthetic scaffolds in this approach is possible. Shinoka *et al.* successfully repaired congenital defects such as a total cavopulmonary connection and patch for the pulmonary artery in children 3 – 14 years old. Biodegradable scaffolds made from PGA, PLLA combined with PLCL were seeded with various cell sources such as vein ECs and bone marrow. Postoperative examinations revealed no dilatation or rupture of grafts, and there were no complications related to tissue-engineered autografts [57].

2.1.4 Cell Type

In the above example, various cell types and sources were used. The decision on what cell type to use for tissue engineered vascular grafts has been debated for many years [58]. If an *in vivo* tissue engineering approach is to be taken, then there are two sources that can be used to comply with the off the shelf time constraint.

The first is recruitment of autologous vascular endothelial and smooth muscle cells. It has been suggested that cells could possibly be recruited from the sites of anastomosis. It has been possible in some animal models, but it has never been successfully demonstrated in humans [58]. Another source of cells is circulating endothelial (EPC) and smooth muscle progenitor cells (SMP). Aggressive research to characterize these cells are underway [59,60]. The second cell source is allogeneic cells. However, immune acceptance would need to be considered. There is interest in using embryonic stem cells and some success has been achieved [61]. Autologous cells from various sources (vein harvest, liposuction, laparoscopy, and bone marrow) have also been used [56]. However, these additional surgical interventions to obtain the cells and then the subsequent expansion make these sources non-ideal in the context of 'off the shelf' availability. It is evident that tissue engineering approach and cell source must be considered in conjunction with the scaffold when deciding on an appropriate design.

2.2 Key Design Parameters for Scaffolds in Tissue Engineering

There are a number of key design parameters that have proven to be important regardless of approach when dealing with scaffolds. These include: porosity, thrombogenicity and mechanical properties. These concepts are not exclusive to tissue

engineering and have been derived from extensive studies in previous non-tissue engineering approaches.

2.2.1 Porosity

Numerous researchers have shown that a porous lumen is a prerequisite to anchor the neointima in position, while a porous outer surface promotes infiltration of perigraft tissue, holds the prosthesis in place, and permits transmural endothelialization by encouraging angiogenesis [62] . A porous scaffold can also increase compliance, a lack of which has been thought to be a contributing factor to neointimal hyperplasia.

A study by Doi and Matsuda [63] examined this phenomenon in more detail by comparing various polyurethane grafts. Compliant, nonporous grafts had less intimal thickening compared to noncompliant, nonporous grafts, but were inferior to grafts with the same compliance and were porous. Thus, porosity and compliance synergistically prevent neointimal hyperplasia. It was hypothesized that tissues firmly attached to the porous scaffold were able to normally respond to cyclical distension, thereby providing biomechanically controlled cellular activities.

Nevertheless, the role of porosity is not without controversy. Both Contreras [64] and Wong [65] have reported that porosity did not improve neointima formation or patency when comparing impervious and porous ePTFE grafts. In those cases, compliance mismatch may have contributed to failure as ePTFE is less compliant than polyurethane.

For tissue engineering of vascular tissue, it is generally accepted that porosity should be at least 90%. This guarantees a high surface area for cell-polymer interactions, sufficient space for extracellular matrix regeneration and minimal diffusional constraints during *in vitro* culture [66].

Scaffold Fabrication

Porous scaffolds can be divided into two classes based on morphology: fibrillar and foams.

Fibrillar : These scaffolds are produced by knitting and weaving, melt or solution spinning, electrostatic spinning and other nonwoven techniques. A potentially advantageous property of such techniques is that the fibres can be oriented. Thus, mechanical properties can be controlled in different directions.

These techniques, electrostatic spinning (ES) in particular, are attractive because they replicate the structure of natural ECM. The ECM is composed of a chemically and physically cross-linked network of proteins and glycosaminoglycans. With ES, fibres in the nanoscale can be created [67]. Studies have shown that cells recognize and respond to the nanometric topologies of the ECM [68]. Electrospun mats of poly(L-lactide-co-ε-caprolactone) (75:25) copolymer were shown to be capable of supporting cell attachment and proliferation of smooth muscle cells (SMC) and endothelial cells (EC). Both cell types maintained their phenotypic shape and integrate with the nanofibers to form a three-dimensional cellular network [67]. Nevertheless, mechanical properties could be improved. The electrospun mats had similar tensile strengths to the coronary artery (mat: 5 MPa, artery: 1.40-11.14 MPa) however the tensile modulus (156 MPa) [67] was much higher than collagen or elastin – the main components in arterial tissue (Table 2). This may have been due to scaffold material selection and not ES technique. Kwon *et al.* created nanofibrous mats of elastomeric poly(L-lactide-co-ε-caprolactone) (50:50) copolymer that had a tensile modulus of 0.8 MPa [69]. A potential drawback to this technique as well as other fibrillar techniques is the low porosity. The mats by Kwon *et al.* only had a calculated porosity between 69 to 76 percent [69].

Other fibrillar type techniques include rapid prototyping (RP) or solid free form fabrication (SFF), which use computer-aided design (CAD) software. The main advantage of RP techniques is their ability to delicately control the microstructure and macrostructures of scaffolds. However, their main drawbacks are the limited types of polymeric materials that can be used and the low porosities obtained [70].

Foam: These scaffolds are produced by thermal inversion, blowing/reticulation, gas expansion, liquid-liquid phase inversion, particulate leaching and emulsions.

Particulate leaching is the most popular technique for fabricating foam scaffolds. The porogen is usually a salt. However, several studies have used paraffin [71], gelatin [72] and sugar [73], among others. A simple technique, the pore size is controlled by the size of the porogen and porosity is controlled by the porogen/polymer ratio. Porogen removal is accomplished by immersing the scaffold in the appropriate solvent. Since the porogen arrangement is random and similar in all directions, there is little control over directional mechanical properties. Nevertheless, small arteries such as the carotid artery have been found to be isotropic [74] in the physiological pressure range and thus simple techniques such as particle leaching may be sufficient. Also, it is possible that when seeded cells are subjected to mechanical stimulation, the synthesized ECM may be oriented.

Pore Size

Pore size can affect cell growth and in many cases different tissues prefer certain pore sizes as shown in Table 5. As with any foreign body, an inflammatory response occurs upon implantation. It has been shown that pore size has an influence on this response and can be decreased without adversely affecting the degree of neovascularization by using a pore size of approximately 160 μm [75].

Table 5: Tissue Ingrowth and Pore Size [75]

Pore Size (μm)	Tissue Ingrowth
< 0.5	Passage of fluids Prevents ingrowth of cells and bacteria (preferred for wound dressing)
5-10	Limited cell ingrowth
10-30 (interconnected)	Fibrohistiocytic tissue and capillaries
30-100	Organized fibrous tissue
100-300	Fibrocartilaginous tissue

With regards to arterial tissue, specifically small-diameter arteries, a consensus has yet to be achieved as to the optimal pore size. Several researchers use porogens between 50 – 150 μm in diameter [52,63]. Nevertheless, Matsuda and colleagues reported optimal endothelialization with pore diameters between 18 – 50 μm [76].

Pore Shape and Selection

The choice porogen in many grafts that use the particulate leaching method technique is NaCl salt. It is inexpensive, readily available, easy to extract and porosity can be controlled based on quantity. Nevertheless, the cubic crystal shape of salt limits pore interconnectivity. Using spherical porogens such as gelatin and paraffin microbeads can increase interconnectivity and improve mechanical properties.

Zhang et al [77] conducted a comparative study of porous PLGA scaffolds with cubic and spherical macropores and found that at high porosities grafts with spherical pores exhibited better compressive properties in contrast to those with cubic pores. The compressive modulus and strength of scaffolds with spherical pores were less sensitive to batch differentiation. Thus, the regular packing of spherical porogens leads to consistent foams, while cubic porogens may have a dispersed distribution of interconnectivity that can differ from batch to batch. Draghi *et al.* [78] measured pore interconnectivity by flow resistance. They found that grafts with NaCl porogens had

higher flow resistances as well as a wider range for similar porosities. Creep deformation was also measured and similar to Zhang's observations, better mechanical properties for grafts prepared with spherical porogens were found.

Nevertheless, spherical porogens are not all created equally. Theoretically, a regularly packed bed can only have a maximum volume fraction of approximately 70%. Grafts using gelatin porogens have reported such porosities [72,78]. Porosities upwards to 90% can be accomplished with paraffin porogens. Paraffin porogens were first introduced by Ma and Choi [71]. No sophisticated equipment was required and a homogeneous foam could be fabricated. The increase in interconnectivity was attributed to a heat treatment that merged adjacent paraffin porogens.

2.2.2 Thrombogenicity

Early prostheses were limited because materials such as Dacron and ePTFE are inherently thrombogenic. Several strategies to overcome this include carbon-coating ePTFE to improve electronegativity and covalently binding heparin for controlled release. Nevertheless, these strategies have not improved vessel patency rates when implanted *in vivo* [79,80]. Vast improvements on patency were seen when grafts were coated with autologous endothelial cells [81]. Thus, it is now well recognized that a layer of endothelial cells is the best way to prevent thrombogenicity.

Surface modifications to increase cell adhesion include plasma deposition [82] and surface hydrolysis [44]. These techniques increase the hydrophilicity of the surface by exposing functional groups such as carboxylic acids and hydroxyls. Surface hydrolysis may also expose a nanoscale topography that enhances cell function [83]. The most popular surface modification to promote EC adhesion and growth is by covalently

binding the peptide sequence Arg-Gly-Asp (RGD). The RGD sequence is found in fibrinogen and other proteins, and promotes EC and SMC adhesion while reducing platelet aggregation [84]. Nonetheless, it has been shown that the RGD signal loses both affinity and specificity when taken out of the context of a protein; however activity is retained when the C-terminal carboxyl group is blocked or flanking amino acids are added [85].

Several techniques exist to covalently bind RGD to polymer surfaces, such as blending with polymers that contain functional groups and co-polymerization. Herel *et al.* gives an extensive review on RGD modified polymers as well as the technical aspects of RGD immobilization on polymers [85]. Peptide sequences, such as REDV (Arg-Glu-Asp-Val) are EC specific and advantageous to limit hyperplastic ingrowth of smooth muscle cells and fibroblasts [86].

2.2.3 Mechanical Properties and Material Selection

Material selection is very important in designing a small diameter blood vessel substitute. From the failure of early prostheses, it was quite evident that matching mechanical properties is one of the keys to success. The major mechanical property that needs to be matched is compliance. Arterial wall elasticity plays a pivotal role in blood flow distribution. A lack of elasticity leads to high turbulence. Under these unfavorable flow conditions, formation of anastomotic aneurysms, development of hyperplastic neointima, and failure of sutures or tearing of the host artery are prevalent [87].

As such, there has been a move towards elastic materials. In particular, a large amount of research has been devoted to polyurethanes (PU). Several products such as the Corvita® graft and Cardiotech® graft are made from compliant polycarbonate PU

and are commercially available or undergoing clinical trials as peripheral grafts [27]. Early PU grafts were prone to aneurismal dilation and rupture [88]. Current polycarbonate-based polyurethanes (PU) have most of the ether linkages eliminated and therefore are hydrolytically and oxidatively stable[89].

Although it is important to keep the integrity of the scaffold, tissue ingrowth and the deposition of native ECM will change the compliance of the vessel. In a study using iliofemoral artery woven Dacron grafts, the average graft diameter variation during the cardiac cycle decreased from 6% at 1 month after implantation to 1% after 1 year [90].

It should also be noted that material composition affects cell function. In particular, a study by Kim and Mooney found that scaffold chemistry regulated SMC phenotype. The rate of elastin production on PGA scaffolds was higher than that on type I collagen sponges, while collagen production was higher on the type I collagen sponges. It is postulated that this is likely due to different ligands for cell attachement. The major protein adsorbed onto the scaffold was different for each case [91].

2.3 Biomimetic Designs

Learning from previous studies, several groups have developed vascular grafts, where the biochemical and mechanical properties of native vessels are emulated through biomimetic designs. Sonoda and Matsuda produced a coaxial double tubular graft design with the same 'J' distension profile as canine carotid arteries. This was achieved by using an inner compliant graft and an outer less compliant graft of segmented PU and adjusting porosity and graft thickness [92]. This design looks promising, but the segmented PU is not degradable. It would be interesting to investigate the effects this design has on cell infiltration and how mechanical properties would be affected.

Jun and West incorporated a diazeniumdiolate-modified nitric oxide -producing peptide into polyurethane to simulate EC function and showed a decrease in platelet adhesion and SMC growth while stimulating EC growth in vitro [93]. Mechanical properties were similar to other polyurethane grafts, but not comparable to arteries, with tensile strength approximately 25 MPa and elongation almost 2500%.

Similarly, Zilla *et al.* have a patent that incorporates a luminal film to prevent fibrin from depositing in pores and hindering transmural ingrowth[94]. Nevertheless, this design could be improved. The materials for the luminal film (polysiloxanes, polyurethanes, etc.) are not necessarily nonthrombogenic [95].

Chapter 3
Scope of Research

Evidence from the literature review indicates that, although there has been some success in finding a suitable scaffold for small diameter vascular tissue engineering, there is room for improvement. There are only a few crosslinked elastomers being investigated and with that, SMC elastin production, a key component of the arterial wall, is greatly missing. Thus, the use of elastomers as scaffolds with their similar mechanical properties may increase the synthesis of this important component. As well, manufacturability of these scaffolds is not ideal. Many processes need high temperatures to crosslink and are not robust for the future incorporation of peptides or drugs.

A photo-cross-linked biodegradable elastomer has been effectively synthesized and characterized as a biomaterial [96]. Mechanical properties of the photo-cross-linked star-poly(ε-caprolactone-co-D,L-lactide) (ASCP) can be controlled by adjusting prepolymer molecular weight and are in the vicinity of several bodily tissues. *In vitro* and *in vivo* studies have also shown good biocompatibility [97]. There have also been previous attempts to modify the surface of this elastomer. Due to the mild processing, the elastomer has great potential for future use as a scaffold with drug delivery capabilities. Thus, it is believed that the ASCP is an excellent candidate as a scaffolding material for tissue engineering of the medial layer of small diameter blood vessels.

3.1 Objectives of Research

To investigate the feasibility of ASCP as a scaffolding material for small diameter blood vessel tissue engineering, the following objectives were pursued:

- Create a scaffold with adequate porosity (greater than 90%). Paraffin and alginate spherical porogens were compared and the porogen that resulted in the highest porosity was chosen for the remainder of the experiments.
- Fabricate a scaffold with mechanical properties similar to native arteries. To do this ASCPs of various molecular weights were tested.
- Investigate the effect of degradation on the mechanical properties of the scaffold.
- Modify the surface of the ASCP scaffold to improve cell attachment of SMCs. For this purpose, base etching and grafting of RGD were examined.
- Incorporate the ASCP scaffold into a biomimetic artery design. The ASCP would act as the media and support SMC growth, while a thin PEG hydrogel layer would act as the intima and support EC growth.

Chapter 4
Materials and Methods

4.1 Porogen Selection and Scaffold Characterization

4.1.1 Reagents

Low viscosity alginate, paraffin, polyvinyl alcohol(PVA), phenol, sodium citrate, calcium dihydride, glycerol, stannous 2-ethylhexanoate, acryloyl chloride, triethylamine, 4-(dimethylamino)pyridine, 2,2-dimethoxy-2-phenyl-acetophenone, and Dulbecco's phosphate buffered saline -without calcium chloride and magnesium chloride (PBS) were purchased from Sigma-Aldrich (Canada). Sulphuric acid, methanol, 2-propanol, hexane, tetrahydrofuran (THF) and dichloromethane (DCM) dried over CaH_2 and distilled under argon were purchased from Fisher Scientific (Canada). Purasorb D,L-lactide (DLLA), 99+% purity was purchased from Purac (The Netherlands) and used as received. 99% ε-caprolactone (CL) from Lancaster (Canada) was dried over CaH_2 (Aldrich, Canada) and distilled under nitrogen. Dimethyl sulfoxide D-6 (d_6-DMSO) for ^1H NMR (Nuclear magnetic resonance) was purchased from Cambridge Isotope Laboratories Inc. (USA).

4.1.2 Porogen Fabrication

Alginate

Ca-alginate microbeads used as porogens were generated using an electrostatics technique adapted from Bugarski *et al*. [98]. Briefly, a 1% alginate solution was added dropwise through a Hamilton 33G needle into a gelling solution of 100 mM $CaCl_2$ using a

syringe pump (Sage Instruments Model 220) at a rate of 0.044 ml/min. A high voltage power supply (Bertan Associates Inc. Series 230-30R) was used to vary voltage from 3 to 13 kV to produce spherical microbeads porogens with diameters between 130 – 60 µm. The distance of the needle tip from the gelling solution was approximately 2 cm. The resulting microbeads were collected on a 45 µm sieve and dried for several days at room temperature. Microbead diameters were measured from light microscope images. A minimum of 10 samples were taken at each voltage. A Hund Wetzlar inverted microscope (model Wilovert S) with a mounted Leica camera (model DFC320) and Leica IM50 software was used to capture images.

Paraffin

Paraffin microbead porogens were fabricated using the method established by Ma et al[71]. Melted paraffin wax was added dropwise to a 0.003% PVA solution vigorously stirred and heated to 65°C. Paraffin droplets were quickly solidified by quenching in ice cold water and stirred. The paraffin beads were then sieved through a 250 µm sieve and collected on a 45 µm sieve. The porogen diameters were measured similar to the Ca-alginate porogens.

4.1.3 ASCP synthesis

Synthesis of star-poly(ε-caprolactone-co-D.L-lactide) (SCP)

Various molecular weights of *star*-poly(ε-caprolactone-*co*-DL-lactide) (1800, 4500 and 7800 Da) were prepared by ring-opening melt polymerization of D,L-lactide (DLLA) and ε-caprolactone (CL) initiated with glycerol (Figure 9). Equation 3 was used to determine the amount of glycerol needed to yield a polymer of a desired molecular weight:

$$M_n = \left[\frac{m_{CL}}{m_I} \left(\frac{MW_{CL} + \gamma MW_{DLLA}}{MW_{CL}} \right) + 1 \right] MW_I \qquad (3)$$

where γ is the molar ratio of DLLA to CL and I is the initiator (glycerol)

In all cases, a 1:1 mol ratio of DLLA to CL was used. DLLA, CL and glycerol were combined in a flame-dried glass ampoule and placed in a 140°C oven until the DLLA was melted. 10^{-3} mol of stannous 2-ethylhexanoate per mole of glycerol was then added and the ampoule flame sealed under vacuum and placed at 140°C for 48h.

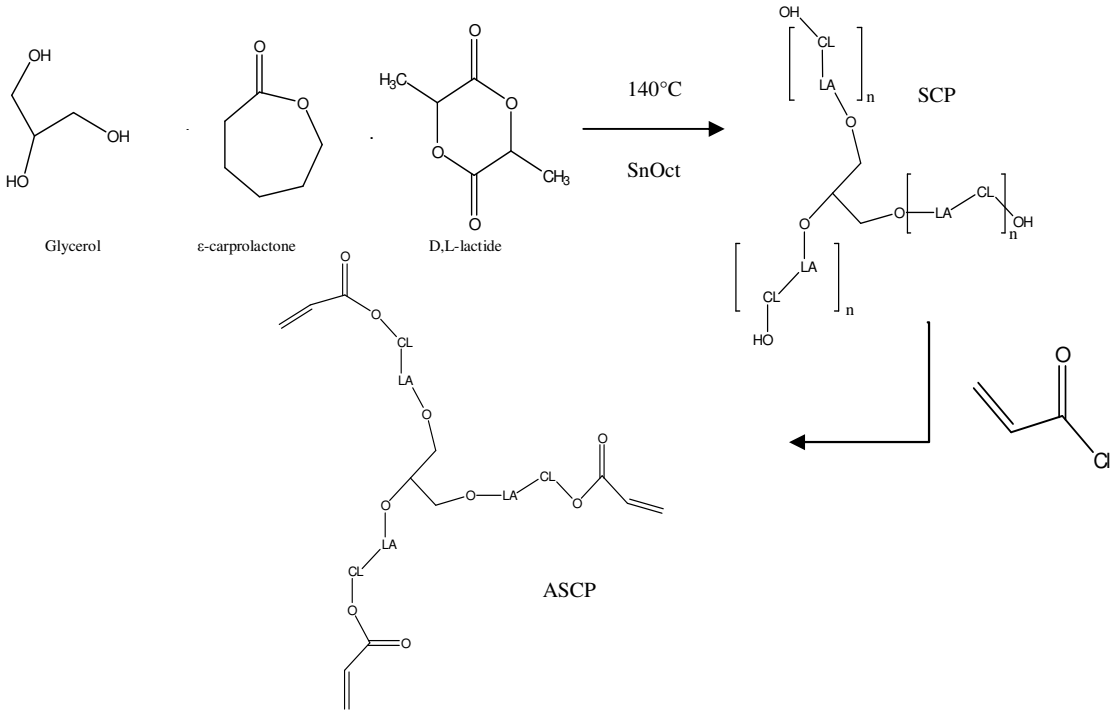

Figure 9: Synthesis of star-poly(ε-caprolactone-co-D.L-lactide) (SCP) and acrylation of end groups (ASCP). SnOct refers to stannous 2-ethylhexanoate.

Synthesis of acrylated star copolymer (ASCP)

The terminal hydroxyl groups of the SCPs were acrylated by reacting acryloyl chloride (ACl) in the presence of triethylamine (TEA) as a hydrochloric acid scavenger, and a catalyst, 4-dimethylaminopyridine (DMAP) (Figure 9). SCP was dissolved in anhydrous, distilled dichloromethane (DCM) at a ratio of 1:10 (w/v) in a flame-dried round-bottom flask. The flask was sealed using a rubber septum, flushed with argon and placed in a controlled climate glovebox filled with nitrogen. TEA and DMAP were added to the SCP solution at a molar ratio of 1 and 10^{-3} mol per mole of SCP hydroxyl group, respectively. ACl diluted in DCM was added dropwise to the polymer solution at room temperature at a ratio of 1.2 mol per mole of SCP hydroxyl group. The reaction was continued at room temperature for 48h under mild stirring. The final solution was dried under a stream of air. The dried polymer was then dissolved in ethyl acetate and filtered to remove the triethylamine hydrochloride salt formed during the reaction. The filtrate was dried under air flow. Finally, the dried polymer was purified by washing with methanol or 2-propanol for lower molecular weight polymers. Methanol was added to the ASCP and stirred for 1 h. The mixture was then cooled for 2 h at -20°C and the methanol was decanted. This extraction process was repeated twice. The purified polymer was then dried under vacuum for several days.

Both SCP and ASCP compositions were confirmed using ^{1}H NMR in d_6-DMSO using a Bruker Avance-300 NMR spectrometer. The resulting M_n of the SCP was calculated from equation 4 and the peak intensities pertaining to only DLLA (5.0 – 5.3 ppm) and CL (2.2 – 2.4 ppm) components in SCP and the DLLA end group (5.5 ppm). The degree of acrylation was calculated using NMR end group analysis (equation 5). Only the endgroup from the DLLA portion was used in the calculations, as the endgroup from the

CL portion was negligible. More specifically, the degree of acrylation was calculated from the ratio of the acrylate groups to total end groups (acrylate and DLLA end groups).

SCP Mn

$$3\left[\frac{I_{DLLA}/2}{I_{endgroup}}MW_{DLLA}+\frac{I_{CL}/2}{I_{endgroup}}MW_{CL}\right]+92 \quad (4)$$

where I_{DLLA} = peak integration of DLLA at 5.0-5.3 ppm
I_{CL} = peak integration of CL at 2.2-2.4 ppm
$I_{endgroup}$ = peak integration of DLLA end group at 5.5 ppm
MW = molecular weight

Degree of Acrylation

$$DA=\left(\frac{I_{C=C}}{I_{C=C}+I_{DLLAendgroup}}\right)100\% \quad (5)$$

where $I_{C=C}$ = peak integration of acrylate end group (5.9 – 6.4 ppm)
$I_{DLLAendgroup}$ = peak integration of DLLA end group at 5.5 ppm

UV crosslinking of ASCP

The ASCP was dissolved in ethyl acetate at a 1:1 (w:v) ratio. 1.5 wt% of the UV initiator, 2,2-dimethoxy-2-phenyl-acetophenone (DMPA) was then added and the solution vortexed. The ASCP prepolymers were cast onto glass molds and exposed to UV light at room temperature using a Blak-Ray® high-intensity long-wave lamp at a relative intensity of 10 mW/cm^2 for 10 minutes. The resulting elastomer was dried under vacuum and kept in a desiccator under vacuum until required for analysis and characterization.

4.1.4 Construction of Porous Scaffold

Alginate

ASCP in ethyl acetate with DMAP (as described above) were added to the Ca-alginate microbead porogens at a maximum weight fraction of 77%. The Ca-alginate porogens were pre-wet with ethyl acetate to facilitate good mixing. The ASCP/Ca-alginate mixture was vigorously vortexed, poured into a glass mold and exposed to UV light (10 mW/cm^2) for 10 minutes. Ca-alginate was removed by immersing scaffold in 500 mM sodium citrate for 24 hrs with frequent changes.

To confirm and quantify the amount of alginate removed, a colorimetric assay based on phenol and sulphuric acid was employed [99]. Alginate monosaccharides will degrade upon exposure to acid to form 5-formylfuran-2-carboxylic acid which then forms a colored product with phenol that can be measured with a UV-spectrophotometer (μQuant microplate reader - BioTek Instruments, Inc.). However, the elastomer also formed a colored product when performing the phenol/sulphuric acid assay. The background absorbance from the elastomer was so great that it was hard to distinguish between samples with and without alginate, thus interfering with the assay. Uncrosslinked linear poly(ε-caprolactone-co-DL-lactide) (PCL/DLLA) was used to resolve this issue as it can be removed with DCM leaving the alginate porogens intact. It was assumed that using the same procedure to make the porous constructs would lead to similar structures and thus was a valid model to confirm alginate removal. Specifically, for a 100μl sample, 44.4 μl of liquefied phenol was added to the sample and vortexed. 2 ml of concentrated sulphuric acid was then added as a stream. The samples were left at room temperature for 5 hrs before being measured at an absorbance of 490 nm.

Paraffin

Scaffolds made with paraffin microbead porogens were fabricated in a similar manner to those with alginate. In this process, paraffin porogens were not pre-wet, but added slowly to the ASCP solution with mixing after each addition. Adding the ASCP solution to the paraffin porogens did not result in good mixing and constructs did not form. The suspensions were cast on glass molds with a glass slide on top and each side was exposed to UV radiation (10 mW/cm^2) for 10 minutes each. An icepack was placed underneath the mold to maintain the temperature below the melting point of paraffin during crosslinking (~55℃).

Paraffin and Emulsion Scaffolds

Increased porosity was achieved by using an emulsion of ASCP with water and the paraffin porogens. The emulsion was prepared by adding 1ml SPAN 80/g ASCP to the ASCP solution (ASCP, solvent, initiator) and vigorously mixed with a vortex. An equal volume of 0.5% PVA was then added dropwise to the mixture (providing a 67 wt% mixture). The mixture was vortexed until the viscosity was significantly thicker. The emulsion was then mixed with the paraffin porogens and cast as before. The paraffin porogens were removed by either immersing in hexane or THF for 24 hrs with frequent changes. In the case of THF, the elastomer sol component was also removed. The scaffolds were then dried for several days under vacuum (20 inHg) and stored in a dessicator. Complete removal of paraffin porogens was assumed since porosity was equal to or higher than the added porogen.

4.1.5 Scaffold characterization

Porosity

Scaffold porosity was measured using a modified Archimedes Principle technique. Dry samples were massed, then immersed in 2-propanol. After sonicating for 30 – 60 seconds to remove trapped air bubbles, the samples were placed in a dessicator under vacuum (20 inHg) for 1 h. In this time, all voids would be filled with 2-propanol. The samples were then weighed after carefully removing excess liquid. Equations 6 - 8 were used to calculate the porosity.

$$V_{voidspace} = \frac{m_{wet} - m_{dry}}{\rho_{2-propanol}} \quad (6)$$

$$V_{elastomer} = \frac{m_{dry}}{\rho_{elastomer}} \quad (7)$$

$$Porosity(\%) = \left(\frac{V_{voidspace}}{V_{voidspace} + V_{elastomer}} \right) 100\% \quad (8)$$

where $V_{voidspace}$ = volume of pores (cm^3)

$V_{elastomer}$ = volume of elastomer (cm^3)

m_{dry} = mass before 2-propanol immersion (g)

m_{wet} = mass after 2-propanol immersion (g)

ρ = density (g/cm^3) 1.18 g/cm^2 was used for the elastomer

Pore Size

To visualize the porous scaffold, scanning electron microscopy (SEM) was employed. A Jeol JSM-840 scanning electron microscope with an accelerating voltage of 10 kV (Queen's University Mechanical Engineering Department) was used. Samples were cross-sectioned by freeze-fracturing in liquid nitrogen, and then were gold coated.

ImageJ software was used to measure a minimum of 20 pores per sample from images of cross-sectioned porous scaffolds at 100 times magnification.

Sol Content

The sol content of the elastomers was determined by washing samples with THF for 24 h and then completely drying under vacuum with mild heat. The mass loss from this wash can be attributed to the uncrosslinked portion of the elastomer (equation 9).

$$SolContent(\%) = \left(\frac{m_{wash}}{m_{before} - m_{wash}} \right) 100\% \quad (9)$$

where m_{wash} = mass after THF wash
m_{before} = mass before THF wash

Thermal Properties

Thermal measurements of elastomers were carried out using a TA instruments Q100 DSC (Differential scanning calorimeter). Samples were run using a cooling-heating-cooling cycle from ambient to -80℃ to 80℃ at a heating/cooling rate of 10℃/min. The glass transition temperatures were determined from the inflection points of the second run endotherms, using the internal DSC analysis program.

Mechanical Properties

Uniaxial tensile properties of the elastomers were measured using rectangular slabs (~ 12 mm x 1 mm x 0.5 mm) and an Instron tensile tester model 4443. The crosshead speed was set at 500 mm/min according to ASTM D412 and the load cell used was 1 kN. All specimens were tested at room temperature.

***In Vitro* Degradation**

Elastomer slabs (same dimensions as above) were immersed in 1.5 ml phosphate buffered saline (PBS), pH 7.4 and 37℃, in clear Eppendorf tubes for 8 weeks. Three samples were used for each time point. PBS was replaced every week. At each time point, slabs were removed, blotted dry, and massed. The slabs were then subjected to uniaxial tensile testing while wet. Samples were then dried and massed. For each time point sol content and thermal properties were measured. SEM images were also taken. All measurements were done on triplicate samples, unless otherwise indicated.

4.2 Surface Modifications

4.2.1 Reagents

Sodium hydroxide, bicarbonate buffer, peptide sequences Gly-Arg-Gly-Asp-Ser (GRGDS) and Arg-Phe-Asp-Ser (RPDS), glycine, fluorescamine isomer 1, *N*-hydroxysuccinimide (NHS), 1-Ethyl-3-[3-dimethylaminopropyl]carbodiimide hydrochloride (EDC) and glycidyl methacrylate (GMA) were purchased from Sigma Aldrich (Canada), acrylate- poly(ethyleneglycol)-succinimidyl carboxymethyl (Mn 3400) was purchased from Laysan Bio Inc.(Arab, AL).

4.2.2 Base Etching

Thin elastomeric films were prepared as described above. After removal of residual solvent by air drying, the films were base etched with 0.5 M NaOH for 1 h. The films were then washed in distilled deionized water three times or until the pH of the wash solution was neutral. The extent of the base etching was determined by covalently attaching fluorescamine to any carboxyl or hydroxyl groups on the surface, through

water-based carbodiimide chemistry and imaging with a confocal microscope (Leica TCS SP2 multi-photon confocal inverted microscope). Water sessile drop contact angle analysis (AST Products Inc. VCA Optima goniometer) was also conducted. Briefly, 1 µl droplet of distilled water was placed on the film and an image of the resulting droplet shape was taken with VCA Optima XE v1.90.0.2 software. The software was then used to calculate the contact angle.

SEM and atomic force microscopy (AFM) (Agilent 5500) imaging were used to determine whether the base etching resulted in only a chemical surface modification or if the etching also physically changed the topography of the surface. The surface roughness root mean square deviations of the unmodified and base etched films were calculated from the resulting AFM images with ImageJ software.

Finally, primary bovine fibroblasts at passage 2 were grown for up to 5 days on both base etched and control elastomeric films to determine whether the surface modification improved cell attachment and proliferation. Elastomer films prepared using 4500 Da ASCP were sterilized with UV light in a laminar flow hood for 30 minutes and then 1.05 x 10^4 cells in 20 µl of medium (Dulbecco's Modified Eagle's Medium and 10% fetal bovine serum) were seeded on each film. The films were incubated for 30 minutes before topping up each film with 2 ml of medium.

4.2.3 Peptide Acrylation

GRGDS and RPDS peptides were acrylated following a modified procedure developed by Hern and Hubbell [100]. Both peptides were dissolved in 50 mM bicarbonate buffer at a ratio of 1 mg/ml. A 10 molar excess of GMA also dissolved in bicarbonate buffer (one third final volume), was then added slowly to the peptide solution and reacted under dark

conditions for 2 hours at room temperature. The final solution was quenched in liquid nitrogen and lyopholyzed. The acrylated peptides were then stored in a -20°C freezer until used.

4.2.4 Addition of peptide to PEG spacer

Acrylate-poly(ethyleneglycol)-succinimidyl carboxymethyl (Mn 3400) was used as a PEG spacer to tether the GRGDS away from the surface. Following a procedure developed by Hern and Hubbell [100], peptides were dissolved in 50 mM bicarbonate buffer at a ratio of 1 mg/ml. A 2 to 1 ratio of PEG spacer to peptide was also dissolved in a minimum amount of bicarbonate buffer (200 µl per 1 mg peptide). The PEG spacer solution was added dropwise to the peptide and reacted for 2 hours. The solution was quenched in liquid nitrogen, lyophilized and then stored in a -20°C freezer until used.

4.2.5 Addition of peptide to scaffold

Both acrylated peptides and PEG spacer-peptides were directly added to the ASCP solution and vigorously mixed. Elastomers were then prepared as previously described. Initial work with glycine as the peptide was done to confirm the addition of the spacer as well as incorporation into the elastomer. ^{1}H NMR was used to confirm addition of glycine to the spacer and attenuated total reflection Fourier-transform infrared spectroscopy (ATR-FTIR) was used to confirm surface modification of the elastomer with the acrylated peptides. A Bruker IFS 55 with diamond ATR-FTIR cell from the Dupont Research, Development and Engineering Centre in Kingston, Ontario was used to measure samples.

4.3 Cell Culture

4.3.1 Materials

Bovine smooth muscle growth media, trypsin/EDTA, trypsin neutralization solution, Hank's buffered salt solution (HBSS) were purchased from Cell Applications (San Diego, CA). Dulbecco's phosphate buffered saline (without calcium chloride and magnesium chloride) (PBS) pH 7.4 from Sigma-Aldrich, WST-1 assay kit from Roche Diagnostics. Vectashield™ aqueous mounting medium with 4,6-diamidino-2-phenylindole (DAPI) was obtained from Vector Labs (Canada). Anti-Mouse IgG (whole molecule) TRITC conjugate, monoclonal anti-caldesmon (smooth), clone hHCD (mouse IgG1 isotype), monoclonal anti-α-Smooth Muscle Actin (mouse IgG2a isotype) clone 1A4 FITC conjugate were purchased from Sigma Aldrich.

4.3.2 Cells

A vial of cryopreserved primary bovine coronary artery smooth muscle cells (BCASMC) at passage 2 were purchased from Cell Applications and expanded. All experiments used SMCs of passages 5-9.

Cell expansion

Cell expansion was done according to the protocol provided by Cell Applications. Briefly, cryopreserved cells were quickly thawed and placed in a T-75 flask with 15 ml of bovine smooth muscle growth medium overnight in a 37℃ incubator with 5% CO_2 and 95% relative humidity. The medium was replaced with 15 ml of fresh medium the next day to remove any trace dimethylsulfoxide. Subsequently, the medium was changed every 2-3 days until cells were 80% confluent. To passage cells, the medium was

aspirated and washed with 5 ml HBSS. 6 ml of trypsin/EDTA were then added to the flask and 5 ml trypsin/EDTA immediately aspirated. The flask was then placed in the incubator for 2 min or until the cells were starting to detach from the surface after tapping the flask. 8 ml of trypsin neutralization solution was then added to the flask. The flask was washed with an additional 5 ml of trypsin neutralization solution. The collected cells were centrifuged at 200xg for 5 minutes to pellet the cells. The supernatant was then aspirated and resuspended in 5 ml of Bovine Smooth Muscle Cell Growth Medum. The cells were counted using a hemocytometer and a trypan blue exclusion assay. 5×10^5 cells were seeded in T-75 flasks and expanded as previously described.

4.3.3 Culturing cells for cell studies

Elastomeric films

Elastomeric films were formed directly within the wells of 96 well plates (Costar) for cell attachment/proliferation studies. 1.5 µl of ASCP were spread on each well and the plate was exposed to UV radiation (10 mW/cm^2) for 10 minutes as previously described. A concentration of 1 pmol GRGDS or RPDS/cm^2 and 0.5 pmol PEG spacer and GRGDS or RPDS/cm^2 was added for modified films. Base etching conditions were as previously described (1 hr, 0.5 M NaOH). For SEM and immunofluorescence measurements, thin elastomeric films were prepared between two glass slides. Plates and films were then stored in a vacuum oven for several days to evaporate the solvent. The plates and films were UV sterilized in a laminar flow hood for 30 minutes then incubated with media overnight. The media was aspirated and cells were seeded at a cell density of 10 000 cells/well with fresh media for up to 7 days, with media changed every 2 to 3 days.

Porous scaffolds

Porous scaffolds were sterilized by immersion in 70% ethanol for 30 minutes followed by washing with sterile PBS. Scaffolds were then placed in a 24 well plate with transwell inserts (Corning) and incubated in bovine smooth muscle growth medium overnight. 10^6 SMC were seeded on the porous side of the scaffold and cultured for 1 and 7 days.

4.3.4 Cellular response assays

Cell attachment and proliferation

Cell attachment and proliferation was measured after 1 and 7 days in culture. The WST-1 assay and UV spectrophotometer (μQuant microplate reader - BioTek Instruments, Inc.) at a wavelength of 450 nm and reference wavelength of 690 nm was used. Measurements were taken after a 2 hour incubation period. A minimum of 7 samples were measured for each surface, and statistical analysis was done by 2-sample T-test with Minitab 15 statistical software. Results were corrected using a Bonferroni correction and a significance of $p<0.05$. Tissue cultured polystyrene (TCPS) was used as the control surface. The WST-1 assay is a colorimetric assay based on the cleavage of the tetrazolium salt WST-1 (4-[3-(4-Iodophenyl)-2-(4-nitrophenyl)-2H-5-tetrazolio]-1,3-benzene disulfonate) to fomazan by the cellular enzymes mitochondrial dehydrogenases. The amount of formazan dye formed is directly correlated to the number of metabolically active cells in culture.

Immunofluorescence and phenotype

After 4 days in culture, medium was aspirated from films and cells fixed with 3.7% paraformaldehyde in PBS for 15 minutes at room temperature. The films were then washed 3 times with PBS containing 100 mM glycine. Cells were permeabilized with

0.1% Triton X-100 in PBS for 1 to 4 minutes and then rinsed with PBS. Nonspecific binding was blocked with 5% FBS in PBS for 30 minutes. The films were then incubated with the primary antibodies in 5% FBS in PBS overnight. The primary antibody monoclonal anti-caldesmon (smooth), clone hHCD (mouse IgG1 isotype) was diluted 500x, while monoclonal anti-α-Smooth Muscle Actin (mouse IgG2a isotype) clone 1A4 FITC conjugate was diluted 250x. Subsequently, the films were washed with PBS 3 times for 5 minutes each and incubated with the secondary antibody (only for anti-caldesmon samples) in 5% FBS in PBS for 1 hour. The secondary antibody, Anti-Mouse IgG (whole molecule) TRITC conjugate was diluted 200 times. The films were washed with PBS and mounted with Vectashield™ aqueous mounting medium with 4,6-diamidino-2-phenylindole (DAPI), coverslipped and sealed with nail polish.

Scaffolds at 7 days were fixed in 3.7% paraformaldehyde overnight, washed in PBS and soaked in 70% ethanol before being paraffin embedded and sectioned by the Queen's University Pathology Department. After de-paraffinizing with toluene (2 washes for 2 minutes each), re-hydration by a series of graded alcohol solutions and finally PBS, antigens were retrieved by sodium citrate. 10 mM sodium citrate was preheated to 80℃ and section slides placed in this solution for 30 min. After allowing slides to cool to room temperature, the sections were rinsed with PBS, permeabilized and stained as previously described.

Films and scaffold sections were imaged using an Axioplan 2 Imaging fluorescent microscope equipped with an Axiocam high resolution monochrome camera to capture images. Images were analyzed using Axiovision LE version 4.6 and ImageJ software.

SEM and Cell Attachment

Films were examined by SEM after 1 and 7 days in culture. Similar to the immunofluorescence samples, films were fixed with 3.7% paraformaldehyde for approximately 6 hrs, washed with PBS then soaked in 70% ethanol. The samples were then dehydrated through a series of graded alcohol solutions, chemically dried with hexamethyldisilazane and air-dried overnight. Dry cellular constructs were sputter coated with gold and observed under the SEM at an accelerating voltage of 10 kV. The control surface for both SEM and immunofluorescence studies were glass coverslides.

4.4 Biomimetic Design

4.4.1 Materials

Poly(ethylene glycol) (PEG) Mn 4000, barium chloride and 0.1 M iodine solution was purchased from Sigma Aldrich (Canada).

4.4.2 Acrylating PEG 4000

Terminal hydroxyl groups of PEG were acrylated in a similar manner as SCP. A 1.2 molar excess of ACl per PEG hydroxyl was utilized. The resulting PEG-diacrylate (PEGDA) was purified and collected by dissolving in a minimum amount of chloroform and adding dropwise to excess anhydrous diethyl ether. PEGDA was stored at 4℃ until use.

4.4.3 Adding PEGDA to elastomer

A monolayer of PEGDA was attached to the elastomer by UV crosslinking. A 20% (w/v) PEGDA solution in ethyl acetate containing 0.3% DMPA was added after exposing the ASCP layer to UV light (10 mW/cm^2) for 30 seconds. The whole construct was then exposed to UV light (10 mW/cm^2) for 10 minutes.

Measurement of the sol content of the PEGDA in water, SEM imaging and selective dying were used to confirm attachment of the PEGDA layer to the elastomer as a thin film. SEM imaging was used to confirm attachment of the PEGDA layer to the scaffold. Staining of the PEGDA layer was conducted with a 5% barium chloride and 0.1 M iodine solution combined at a 5:2 ratio[101]. Specific staining of the PEG is from the formation of a barium iodide complex with the PEG molecules.

4.4.4 Tubular construct

A 5 mm straight glass tube was filled the paraffin/ASCP emulsion mixture (prepared as before) and then fitted with rubber septa on either end. The septa had holes cut out in the middle. A glass mandrel with a diameter of 2.5 mm coated in paraffin was then inserted into the septa from end to end. This construct was exposed to UV light (10 mW/cm^2) for 30 seconds and the mandrel removed. PEGDA (as above) was then poured down the lumen of the construct and proper coating was ensured. The construct was then placed back under UV light (10 mW/cm^2) for 20 minutes with frequent turning to ensure even crosslinking. After drying overnight, the glass tube was carefully removed and paraffin removed with hexane as before. SEM imaging was done to visualize the resulting construct.

Chapter 5
Results and Discussion – Porogen and Scaffold Characterization

5.1 ASCP Synthesis

The ASCP platform for making biodegradable elastomers possesses many criteria, such as ease of manufacture and appropriate mechanical properties, making it an interesting candidate for small diameter blood vessel tissue engineering. To further investigate the feasibility of elastomers prepared using ASCPs as a scaffolding material for this application, three molecular weights of ASCP were prepared: 7800, 4500 and 1800 Da. Elastomers prepared with each ASCP would result in different crosslink densities. The 7800 Da ASCP elastomer (ELAS 7800) would have a lower crosslink density versus the 1800 Da ASCP elastomer (ELAS 1800). The crosslink density is proportional to the end group concentration.

Using the peak integrations of the 1800 Da SCP ^{1}H NMR spectrum (Figure 10) and equation 4 the M_n was calculated to be 1967 Da. The degree of acrylation of the resulting 1800 Da ASCP was calculated using the peak integrations of the end groups (Figure 11) and equation 5. The M_n and degree of acrylation for the 7800 and 4500 Da ASCPs were calculated in a similar fashion and from Table 6 it is evident that there was successful acrylation regardless of molecular weight. There was also a high degree of crosslinking as all prepared elastomers had low sol contents. The sol content of an elastomer is a measurement of crosslinking effectiveness. The sol is any ASCP that did not become incorporated into the network during the photo-crosslinking reaction. As

such, this portion would be washed out by THF or any organic solvent. The elastomer, on the other hand, would swell, but not dissolve in the solvent since it is crosslinked.

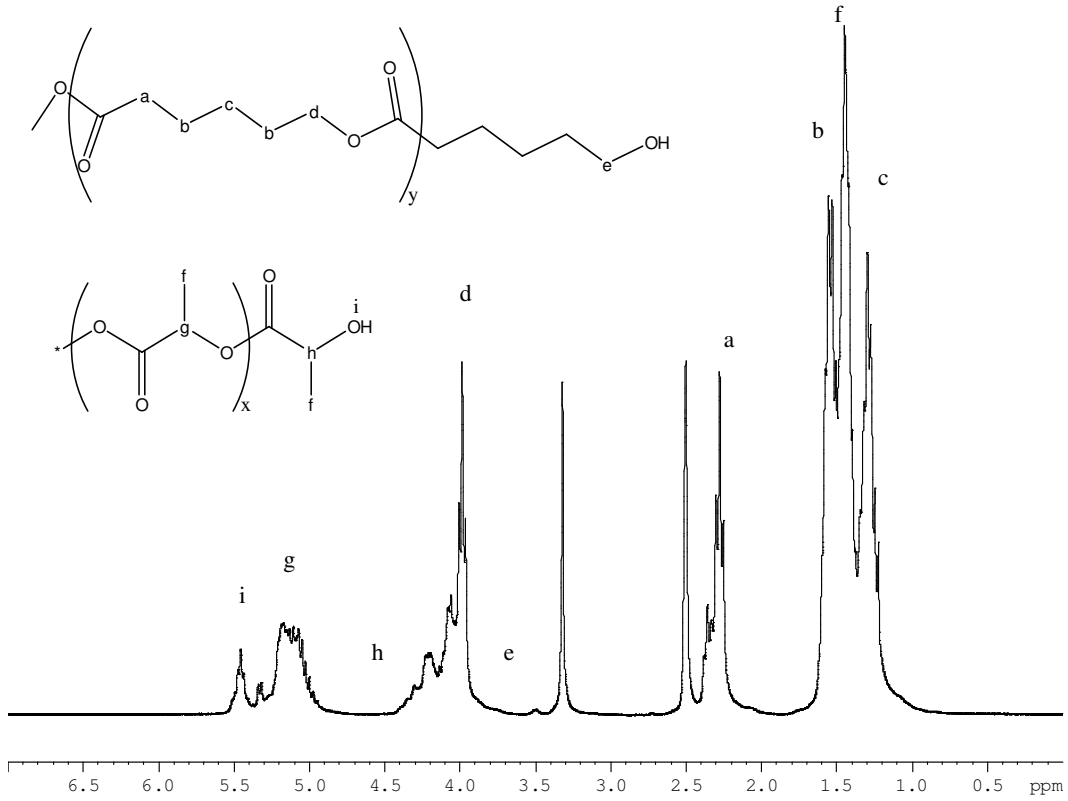

Peak	Integration
i (DLLA endgroup)	0.803
g (DLLA)	3.356
a (CL)	4.559

Figure 10: ^{1}H NMR spectrum and resulting integration of SCP 1800

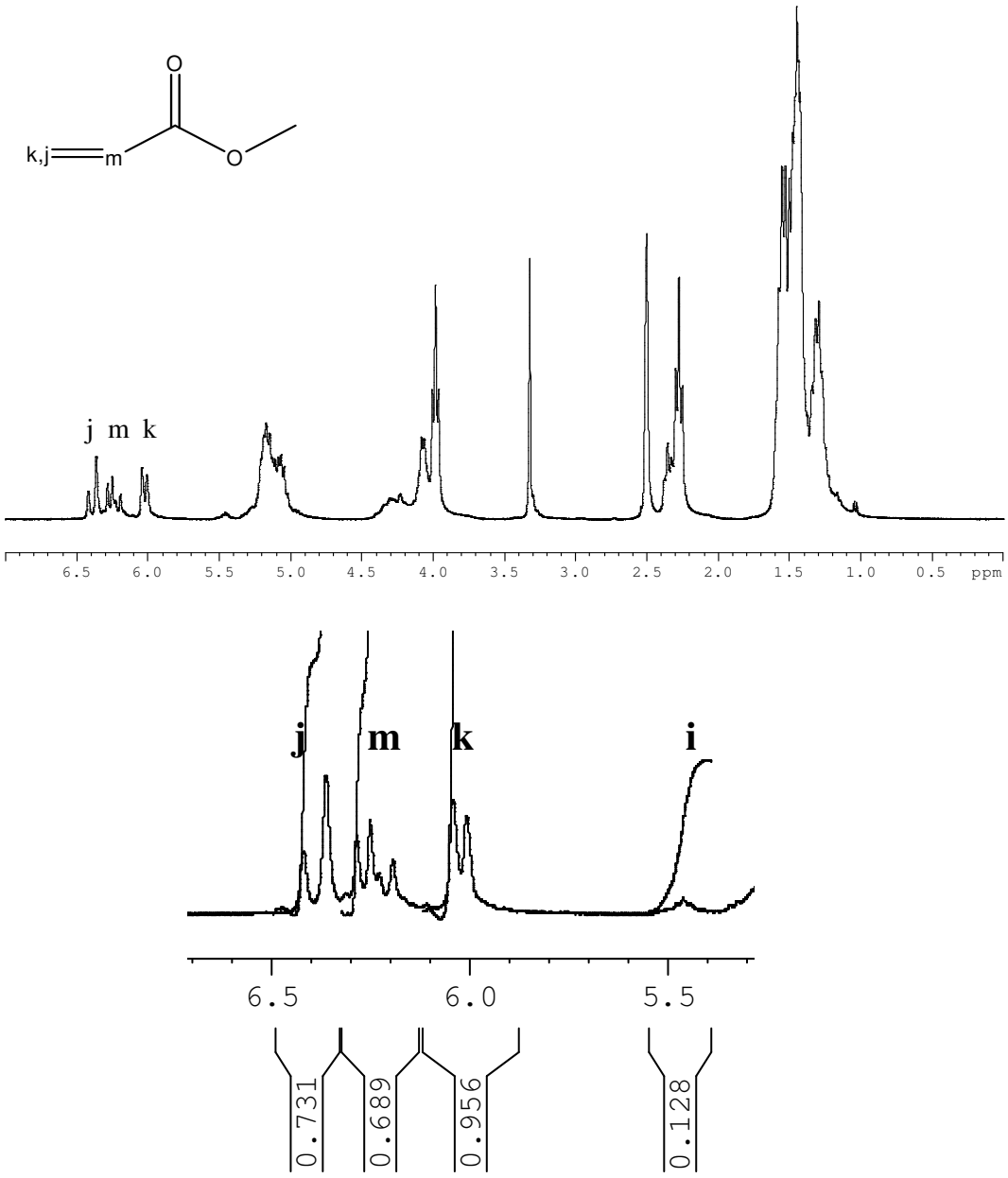

Figure 11: ^{1}H NMR spectrum and resulting integrations of ASCP 1800

Table 6: ASCP properties of various molecular weights

Target SCP molecular weight (M_n)	SCP M_n from NMR end group analysis	Degree of acrylation (%)	Elastomer sol content (%)
7800	8294	98.8	5.42 ± 2.75
4500	4528	98.2	5.76 ± 1.04
1800	1967	88.2	5.82 ± 0.95

5.2 Porogen Selection

5.2.1 Alginate

Alginate was considered a potential porogen because it can be easily made into microbeads and these microbeads are readily dissolved in an aqueous medium. Alginate is a polysaccharide isolated from brown algae. It is composed of D-mannuronic and L-guluronic acid residues, and gels in the presence of bivalent cations such as Ca^{2+} and Ba^{2+}. The most commonly used bivalent cation is Ca^{2+}. The resulting hydrogel is only physically crosslinked. Carboxylate groups on the guluronate chains are ionically bound to the bivalent cation, zipping guluronate chains together, and the crosslink point is further stabilized by hydrogen bonding. Chelating agents, such as sodium citrate, will disrupt the hydrogel because Ca^{2+} has a greater affinity for sodium citrate compared to alginate [102]. Removal of alginate microbeads with sodium citrate may be advantageous since a solution of sodium citrate is slightly basic. Thus, the sodium citrate solution may potentially hydrolyze the surface of the ASCP scaffold and increase the hydrophilicity of the ASCP surface.

Spherical microbeads can be made with a variety of techniques, resulting in a wide range of diameter sizes [103-105]. For this study, the electrostatics technique was chosen since it has been previously shown to readily produce microbeads < 100 μm in

average diameter [98]. In the electrostatics technique, a polymer solution is extruded through a needle which is maintained within an applied electric field. Microbeads are formed when the solution droplets are in contact with the collection solution. For alginate microbeads this solution would be a calcium chloride solution. The electric field induces a charge on the droplet surface. Mutual charge repulsion results in an outwardly directed force acting downwards on the forming droplet. These electrostatic forces pull the droplet from the needle tip at a lower mass, resulting in smaller droplets. Without the electrostatic forces, the droplet would only drop from the needle when its mass is large enough to escape the surface tension at the needle-droplet interface [106].

Alginate microbead diameter was controlled by varying voltage, with a minimum diameter of 60 μm obtained between 10 and 11 kV (Figure 12). Nevertheless, as voltage increased, the shape of the resulting porogens became deformed and irregular as shown in Figure 12. The shape of the alginate microbead is important to ensure maximum surface area contact and regular pore formation within the resulting elastomer scaffold. Considering the shape and size of the resulting alginate microbeads, a diameter of 60 μm was chosen as the preferred porogen size. From Table 5 and previous studies as discussed in Chapter 2, pore sizes of 50 – 100 μm were found to be optimal for organized fibrous tissue generation and used in previous vascular graft designs.

Using alginate as a porogen proved to be fairly difficult in creating a porous scaffold. Mixing between ASCP and alginate was inconsistent, most likely due to the nature of the materials, with ASCP/ethyl acetate being organic, while alginate is aqueous. This resulted in low porosities and inconsistent pore structure. Scaffolds made with 85 wt% alginate only resulted in a porosity of 49.7%. SEM images of these scaffolds (Figure 13)

also revealed that there was very little interconnectivity between pores. From Figure 13 it is evident that the sodium citrate wash removed all of the alginate. This was also confirmed with a phenol/sulphuric acid assay (Figure 14). Regardless of alginate concentration in the scaffold, practically all the alginate was removed by the sodium citrate wash; 98 ± 2% of the alginate was removed by this method. The amount of alginate removed was considered sufficient as residual alginate would not have a toxic effect on cells [103]. However, because of the lack of repeatable results and low porosities, an alternative porogen was tested.

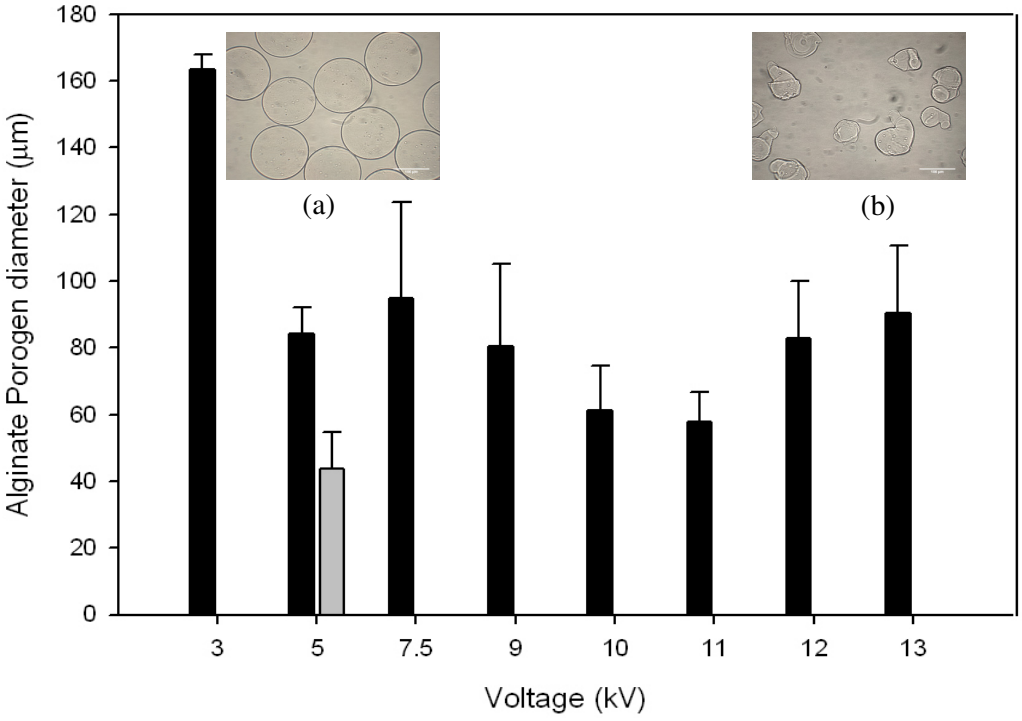

Figure 12: Effect of voltage on alginate microbead diameter. Two populations of microbeads were observed at 5 kV, which disappeared as the voltage increased. Inserts show microbead shape at (a) 3 kV and (b) 13 kV.

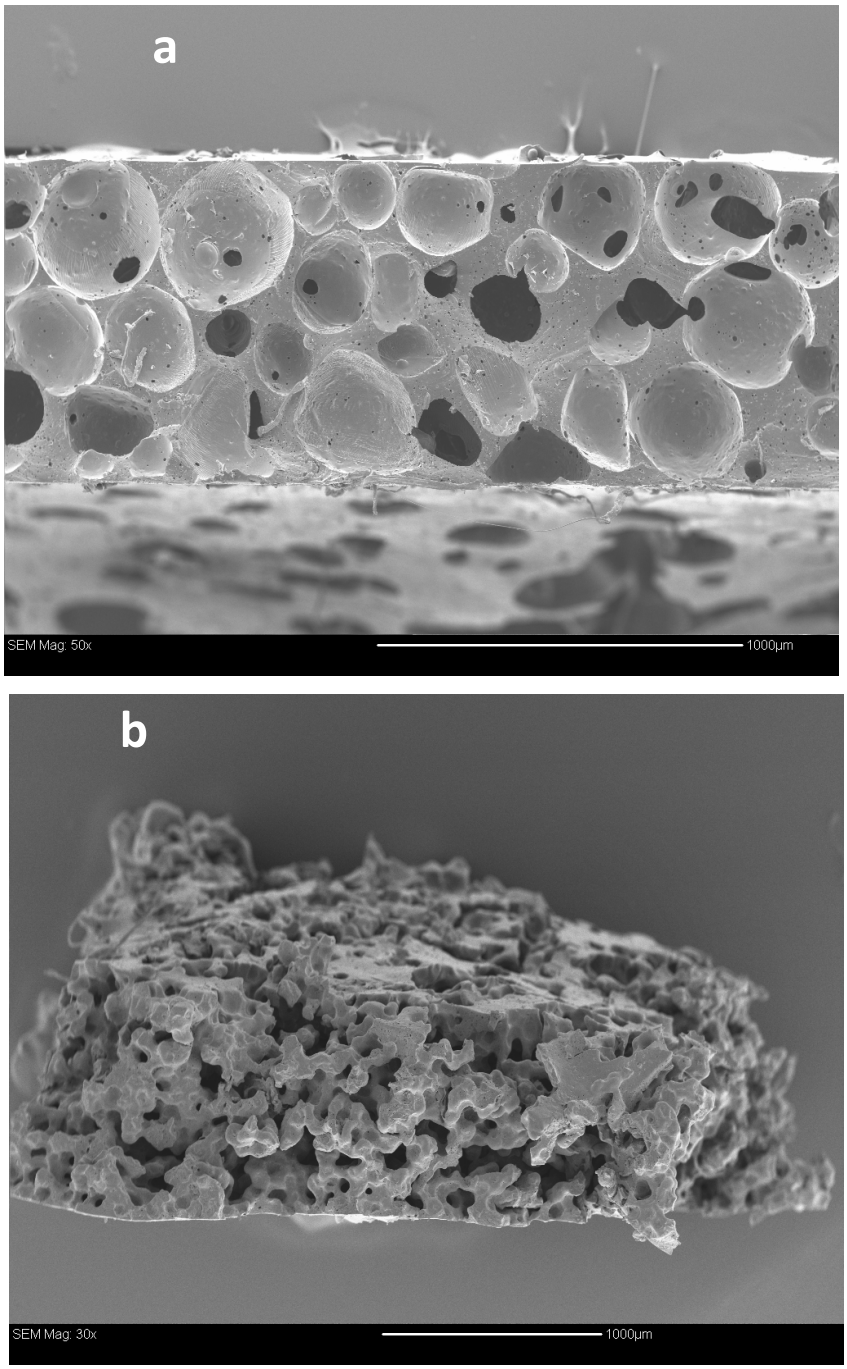

Figure 13: Cross section SEM images of scaffolds using alginate as porogen. Both (a) and (b) were made under similar conditions. The difference in structure is due to inconsistent mixing between the alginate and ASCP.

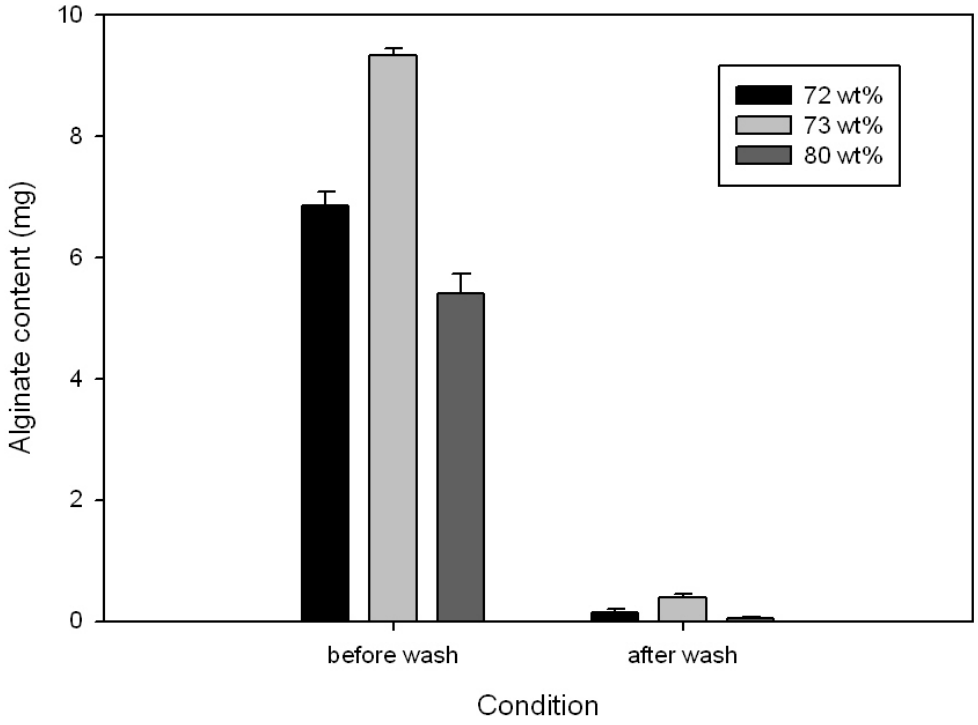

Figure 14: Alginate content removed by 500 mM sodium citrate wash from scaffolds with various weight percents of alginate. There was an average removal rate of 98 ± 2%.

5.2.2 Paraffin

Following the inconsistent results from scaffolds made with alginate microbeads, paraffin microbeads were tested. Ma *et al*. [71] established a method of creating highly porous scaffolds (> 90% porosity) with pore sizes of approximately 100 µm. Paraffin is a good porogen since it is readily available, creating microbeads is quick, the process does not require sophisticated equipment and the paraffin can be removed with hexane or other volatile organic solvents that do not leave toxic residues. Using a modified version of Ma's method, spherical paraffin porogens were fabricated with a mean diameter of 84.3 µm ± 45.4 µm. As seen in Figure 15, there was a wide range of diameters created. This

range in porogen diameters may be beneficial in providing better packing and interconnectivity between pores.

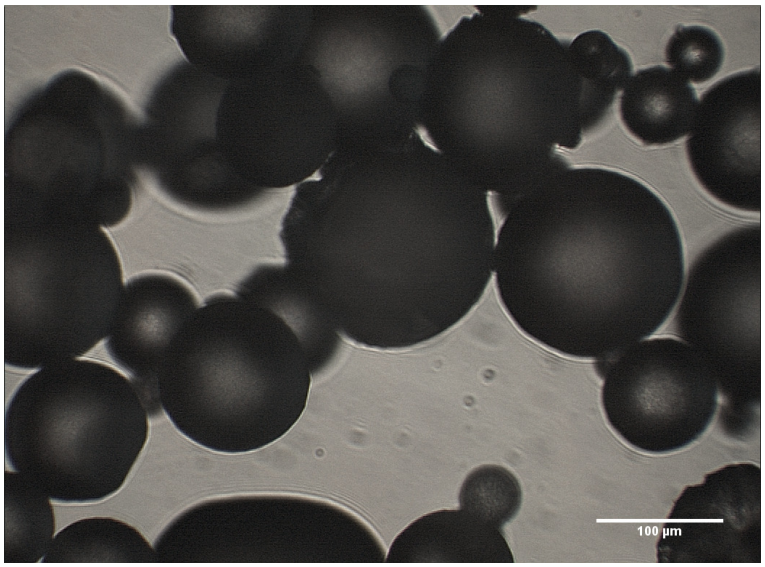

Figure 15: Light microscope image of paraffin microbeads

Working with paraffin was much easier than alginate. The two phases consistently mixed well and resulted in similarly structured scaffolds regardless of paraffin microbead batch (Figure 16). Porosity was also significantly higher. Scaffolds made with 77 wt% paraffin resulted in a scaffold porosity of 84 ± 1.5% and an average pore size of 104 ± 31 µm. The hexane or THF wash was effective in removing all paraffin porogens. No residual paraffin can be detected from the SEM images in Figure 16.

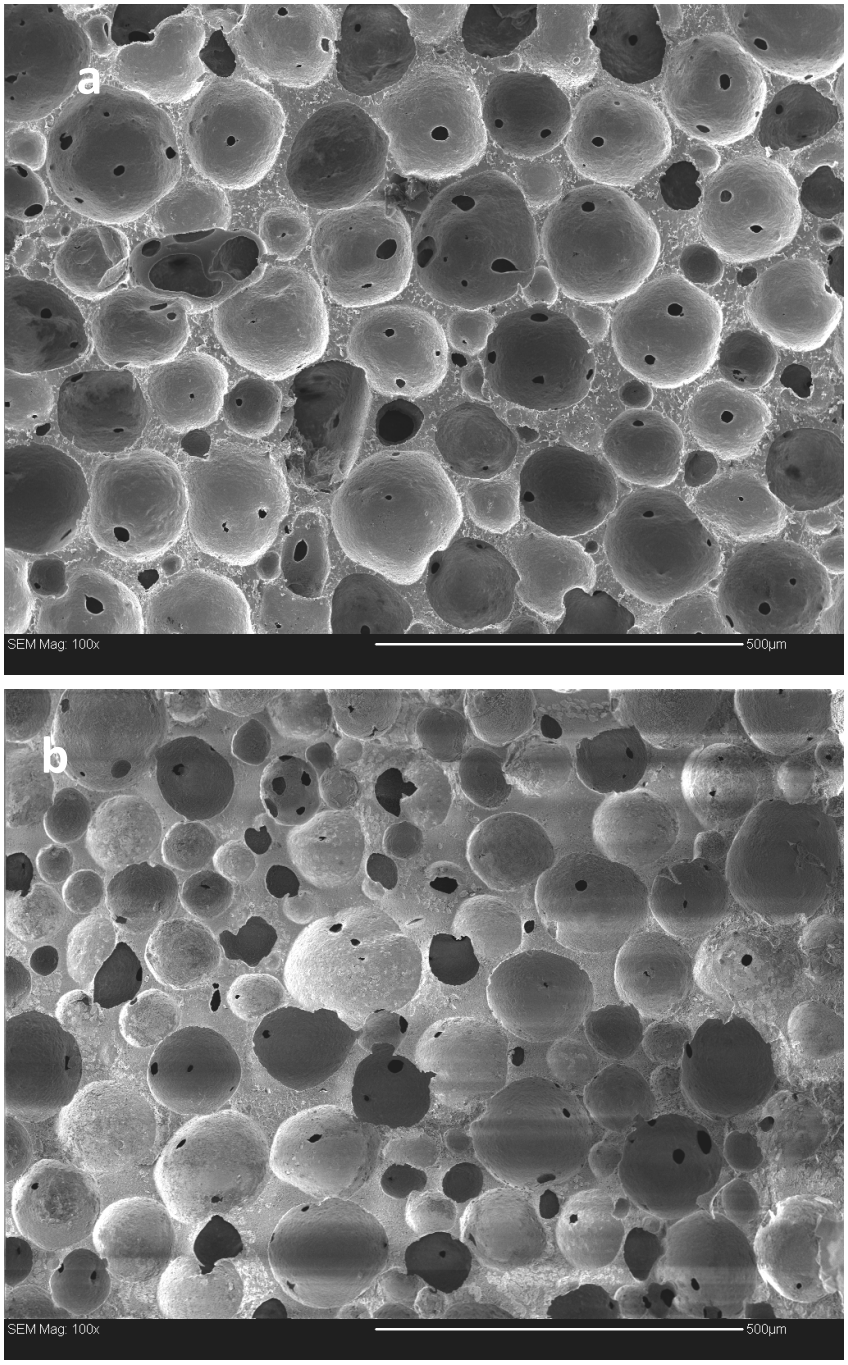

Figure 16: Cross section SEM images of ASCP scaffolds using paraffin as porogen Both (a) and (b) were made under similar conditions. (a) is with ELAS 4500 and (b) is with ELAS 1800.

5.2.3 Increasing Porosity with a Water Emulsion

Although the porosity of the paraffin-made scaffold was high, it was investigated whether a scaffold with a porosity of 90% could be manufactured. A 90% porosity is ideal for sufficient nutrient and waste transport [66]. To achieve this goal, using a water emulsion, along with the paraffin microbeads and different M_n ASCP was examined. Emulsions of water have previously been used in creating scaffolds [107-109]. Nevertheless, the systems used in those scaffolds were quite different than the tested system. Busby *et al.* prepared PCL scaffolds using acrylated macromonomers of PCL diol (M_n=2000) that were thermally copolymerized with styrene or methylmethacrylate. Moreover, the water content of the resulting emulsion was greater than 74% [109]. The maximum amount of water that could be incorporated into the emulsion in this work was 67 wt%. Adding more water interfered with crosslinking and an elastomer did not form.

The difference between these two systems is that the latter is UV crosslinked.To have effective crosslinking by UV radiation, there must not be any obstructions to the UV light path. Opaque materials will disperse and absorb the radiation, thus preventing endgroups farther away from the UV source from becoming crosslinked. Thermal free radical copolymerization, on the other hand provides uniform polymerization as the whole structure can be heated evenly.

Nevertheless, scaffolds made from the 67 wt% water/ASCP emulsion with 77 wt% paraffin resulted in a porosity of 90.5 ± 1.8% (Figure 17 – 1). The scaffolds prepared using the emulsion alone had a porosity of 36.9 ± 5.9% and a pore size of 25 ± 13 μm (Figure 17 – 3). Pore size was similar regardless of the addition of the water emulsion. From the SEM images a pore size of 106 ± 29 μm was measured for scaffolds with the water/ASCP emulsion and paraffin microbeads and 104 ± 31 μm for scaffolds with

paraffin microbeads only. Comparing Figures 17 – 1 and 17 – 2, the addition of the emulsion increased porosity by increasing interconnectivity between pores and creating micropores in the walls between pores (Figure 17 – 1b).

5.2.4 Influence of ASCP M_n on Water Content in Emulsions

The amount of water that could be incorporated into the emulsion appeared to be ASCP M_n specific. Scaffolds would not form using the same procedure with ASCP of M_n 1800 Da (ELAS 1800). When ASCP 1800 and water were vigorously mixed a significant portion of the ASCP 1800 was found in the water phase. A ^{1}H NMR spectrum of the water soluble ASCP (Figure 18) revealed that the water soluble fraction had all the same peaks as the initial polymer and that the M_n was 2020 Da. Thus, all ASCP molecules below M_n 2020 Da were being dissolved into the water phase and not enough end groups were available to crosslink in the organic phase. With this in mind, all ELAS 1800 scaffolds were made with paraffin microbeads only. Although, a porosity of 90% is ideal, for this study 85% porosity was deemed sufficient. As shown in Figure 20, this difference in porosity does not affect mechanical properties.

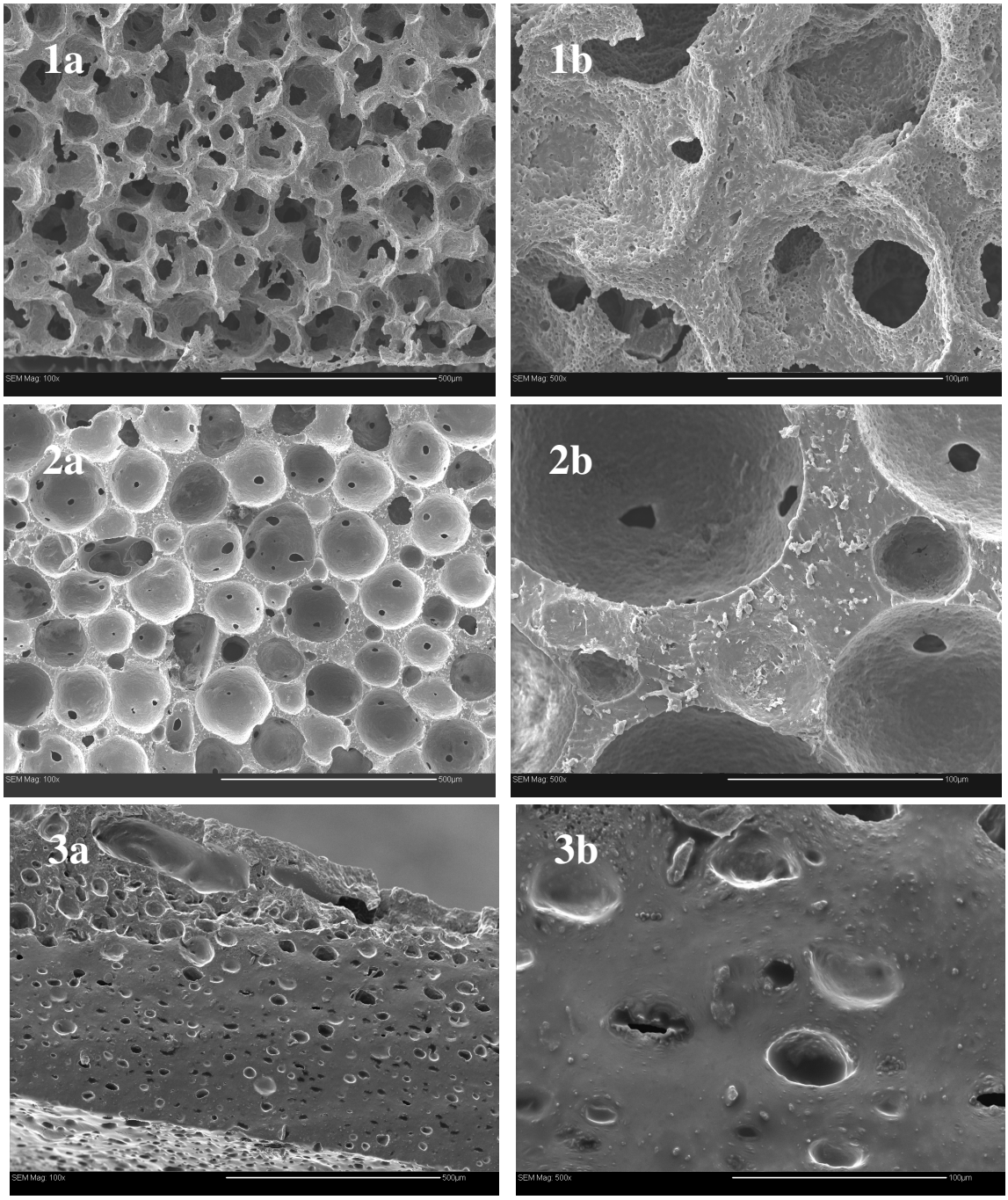

Figure 17: Effect of emulsion addition on scaffold structure. 1a and 1b are scaffold with the emulsion added, 2a and 2b are paraffin only scaffolds and 3a and 3b are emulsion only scaffolds. In 1 and 2, 77 wt% paraffin was added. ELAS 4500 was used in all cases. Scale bar in (a) 500 μm (b) 100 μm.

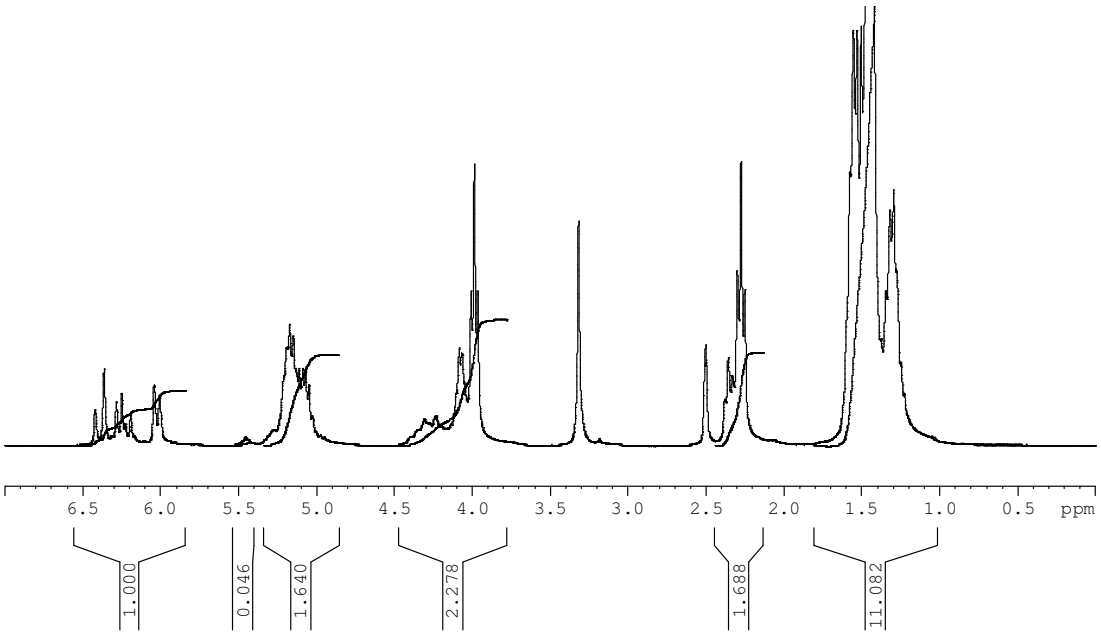

Figure 18: ^{1}H NMR spectrum of water-soluble ASCP 1800 after vigorous mixing with double distilled water.

5.3 Scaffold Mechanical Properties

5.3.1 Effect of Porosity

The porous nature of the scaffold will inherently reduce the mechanical properties of the structure compared to a nonporous slab. This is clearly illustrated in Figure 19; a scaffold with 37% porosity possessed significantly reduced tensile modulus and tensile strength. Increasing the porosity to beyond 80% continues to decrease tensile modulus and tensile strength, but only slightly. Ultimate strain is only mildly affected. When an elastomeric foam is stretched in tension there is initial cell (pore) wall bending giving the foam linear elasticity, at larger strains the cell (pore) walls align and the scaffold behaves as a nonporous entity [110]. The stress – strain curves are similar for both the nonporous slab and porous scaffold, as shown in Figure 20. Moreover, the effect of

porosity on mechanical properties was similar regardless of M_n of the ASCP prepolymer as shown in Figure 21.

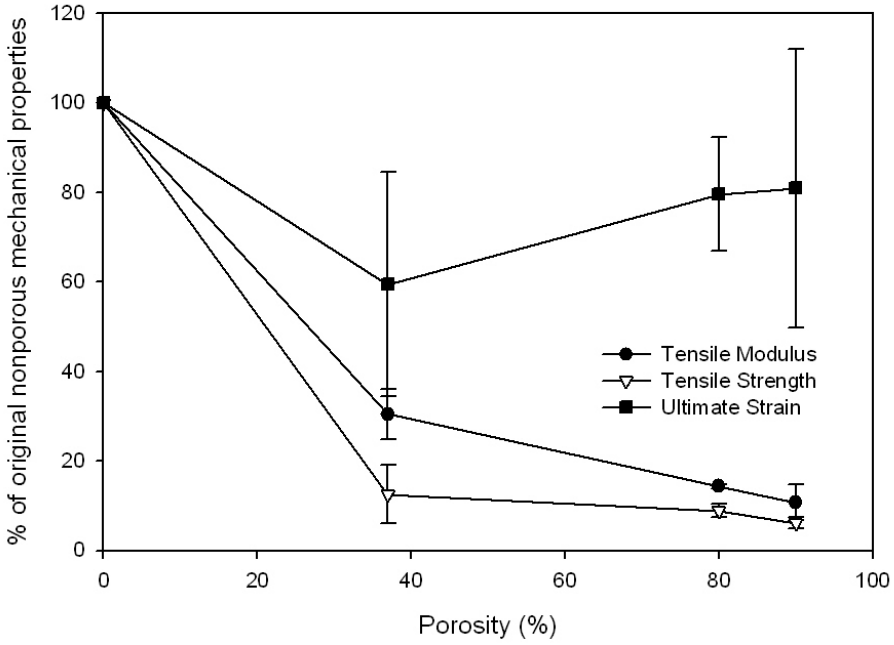

Figure 19: Effect of porosity on the scaffold mechanical properties. ELAS 4500 was used for all samples

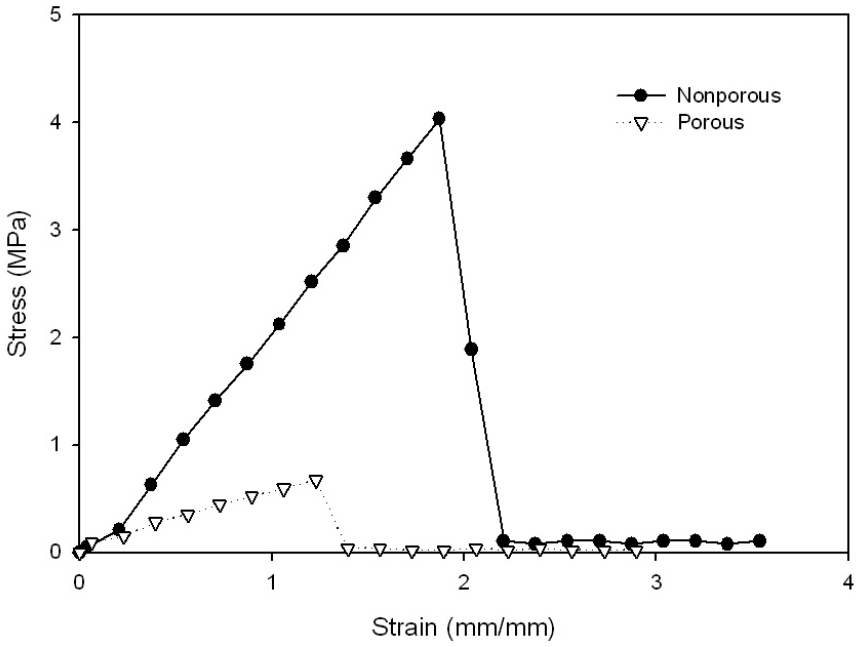

Figure 20: Typical stress - strain curve for ELAS 1800 in nonporous (circle) and 85 % porosity (inverted triangle) configuration.

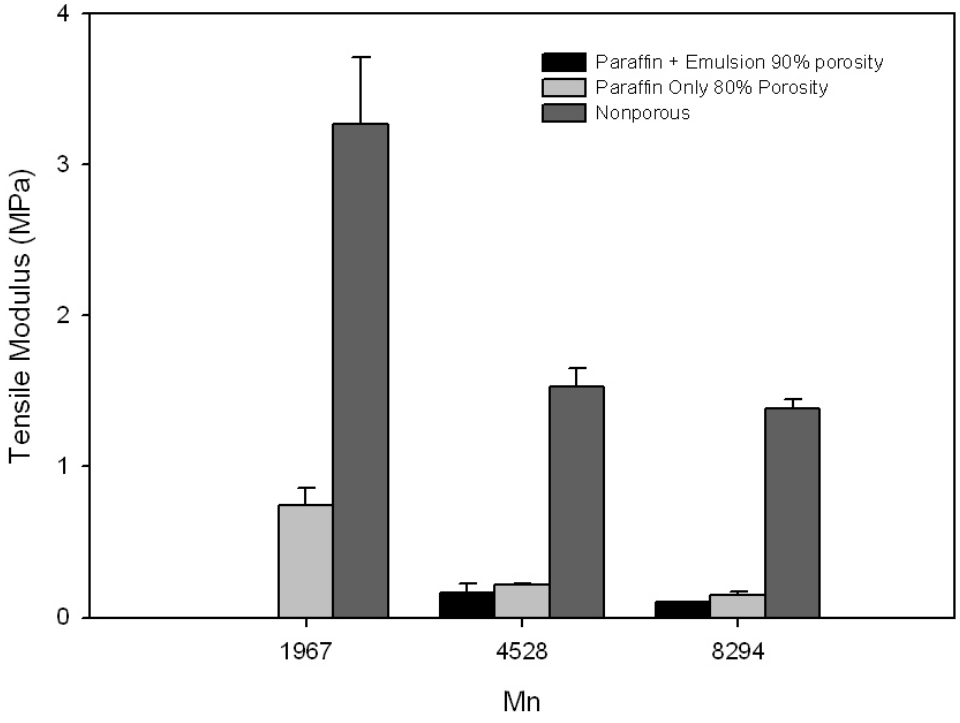

Figure 21: Effect of porosity and ASCP M_n on tensile modulus

5.3.2 Effect of elastomer crosslink density

Comparing mechanical properties of the nonporous and porous elastomers of various crosslink densities (Table 7), the trends are the same. Both tensile modulus and tensile strength decrease with decreasing crosslink densities, while ultimate strain increases. The reduction in mechanical properties from nonporous to porous elastomer is advantageous since it brings the scaffold mechanical properties very close to those of small diameter arteries. From Table 7 it is apparent that the scaffold with the closest mechanical properties is that prepared with ELAS 1800. As such, all cell response studies were conducted with ELAS 1800.

Table 7: Mechanical Properties of various arteries and elastomer scaffolds prepared of different crosslink densities (stat = static conditions, dyn = dynamic conditions, inc = modulus at given pressure)

Material	Tensile Modulus (MPa)	Tensile Strength (MPa)	Ultimate Strain (mm/mm)
Human Coronary Artery[111]	**$E_{(stat)}$: 0.62 $E_{(dyn)}$:0.97**	**1.40-11.14**	**0.45-0.99**
Canine Peripheral Vessels[74]	$E_{(stat)}$: 0.17 – 0.96 E inc $_{(100\ mmHg)}$: 0.4-0.8	n/a	n/a
Elastin[17]	0.1 – 0.6	n/a	n/a
Nonporous ELAS 7800	1.38 ± 0.07	4.39 ± 0.9	4.82 ± 0.26
Porous ELAS 7800	0.10 ± 0.004	0.40 ± 0.16	6.29 ± 1.33
Nonporous ELAS 4500	1.53 ± 0.12	5.22 ± 1.13	2.81 ± 0.31
Porous ELAS 4500	0.16 ± 0.06	0.32 ± 0.068	2.27 ± 0.004
Nonporous ELAS 1800	3.27 ± 0.44	8.26 ± 0.55	2.28 ± 0.23
Porous ELAS 1800	**0.74 ± 0.12**	**0.73 ± 0.14**	**1.12 ± 0.24**

5.3.3 *In Vitro* Degradation

The preferred tissue engineering paradigm for this scaffold is an *in vivo* approach (Figure 2b). The scaffold with its initial mechanical properties matched to the substituted artery would be directly placed in the vasculature without any conditioning within a bioreactor. Native SMCs from peripheral vessels would populate the scaffold while EPCs from the blood stream would populate a nonthrombogenic lumen. With this in mind, it is very important that the *in vitro* degradation of the scaffolds be tunable to the generation of ECM along with SMC infiltration, so that mechanical properties and integrity of the blood vessel is kept constant. To characterize the degradation of porous elastomer scaffolds, an *in vitro* degradation study in PBS, pH 7.4 at 37°C was performed.

Degradation by bulk hydrolysis of elastomers developed with ASCPs has been shown to be similar under *in vitro* and *in vivo* conditions [112]. In hydrolytic degradation there are two possible rate limiting steps, the rate of water penetration into the polymer and rate of bond cleavage. Most polyesters undergo bulk hydrolysis degradation, where the rate of water penetration is greater than the rate of bond cleavage. Thus, there is initial water penetration into amorphous regions and then random backbone cleavage. There is not appreciable mass loss but strength decreases with time. The backbone cleavage results in low molecular weight degradation products and thus increased internal osmotic activity and the device swells. The acid degradation products can lead to an autocatalytic hydrolysis effect, since there is a decrease in pH. Eventually, the device will fragment and there is appreciable mass loss. If the rate of bond cleavage is greater than the rate of water penetration, surface degradation will occur. The bulk properties of the device will not change, but mass loss will be consistent [42].

Both nonporous and porous ELAS 4500 and 1800 were tested and the effects of degradation time on several parameters are given in Figures 22 - 29. In both Figures 22 and 26 the results have been normalized with respect to values prior to degradation. It should be noted that mechanical properties for porous ELAS 4500 samples could not be tested after 45 days *in vitro*. Stresses beyond this time point were below the measurement ranges of the testing equipment.

Influence of Porosity

For both ELAS 4500 and ELAS 1800, porosity did not influence the type of degradation that occurred. In both cases, mass was relatively unchanged while mechanical properties were dramatically reduced. This is characteristic of hydrolytic bulk degradation and it has been previously shown that regardless of crosslink density, elastomers prepared from ASCP degrade in this fashion [96,112]. The porous scaffolds displayed a similar decline in tensile modulus and tensile strength over time as compared to the nonporous samples. Ultimate strain did not change as significantly as tensile modulus or tensile strength (Figures 22 and 26).

The decrease in tensile modulus and tensile strength are related to polymer backbone degradation. As the polymer backbone degrades, the number of effective elastic chains, n, in the network decreases. In rubber networks the tensile modulus and tensile strength are functions of n, reflected in the average molecular weight between crosslinks, as seen in equations 9 and 10 [113].

$$E = 3nRT$$
$$n = \frac{\rho}{\overline{M}_c} \qquad (9)$$
$$E = \frac{3\rho RT}{\overline{M}_c}$$

$$\sigma = nRT\left(\alpha - \frac{1}{\alpha^2}\right)$$
$$\alpha = \frac{L}{L_0} \qquad (10)$$
$$\sigma = \frac{3\rho RT}{\overline{M}_c}\left(\alpha - \frac{1}{\alpha^2}\right)$$

where $\overline{M}_c$ = average molecular weight between crosslinks

α= extension ratio

Thus, as the $\overline{M}_c$ increases, the tensile modulus and tensile strength will decrease. Ultimate strain however, is not a strong function of crosslink density. It is limited by the shortest distance between crosslinks. Unless there is a significant amount of backbone degradation, the ultimate strain will not change.

In terms of degradation rate, it appears that the porous ASCP elastomers degrade more slowly than the nonporous elastomers. From Figure 23, the T_g of the porous ELAS 4500 was constant throughout the degradation study unlike the T_g of the nonporous ELAS 4500 which was decreasing at a constant rate. The decrease in T_g indicates a decrease in $\overline{M}_c$. This phenomenon was not seen in ELAS 1800 scaffolds (Figure 27), and may be due to the time frame. As discussed below, ELAS 1800 appears to degrade more slowly than ELAS 4500. Thus, the 8 week time frame may have been too short to observe a significant amount of chain and crosslink breakage. Nevertheless, the difference in degradation rate is very slight. Sol content was similar regardless of configuration (Figures 24 and 28). Porous scaffolds degrade more slowly, since in this configuration there is a very high surface area to volume ratio. Thus, the acid degradation products (lactic acid and 6-hydroxycaproic acid) cannot accumulate locally

and produce an autocatalytic hydrolysis effect as in the slab configuration [114]. Wu and Ding also observed that highly porous scaffolds degraded slower than lower porosity counterparts [115].

Influence of Crosslink Density

Scaffolds composed of 4500 Da ASCP degraded faster than those created with 1800 Da ASCP. Thus, scaffolds with a lower crosslink density will degrade faster. The sol content for the ELAS 4500 scaffolds (Figure 24) was constantly increasing throughout the length of the study, while the sol content of the ELAS 1800 scaffolds (Figure 28) did not change and was relatively low at approximately 10 %. Therefore, the degradation products in the ELAS 4500 scaffolds resulted in a greater amount of the polymer chains being liberated from the network. Similarly, there was a greater increase in water absorption by the nonporous samples with ASCP 4500 (Figure 30). The decrease in crosslink density, and production of free degradation products, would accommodate more water absorption. The T_g of the ELAS 1800 samples (Figure 27) did not change during the course of the degradation study, which also is indicative of slow degradation. T_g is related to diffusivity. As T_g decreases, solute diffusivity within the polymer increases since the polymer chains are more mobile. Moreover, there is the additional osmotic pressure effect to draw water into the structure.

Nonetheless, the degradation did not affect the physical structure of the scaffolds for both crosslink densities as pore size and porosity remained relatively unchanged (Figures 25a and 29a). A minor decrease in porosity for ELAS 4500 scaffolds may be due to closed micropores caused by swelling from absorption of water (Figure 25b).

At 7 days the porous ELAS 1800 scaffolds had a reduction of approximately 40% in tensile modulus and tensile strength accompanied by an increase of 30% in ultimate strain. This was not seen in the nonporous ELAS 1800 (Figure 26). There was also no sign of this phenomenon in the porous ELAS 4500 scaffolds, although there was a very large standard deviation for all mechanical properties (Figure 22). This decrease only happened at 7 days. Afterwards, the tensile modulus and tensile strength remained unchanged for 4 weeks then slightly decreased at 8 weeks. The large reduction in tensile modulus and tensile strength at 7 days may be attributed to ELAS 1800 interactions with water creating a plasticizing effect. Further investigations should be done to fully understand this mechanism.

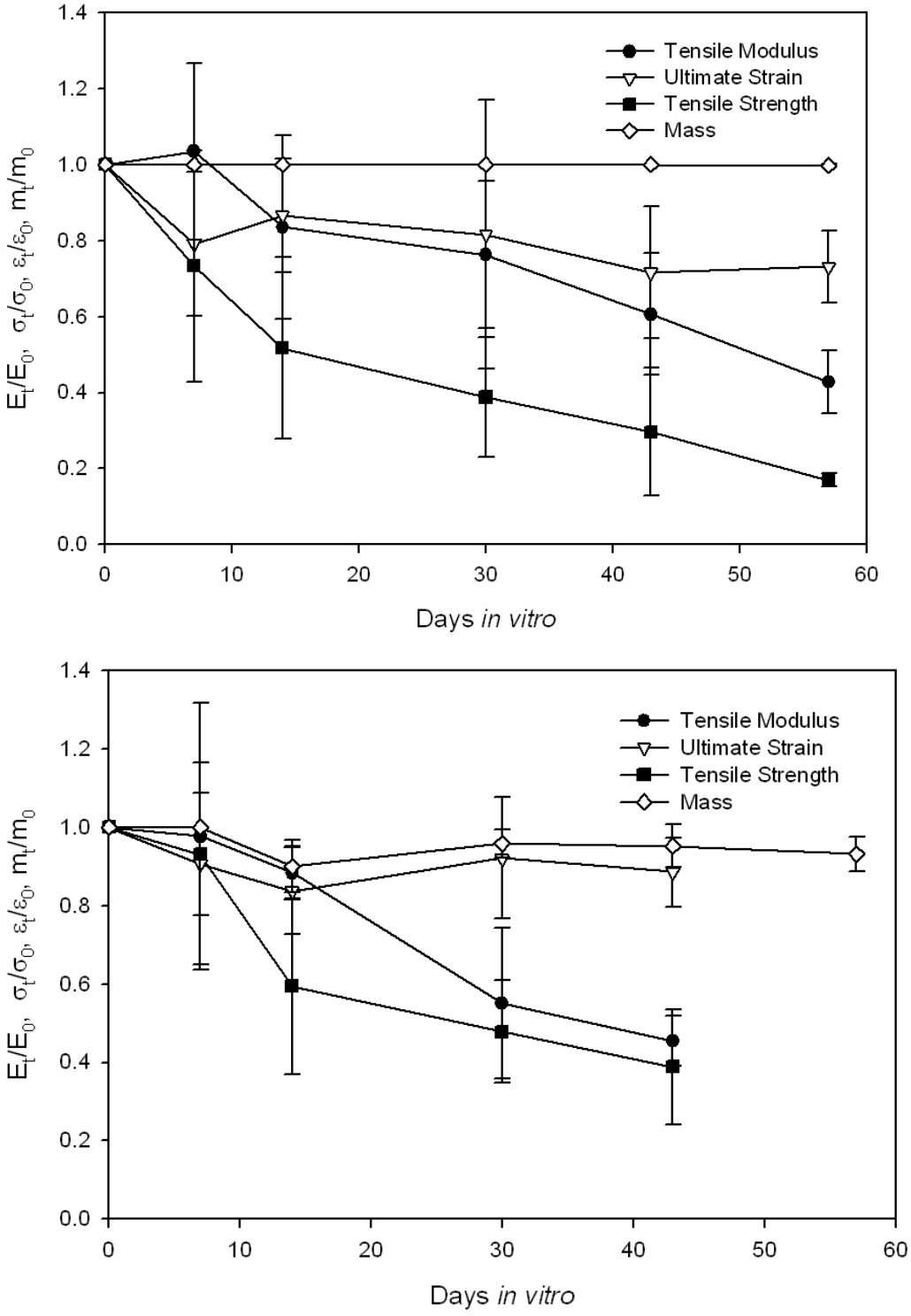

Figure 22: Change in mass and mechanical properties of nonporous (top) and porous (bottom) ELAS 4500 scaffolds during 8 weeks *in vitro* degradation in PBS pH 7.4, 37°C.

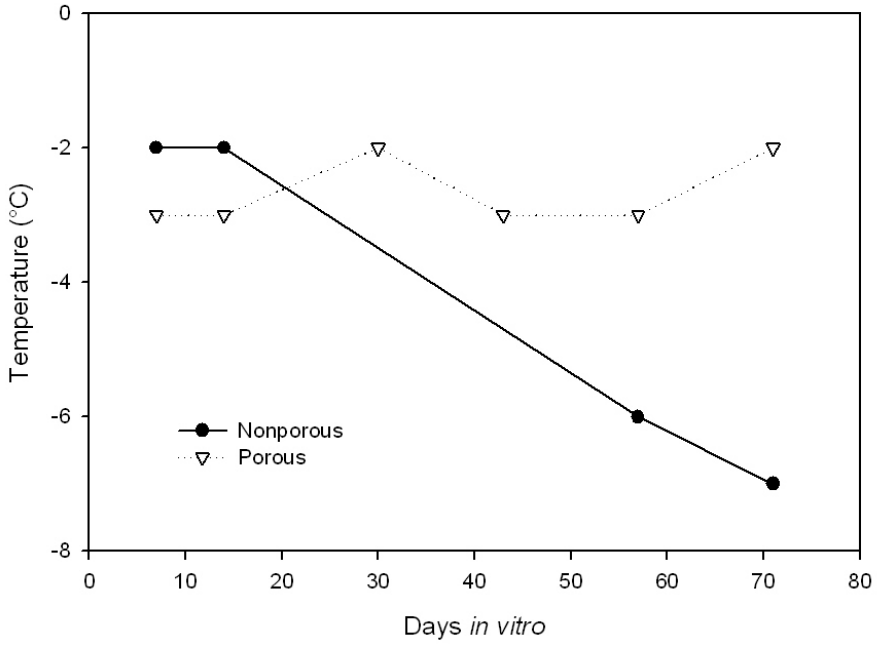

Figure 23: Glass transition temperature of ELAS 4500 scaffolds during *in vitro* degradation in PBS pH 7.4, 37°C.

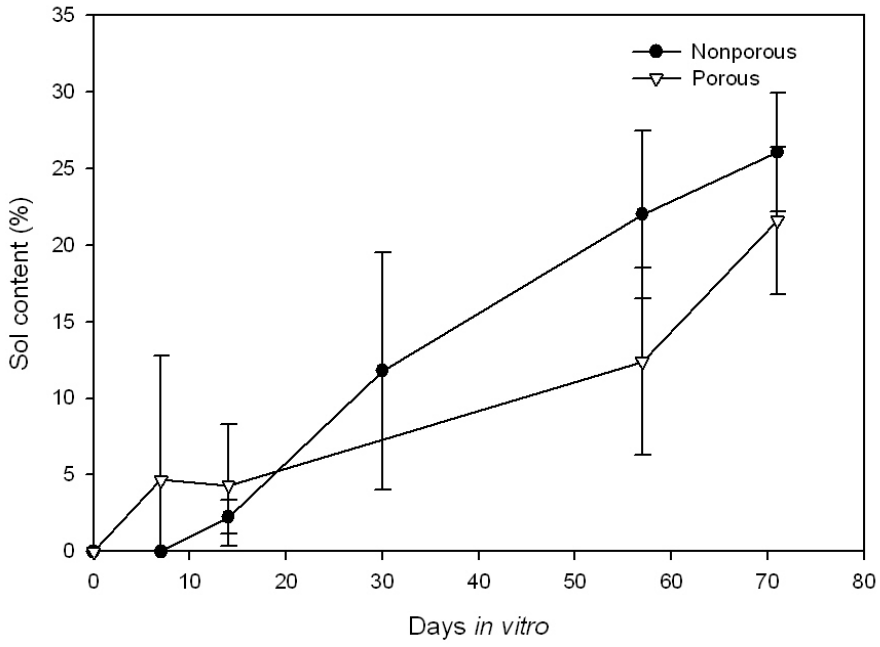

Figure 24: Sol content of ELAS 4500 scaffolds during *in vitro* degradation in PBS pH 7.4, 37°C.

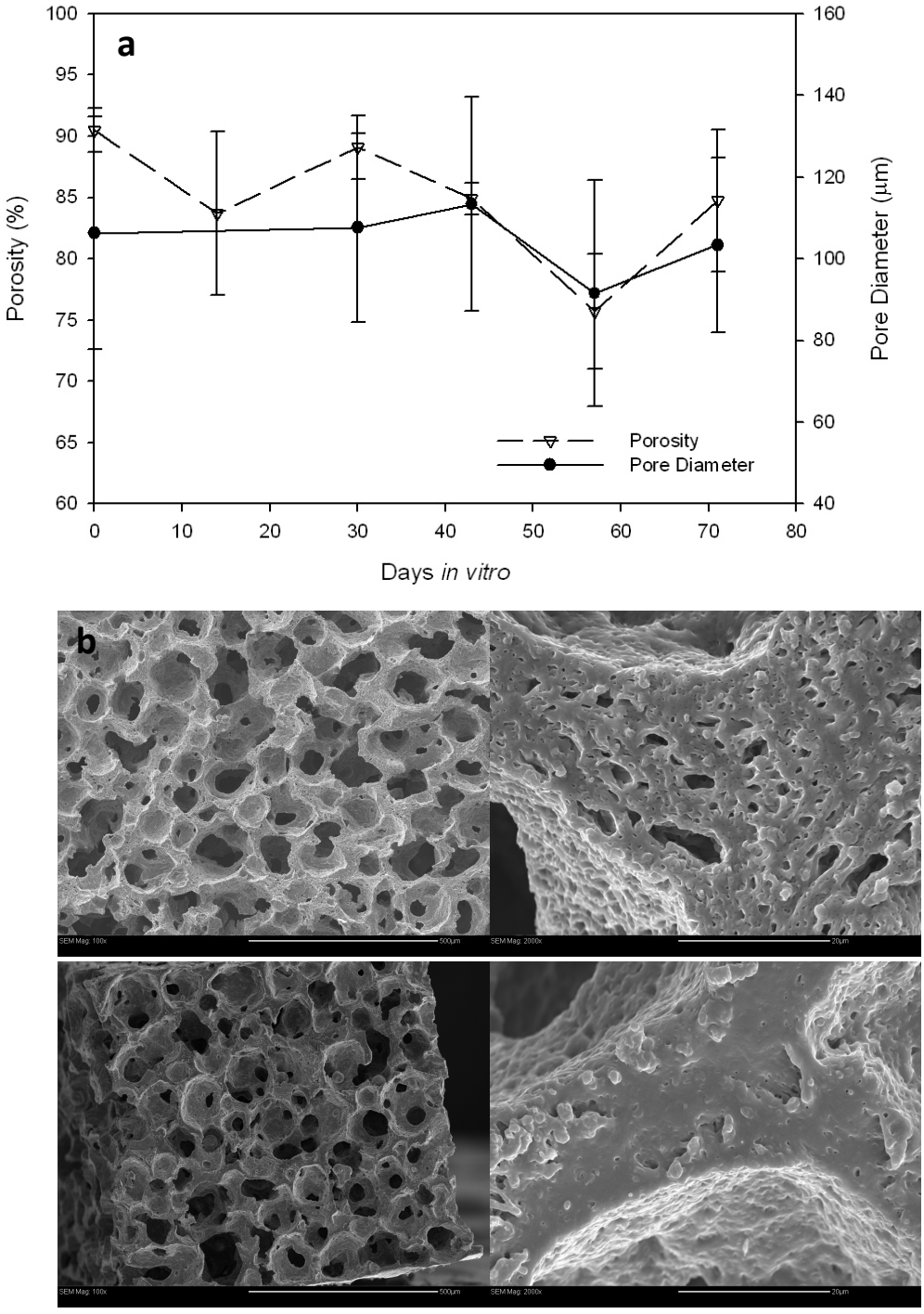

Figure 25: (a) Porosity and pore size of porous ELAS 4500 (b) SEM of porous ELAS 4500 before degradation (top) and after 8 weeks (bottom) *in vitro* degradation in PBS pH 7.4, 37°C. Right side images show closing of micropores after 8 weeks. Scale bar in left 500 µm, right 20 µm.

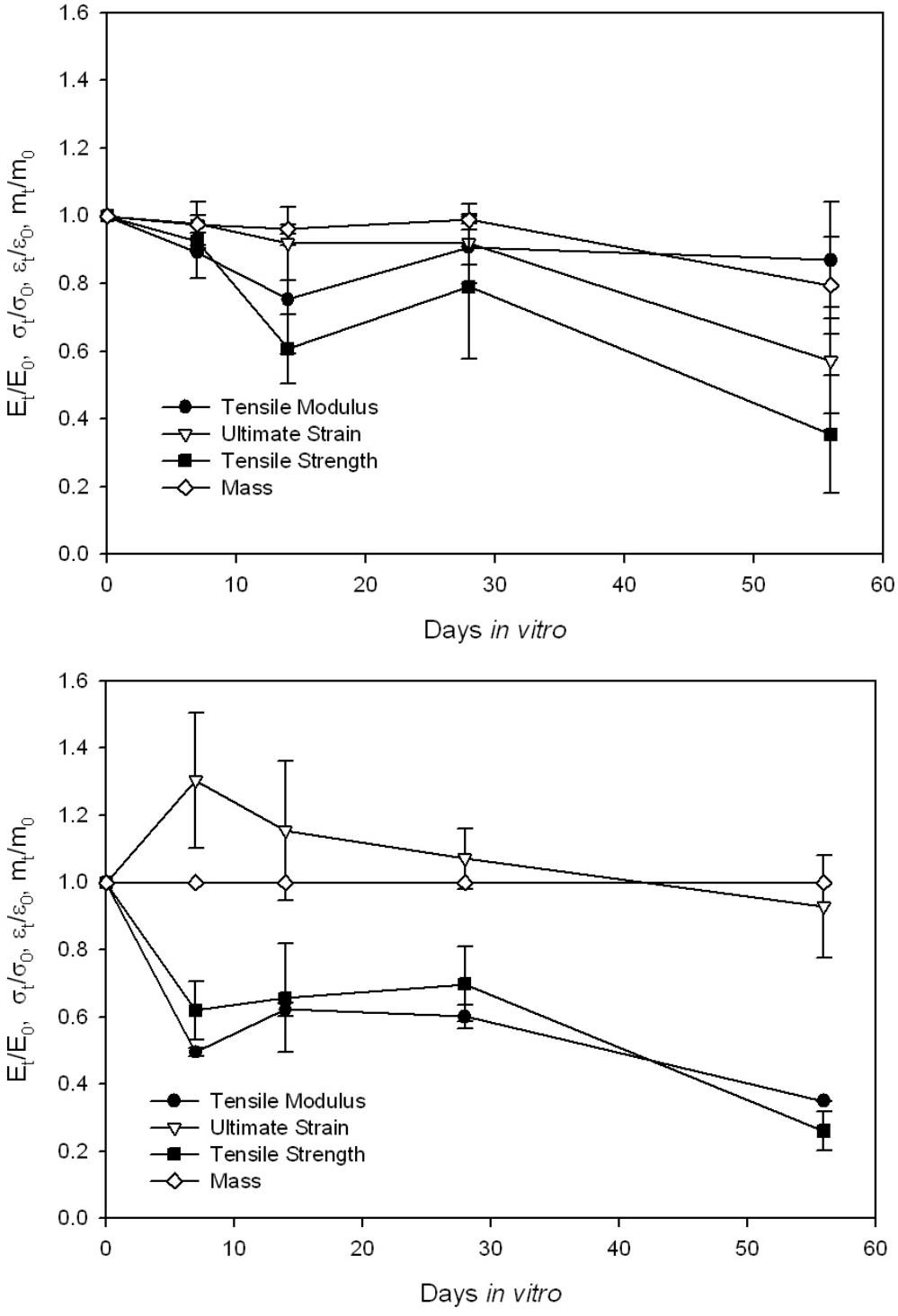

Figure 26: Change in mass and mechanical properties of nonporous (top) and porous (bottom) ELAS 1800 scaffolds during 8 weeks *in vitro* degradation in PBS pH 7.4, 37°C.

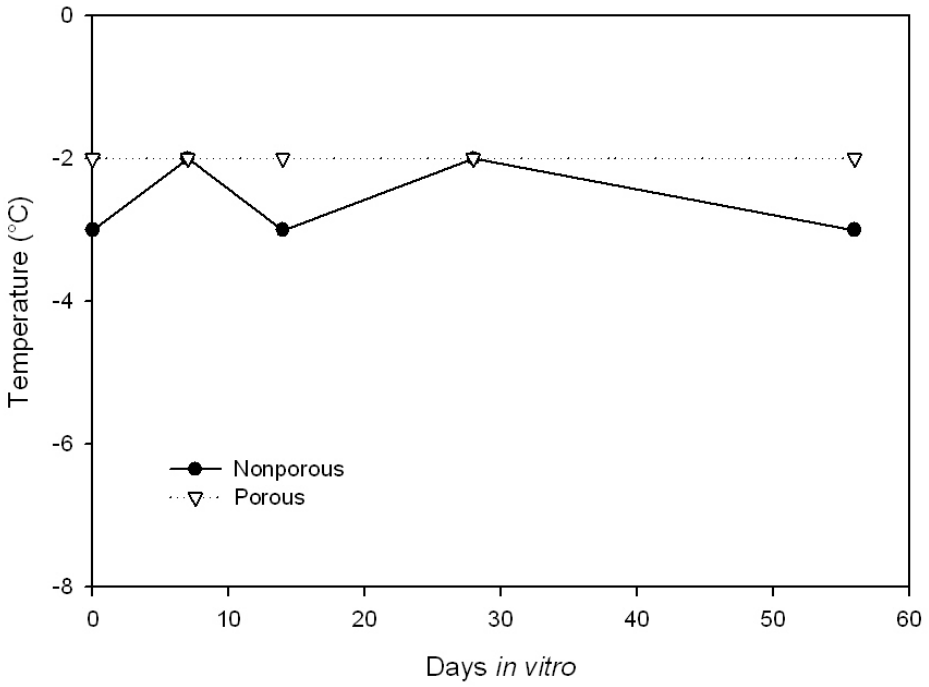

Figure 27: Glass transition temperature of ELAS 1800 scaffolds during *in vitro* degradation in PBS pH 7.4, 37°C.

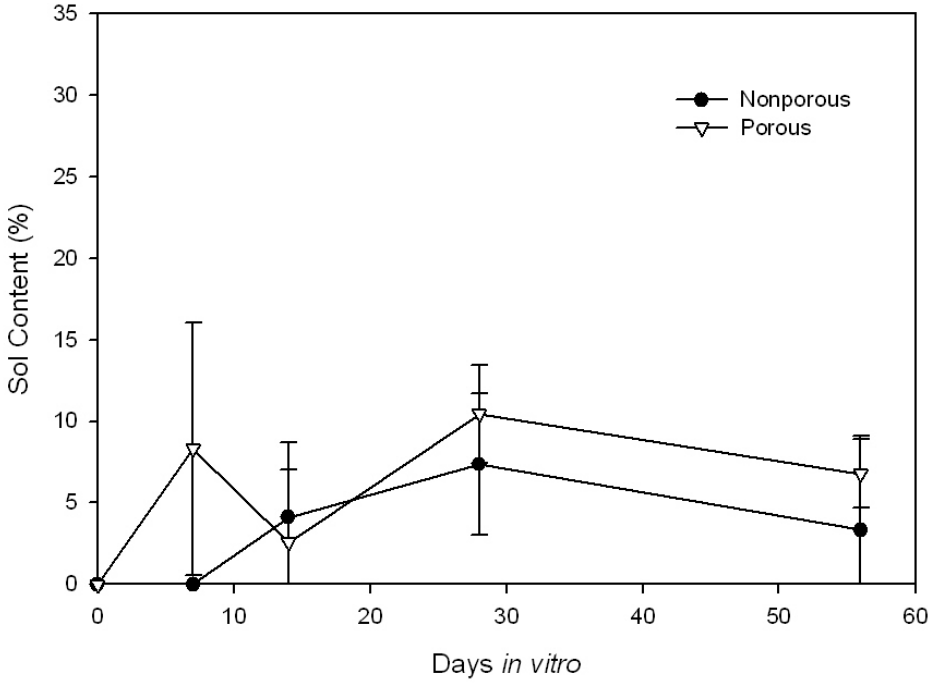

Figure 28: Sol content of ELAS 1800 scaffolds during *in vitro* degradation in PBS pH 7.4, 37°C.

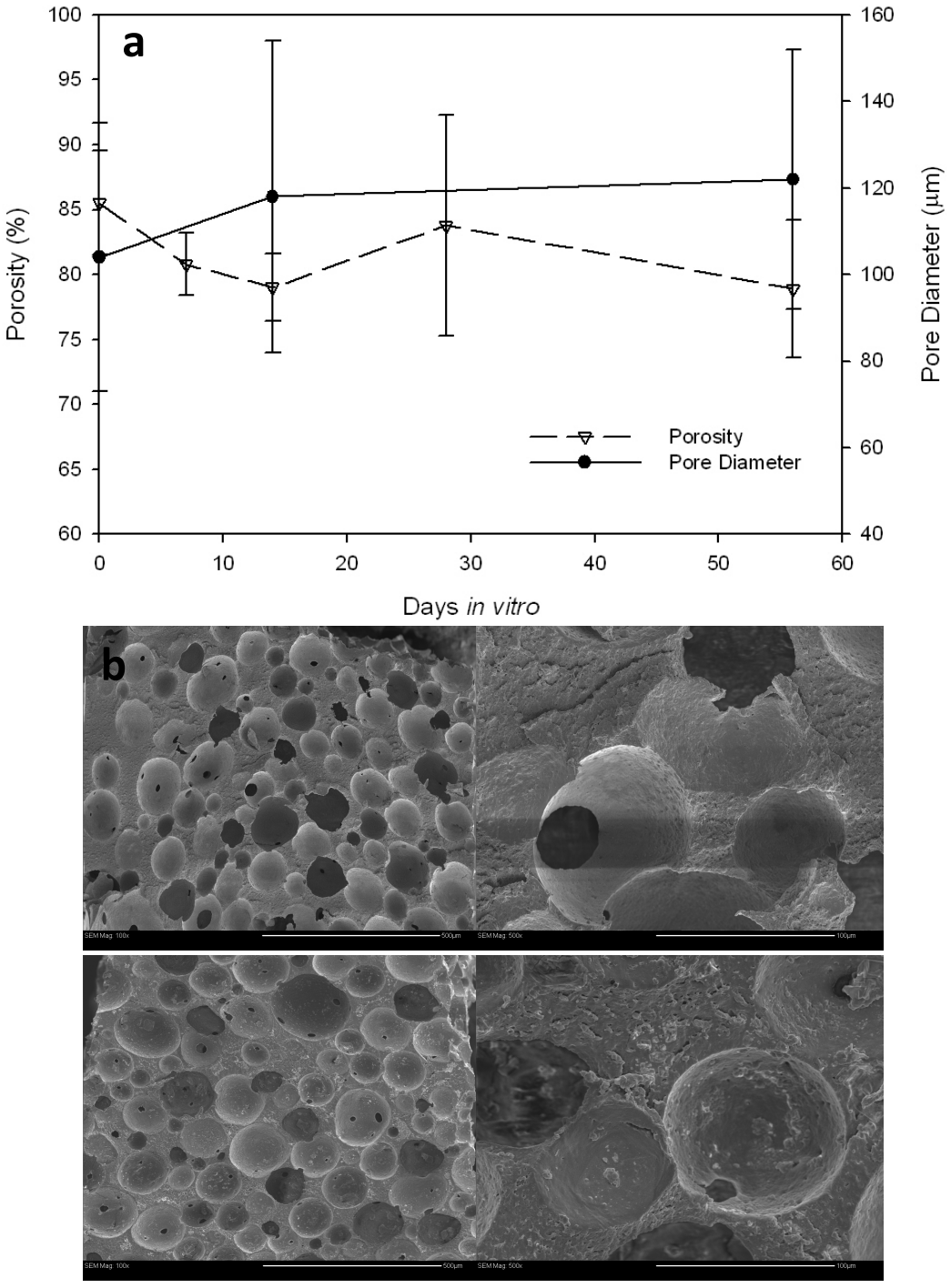

Figure 29: (a) Porosity and pore size of porous ELAS 4500 (b) SEM of porous ELAS 1800 before degradation (top) and after 8 weeks (bottom) *in vitro* degradation in PBS pH 7.4, 37°C. Scale bar in left 500 µm, right 100 µm.

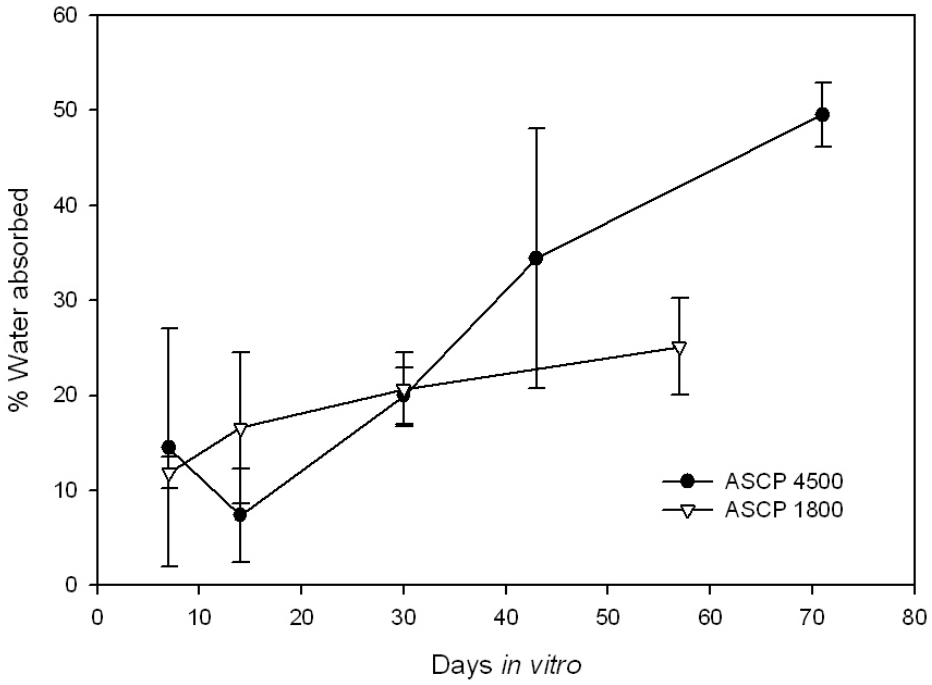

Figure 30: Water absorbed by elastomers with various crosslink densities during in vitro degradation in PBS pH 7.4, 37°C.

Chapter 6
Results and Discussion – Surface Modifications

As with other synthetic polymers, the ASCP does not have cell adhesion sites on its backbone [47,48]. Thus, it is safe to assume that it will most likely have poor cell attachment properties. Anticipating this, two surface modifications were investigated to see if the cell attachment properties of ASCP could be improved. These two modifications were base etching and crosslinking GRGDS (an adhesion-promoting oligopeptide[116]) into the elastomer.

6.1 Base Etching

As discussed in Chapter 2, surface hydrolysis or base etching of polyesters is a popular surface modification to increase cell attachment. To visually determine the extent of surface hydrolysis under the prescribed conditions (0.5 M NaOH, 1 hr), fluorescamine was covalently attached to any carboxyl or hydroxyl groups on the surface through water-based carbodiimide chemistry and imaged with confocal microscopy. Figure 31 is a plot of the surface area versus fluorescent intensity. High intensity (fluorescamine attached) areas are contained to small patches and not widespread. Thus, under these base etching conditions only localized surface hydrolysis occurred. This may be attributed to the different affinities of CL and DLLA to be hydrolyzed. DLLA is more hydrophilic than CL and thus more susceptible to being hydrolyzed. Nevertheless, even under these conditions, a reduction of 20° in water contact angle was observed for both ELAS 4500 and ELAS 1800 films (Figure 32).

Previous studies [83,117] have suggested that base etching improves cell attachment by changing the topography of the surface on a nano scale. From the SEM images in Figures 33 it was evident that under the tested base etching conditions, there was no change in surface roughness. There were no noticeable grooves, pitting, or other changes in topography on the macroscale. Even on the nanoscale there was no change in surface roughness. The surface roughness root mean square deviations were calculated for AFM images of unmodified and base etched ELAS 4500 films (Figure 34). The surface roughness was the same for both films regardless of surface area. As well, the root mean square deviations were on the order of angstroms, indicating a very smooth surface. The root mean square deviation is a measurement of error or residuals. A large root mean square deviation would indicate a rough surface since each point of the surface would be different from each other. From these three techniques it was concluded that base etching only changed the surface chemistry of the elastomer films. To quickly test the effectiveness of the base etching conditions on cell attachment, primary bovine fibroblasts were seeded on unmodified and base etched films of ELAS 4500 and cultured for up to 5 days. At 3 days, the base etched films had more cells attached versus the unmodified films (Figure 35) and the cells were more spread out.

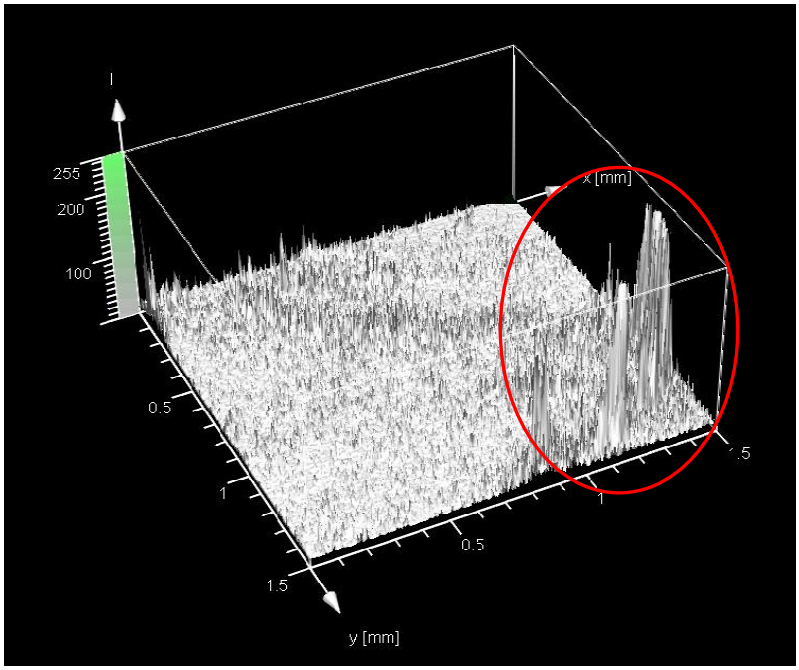

Figure 31: Visualization of base etched areas covalently linked with fluorescamine on ELAS 4500 films. High intensity area (circled) is covalently linked with fluorescamine.

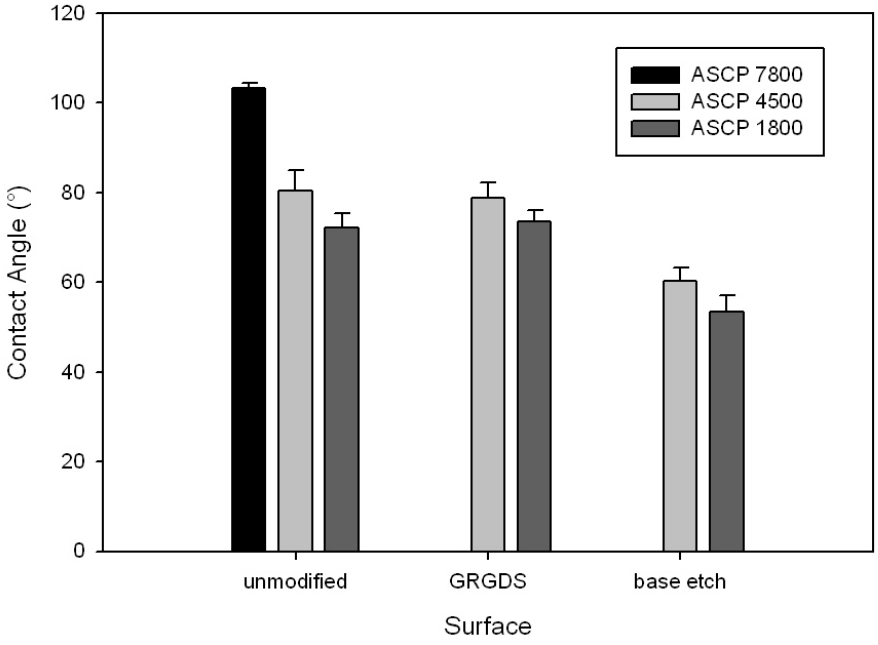

Figure 32: Effect of surface modifications to elastomers made with various ASCP M_n on water contact angle. All M_n and base etched samples were statistically significant ($p < 0.01$) while GRGDS surfaces were not statistically significant.

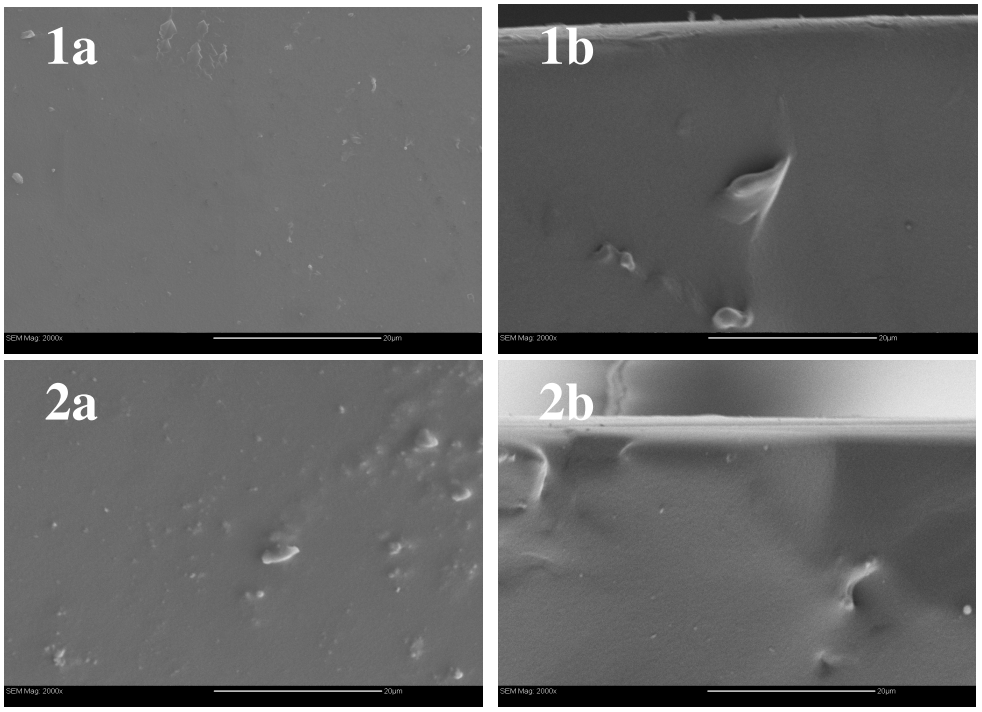

Figure 33: SEM images of 1- umodified ELAS 4500 and 2 – base etched ELAS 4500 (a) are taken at the surface while (b) are cross-sectional images. Base etching conditions: 0.5 M NaOH, 1 hr. Scale bar = 20 μm

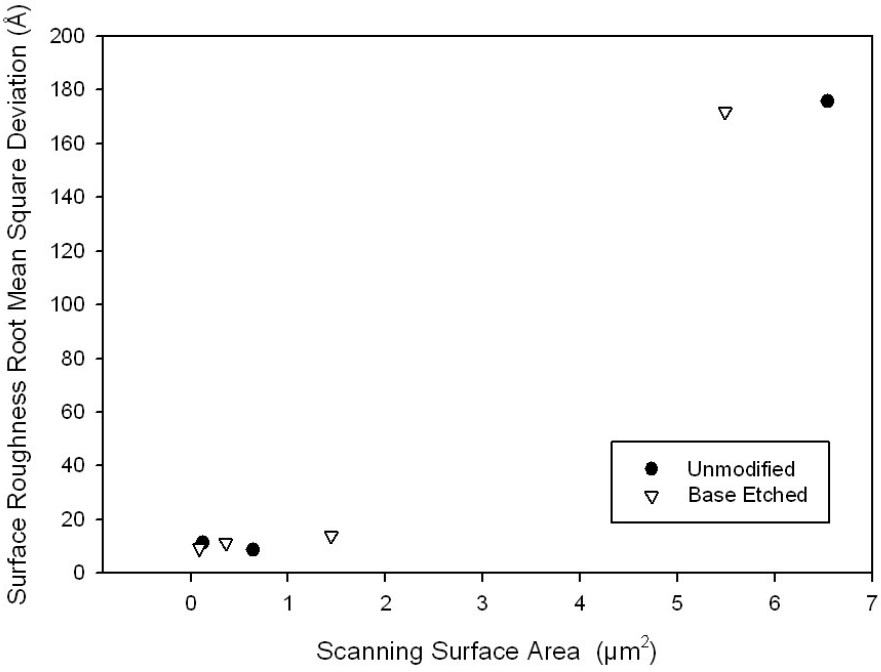

Figure 34: Surface roughness of unmodified and base etched ELAS 4500 measured by AFM.

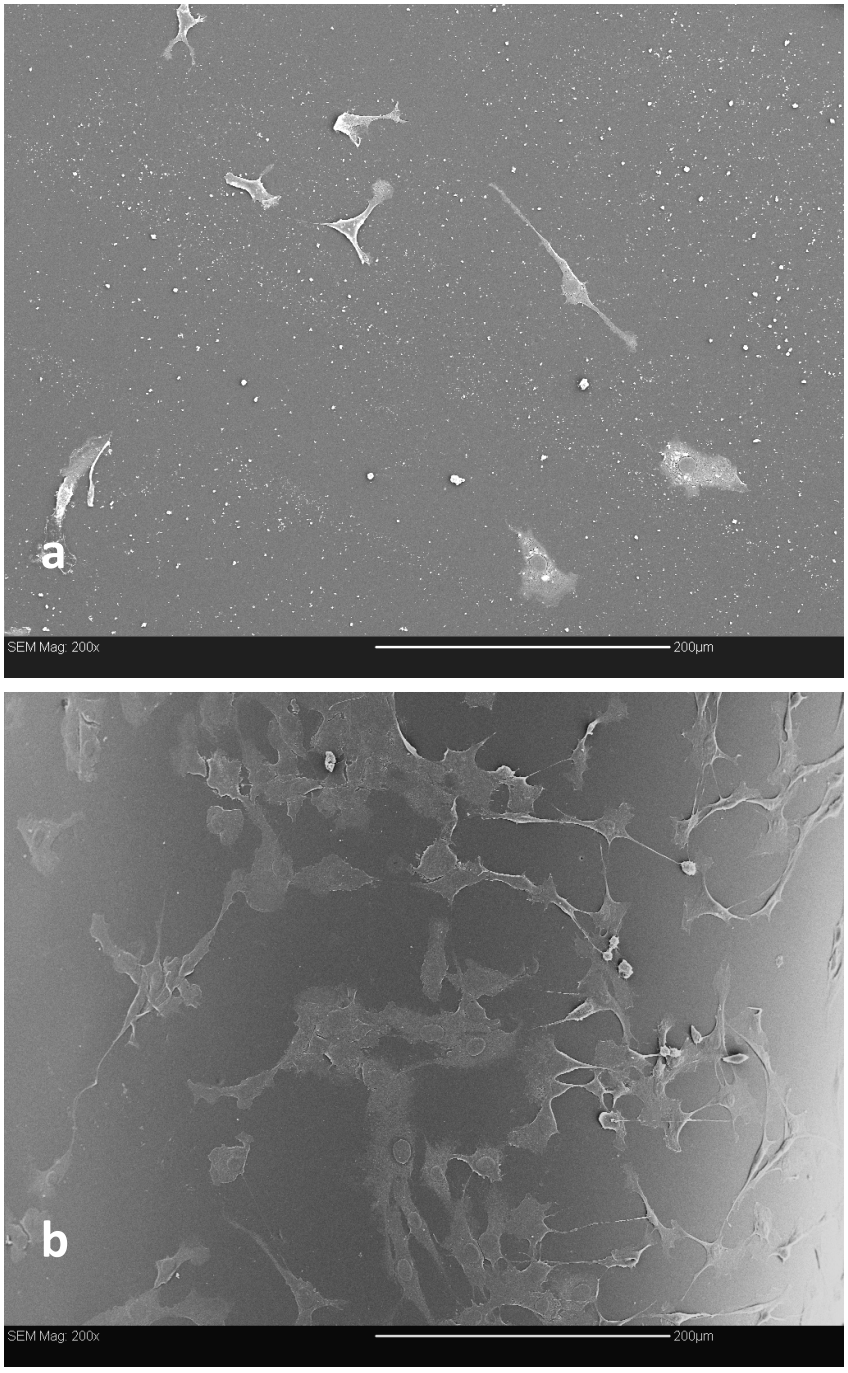

Figure 35: SEM images of primary bovine fibroblasts (passage 2) after 3 days in culture on (a) unmodified and (b) base etched ELAS 4500 films. Scale bar = 200 µm

6.2 Peptide incorporation into ASCP elastomeric network

The RGD sequence is the most often used peptide sequence for stimulated cell adhesion on synthetic surfaces. This is due to its use throughout the organism; the sequence is found in many ECM proteins including fibronectin, vitronectin, fibrinogen and collagen. Cells are attached to RGD through integrin mediated cell adhesion. Moreover, this short peptide sequence has been found to have an extraordinary ability to address more than one cell adhesion receptor and is very influential on cell anchoring, behavior and survival [85]. In this work, the peptide sequence GRGDS was used as the RGD source.

Nevertheless, there is contradictory evidence that there is a minimum distance needed from a surface to reach cell receptors. A detailed study by Beer *et al.* concluded that virtually all receptors can be reached with a spacer length of 46 Å [118]. However, Massia *et al.* directly attached RGD to a poorly adhesive glass substrate and also observed excellent cell adhesion [119]. Since no conclusions can be made from published data and could be situation specific, GRGDS was tested for both cases, *i.e.* directly attached to the elastomer, and tethered with a PEG spacer. Glycine was used a model peptide to test the effectiveness of the PEG spacer linkage.

The ^{1}H NMR spectra of the PEG spacer alone and tethered with glycine (Figure 36) clearly shows that the glycine molecule is attached to the PEG spacer and that the acrylated ends are left intact. The PEG spacer has a reactive succinimidyl carboxymethyl end which couples with the N-terminal glycine side chain. Thus, after successfully tethering the glycine on the PEG spacer, the succinimidyl carboxymethyl end at 2.7 ppm disappears and glycine peaks at 4.1 and 7.6 ppm appear. ATR-FTIR

also showed that the PEG spacer with glycine was successfully on the surface (Figure 38) with peaks at 1637 cm^{-1} and 1620 cm^{-1}. Peaks in this range correspond to amide vibrations which are only present on the GRGDS peptide. Similarly, ATR-FTIR spectra of ELAS 1800 films with the PEG spacer and GRGDS (Figure 38) and GRGDS directly crosslinked to the elastomer (Figure 37) showed peaks at 1637 cm^{-1} and 1593 cm^{-1} respectively. It was assumed that the negative control peptide RPDS would be coupled in a similar fashion and thus was not tested.

It has been suggested by Lin *et al.* that the attachment of RGD on the surface also introduces charged functional groups that may change surface hydrophilicity [120]. In this study, the addition of GRGDS to the surface did not change the hydrophilicity of the elastomer film surface. The contact angle did not change after the addition of GRGDS to the surface for either ELAS 4500 or ELAS 1800 (Figure 32). The study by Lin et al. added a 1.1 molar excess peptide to carboxylate groups of a polyurethane polymer. In the current study the amount of peptide added was on the order of 1 $pmol/cm^2$, much less then the Lin study. Thus, the amount of peptide on the elastomer surface was not enough to change the contact angle.

6.3 Influence of crosslink density on surface chemistry

Comparing elastomer films of various crosslink densities, the water contact angle increases as crosslink density decreases (Figure 32). This phenomenon may be due to the acrylate content at each M_n; acrylate content in the elastomer increases at higher crosslink densities since there are more end groups in the ASCP used to make the elastomer. Thus, the greater acrylate content in the ELAS 1800 film would attract more water to the surface, creating a more hydrophilic surface.

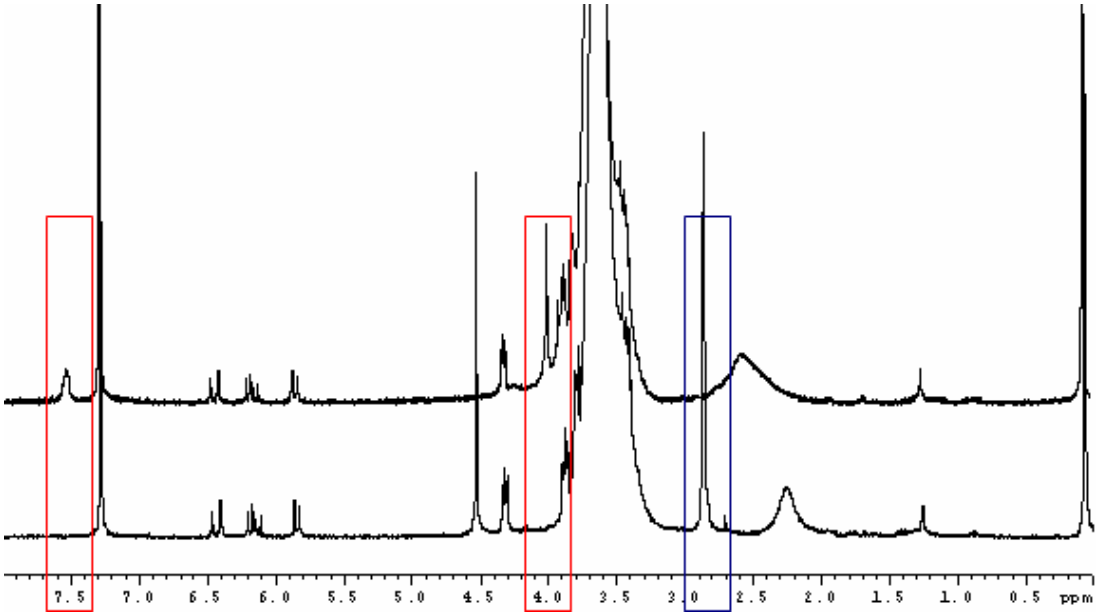

Figure 36: 1H NMR spectra for PEG 3400 spacer in $CDCl_3$ before (bottom) and after (top) coupling with glycine. Coupling was successful as the succinimidyl carboxymethyl (blue) peak at 2.7 ppm disappears and glycine peaks (red) at 4.1 and 7.6 ppm appear.

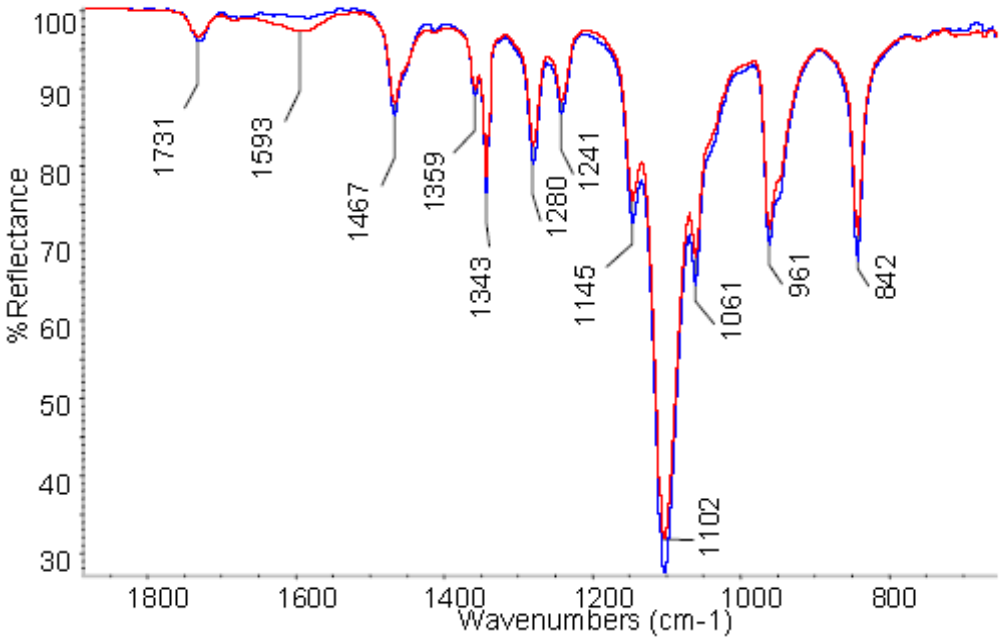

Figure 37: ATR-FTIR spectrum of unmodified and GRGDS-modified ELAS 1800 films. Blue line is unmodified surface while red is GRGDS-modified surface.

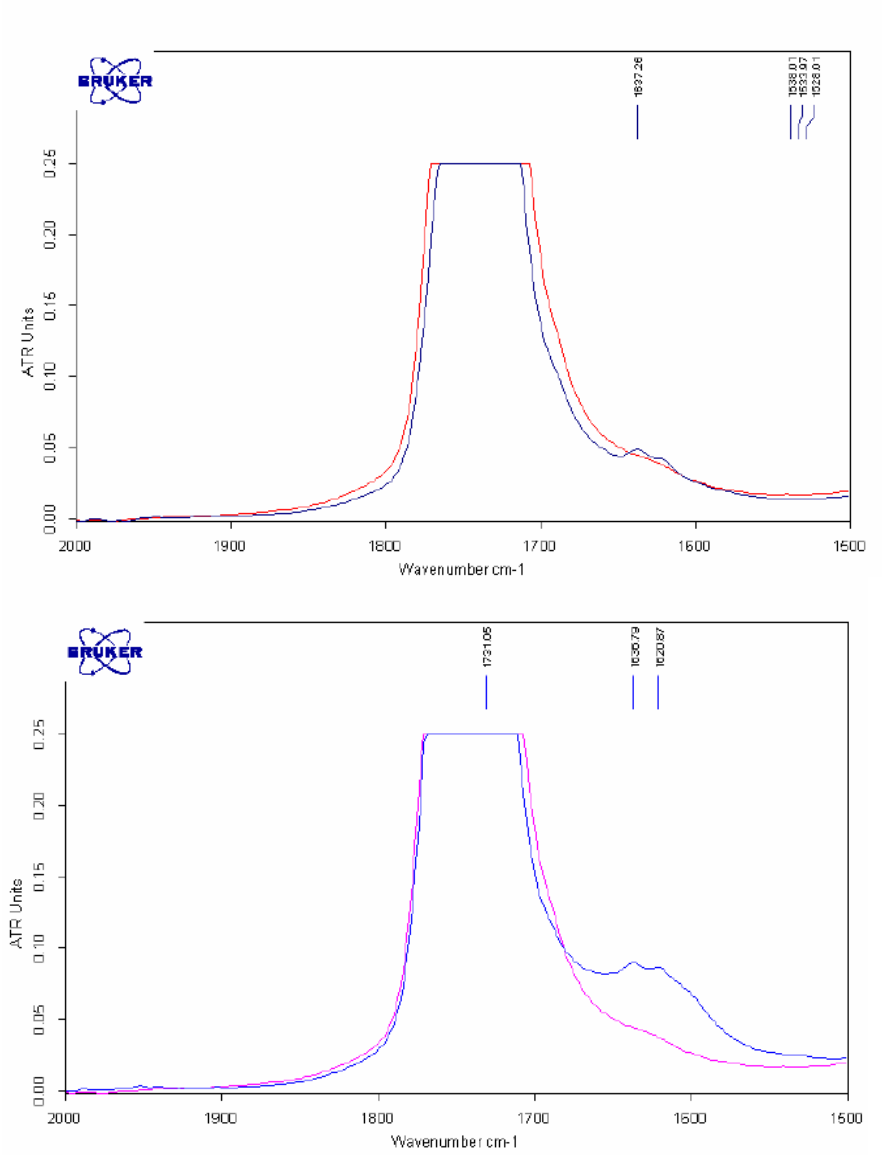

Figure 38: ATR-FTIR spectra of unmodified and PEG spacer with peptide-modified ELAS 1800 films. Peptide in top is GRGDS and bottom is glycine. Blue line is modified surface while red/pink is unmodified surface.

Chapter 7
Results and Discussion – Cellular Response

7.1 Cell attachment and proliferation

Attachment of SMCs to unmodified and modified ELAS 1800 and ELAS 4500 surfaces were measured after 1 day in culture (Figure 39). It was assumed that the cells on the surface after 1 day were from the seeding and not due to proliferation. This was confirmed as the calculated number of cells on the TCPS (tissue culture polystryrene) control surface was 12 888 ± 1439, and the seeding density was 10 000 cells. Proliferation was measured after 7 days in culture (Figure 40), it was assumed that by this time a confluent layer of SMCs would be present. All data was normalized against the number of cells on TCPS at 1 day.

7.1.1 Influence of crosslink density

Crosslink density did not influence cell attachment on unmodified elastomers. Cells did not attach as well on the unmodified elastomers as they did on the TCPS control, regardless of crosslink density (Figure 39). This was expected, since it is well known that cells attach poorly to hydrophobic surfaces. Surprisingly, crosslink density did have a dramatic effect on cell proliferation. The unmodified surfaces were significantly different, with ELAS 4500 having over 3 times the number of cells on the surface, which was similar to the number on TCPS (Figure 40).

This difference may be due to differences in surface chemistry. A 10° difference in water contact angle was observed between ELAS 4500 and ELAS 1800 (Figure 32). This difference in surface hydrophilicity could affect long term protein deposition (nature,

amount, and orientation). Initially the type of proteins adsorbed on the surface may have been the same, thus creating no difference in cell attachment. Over time, the Vroman effect would cause the protein composition for each film to be different. The highest mobility proteins arrive first and later are replaced by less mobile proteins that have a higher affinity for the surface. It is possible that the proteins deposited on the ELAS 4500 surface are similar to those on the TCPS surface and as such have similar cell densities after 7 days. In the same way, it has been reported that different ECM materials promote SMC proliferation. Fibronectin substrates caused modulation of SMCs from a contractile to a synthetic phenotype. However, there was a delayed phenotypic modulation of SMCs when grown on laminin [121]. Orientation of the adsorbed proteins also affects cell behaviour. On hydrophobic surfaces, proteins are spread out while on hydrophilic surfaces, they are less likely to undergo significant changes in configuration [95]. This change in configuration can lead to undesirable cell response.

7.1.2 Influence of base etching

Initial work with fibroblasts suggested an improvement in cell attachment with base etching. Under the tested conditions, base etching did not increase cell attachment for both ELAS 4500 and ELAS 1800. Base etching also did not have an impact on cell proliferation on either elastomer. This result is similar to those reported by Miller *et al*. [117] who showed that for vascular smooth muscle cells, there was no influence of surface chemistry on cell attachment. The increase in cell attachment was attributed to a change in surface topography.

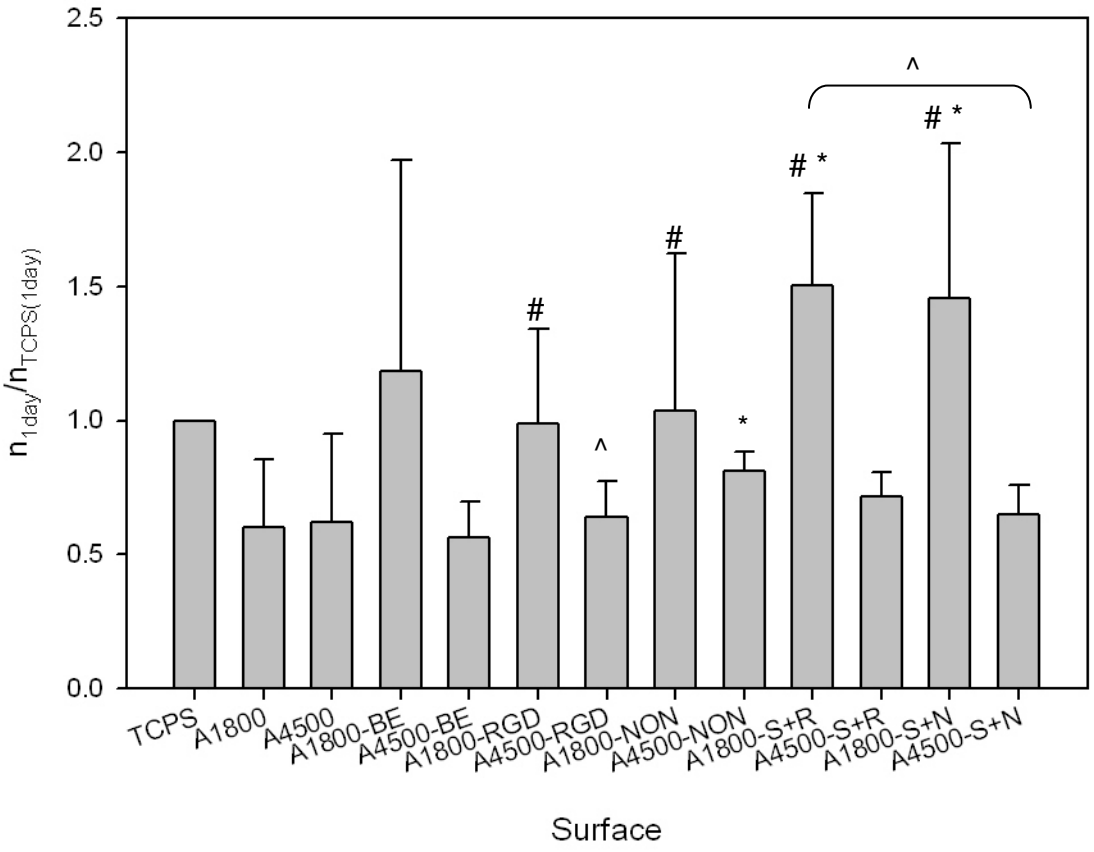

Figure 39: Cell attachment of SMCs to various ELAS surfaces after 1 day in culture. WST-1 was used to measure cell numbers and all data was normalized against the number of cells on TCPS at 1 day. Initial seeding density 10^4 cells/well. TCPS = tissue cultured polystyrene, BE= base etched, RGD = GRGDS, NON = RPDS, S+R = PEG spacer and GRGDS, S+N = PEG spacer and RPDS. Significance = $p < 0.05$. (+) ASCP 4500, (#) ASCP 1800, (*) between GRGDS of the same Mn, (^) between Mn

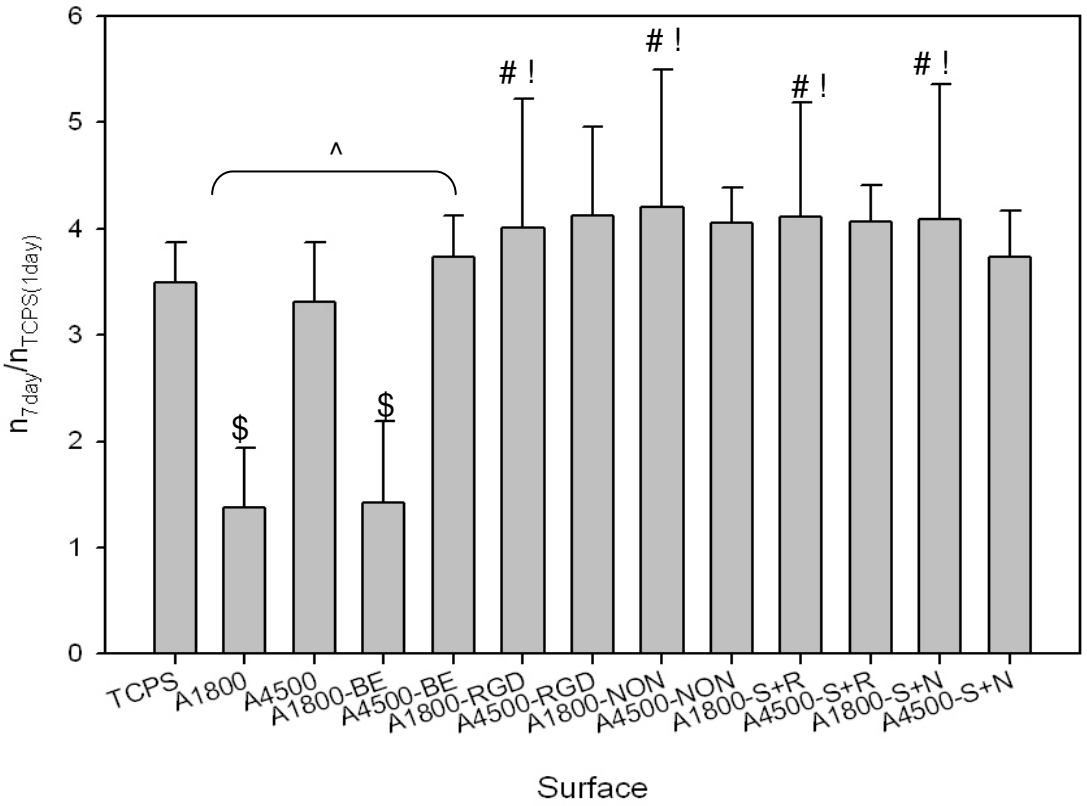

Figure 40: Cell proliferation of SMCs on various ELAS surfaces after 7 day in culture. WST-1 was used to measure cell numbers and all data was normalized against the number of cells on TCPS at 1 day. Initial seeding density 10^4 cells/well. TCPS = tissue cultured polystyrene, BE= base etched, RGD = GRGDS, NON = RPDS, S+R = PEG spacer and GRGDS, S+N = PEG spacer and RPDS. Significance = $p < 0.05$ (#) ELAS 1800, ($) TCPS, (!) ELAS 1800 BE (^) between Mn

Surface chemisty may still have a role in cell attachment. Salloum *et al.* showed that on polyelectrolyte multilayers, cultured rat aortic smooth muscle A7r5 cells adhered and spread better on hydrophobic, negatively charged surfaces [124]. Base etching imparts a negative charge on the surface from exposed carboxylic acid groups. However, the localized base etching (Figure 31) may not have been sufficiently significant to increase cell attachment.

7.1.3 Influence of peptide activity and configuration

Addition of a peptide to the surface significantly increased cell attachment on the ELAS 1800 elastomer but not on the ELAS 4500 elastomer as compared to the unmodified elastomers. The bioactivity of the peptide did not influence cell attachment as both inactive and active peptides on ELAS 1800 produced the same cell response. The inactive peptide sequence RPDS was used to test for cell attachment based on specific binding to integrins and not from surface hydrophilicity or other similar surface properties. There have been a few cases where there was a cell response to negative controls [125], however, there has yet to be an explanation for this phenomenon. It has been suggested that the interaction might be due to residual peptide affinity or changed surface properties that enable deposition of soluble cell adhesive serum proteins [125]. The above rationalization is quite probable since the medium used for all studies contained serum. Nonetheless, it can be assumed that this behaviour is not due to surface hydrophilicity, as there was no difference in water contact angle between films with and without GRGDS (Figure 32).

A spacer significantly increased cell attachment, greater than surfaces with the peptide directly attached to the surface, but only for ELAS 1800 films. The active and inactive

peptide also produced the same response. This nonspecific increase in cell attachment may be due to the PEG spacer promoting an increase in the deposition of soluble cell adhesive serum proteins compared to films with peptides directly attached. Although, PEG hydrogels do not promote protein deposition, the concentration of the PEG spacer on the films (pmol range) may not be sufficient to deter protein deposition. ELAS 4500 films with the PEG spacer did not exhibit the same response. This may be due to differences in surface concentrations. Although, the same amount of peptide was added to each film (0.5 pmol/cm^2), the amount of polymer end groups available to crosslink with the PEG spacer were different. In the ELAS 4500 films, there were fewer available end groups. Thus, the amount of peptide on the surface would be less than on the ELAS 1800 films. A similar concentration difference also occurred on the surfaces with peptides directly incorporated into the network. Concentrations in both cases are likely below the values needed to increase cell attachment.

At 7 days, all ELAS 1800 peptide modified surfaces had a significant influence on cell proliferation compared to the unmodified surface. These surfaces were also similar to the TCPS control. There was no difference between peptide modified surfaces with or without a spacer and between the two crosslink densities. The enhanced cell proliferation may be due to integrin binding to the RGD motif grafted to the surface or to the cell adhesive protein fibronectin found in serum. Neff *et al.* observed an increase in cell attachment and cell proliferation of NIH 3T3 fibroblasts on GRGDSY grafted polystyrene. However, there was a maximum peptide density before cell proliferation began to decrease [126]. Mann and West conducted a similar study with human aortic smooth muscle cells, but did not observed an increase in cell proliferation [127]. Nevertheless, they contribute this observation to using concentrations above the

maximum peptide density. In their study peptide concentrations were on the order of 2 nmol/cm^2, while in the current work the peptide concentration is 0.5 – 1 pmol/cm^2. It should be noted that in the study by Neff, an inactive peptide control was not tested. Thus, it is unknown whether the inactive peptide has the same influence on cell proliferation. From the cell proliferation results in this work, it appears that the inactive peptide may have an influence on cell proliferation. Whether this influence is direct or indirect from the cell adhesive peptides that are deposited on the surface needs to be further investigated. Similar to the cell attachment results, peptide modified ELAS 4500 films did not have an influence on cell proliferation. Again, this is likely due to the low concentration of grafted peptides to the surface.

7.2 Morphology

From Figures 39 and 40 it was evident that modifying the surface with a peptide increased cell attachment. Cell morphology was also investigated on unmodified and modified ELAS 1800 films to see if the SMCs were well spread on the surface. A well spread cell indicates good attachment to the surface. It may also give indications about phenotype as contractile SMCs are spindle shaped while synthetic SMCs are more rhomboid shaped [11,20] (Figure 6). The positive control was a glass cover slip. Glass was chosen as the control because it is routinely used for SMC studies [128]. Thus, its cell adhesion and effect on phenotype are fully characterized. It has been observed that SMCs seeded on glass substrates exhibit a synthetic phenotype.

After 1 day in culture, SMCs on peptide modified surfaces were all well spread out and similar to the positive glass control (Figure 41). Similar to the cell proliferation results, SMCs on the unmodified ELAS 1800 and base etched films were not as spread out as

the glass control or GRGDS modified surfaces. SMCs on these surfaces were more spindle-shaped and not spherical-shaped. Spherical cells indicate unfavourable surface conditions and can lead to detachment and apoptosis [85]. The spindle shape may be more indicative of a contractile phenotype. If this is the case, then the cell proliferation results support this case as there was a small change in cell number from 1 and 7 days on ELAS 1800 base etched films indicating a slow cell proliferation rate. A slow cell proliferation rate is characteristic of the contractile SMC phenotype [11]. Unmodified ELAS 1800 films showed both spindle shaped and well spread cells. Similarly, the cell proliferation rate reflected the presence of these two populations as cell numbers were reached those of the base etched films, but not on the peptide modified surfaces.

At 7 days, a confluent layer of SMCs was observed on all surfaces and it was very difficult to identify individual cells and morphology (Figure 42). The observed surface was similar to other studies [129]. This might be an indication that the attached SMCs are contractile. It has been observed that the contractile phenotype returns after becoming confluent [19]. If the SMCs were synthetic a characteristic “hill and valley” growth pattern would be seen. The hills contain cells that have piled up on one another to form as many as 10-15 cell layers, while the valleys may contain no cells or 1-3 layers [19].

7.3 Phenotype

Due to the flexible nature of SMC phenotypic modulation, it is important to characterize if the elastomer surface will influence phenotype. The SEM images suggest that immediately after seeding SMCs may become synthetic. However at 7 days, once the SMCs are confluent, the phenotype is modulated to the contractile state.

In this work, immunofluorescence of two contractile marker proteins, α – actin and h – caldesmon, was used to observe the phenotype of the SMCs attached to the various ASCP surfaces. Smooth muscle α – actin is a protein filament used for contraction. It is the most abundant protein in SMCs making up 40% of total cell protein. The high α – actin content is required for their high force-generating capabilities [20]. It is also one of the earliest contractile markers present during SMC phenotypic modulation from the synthetic phenotype to the contractile phenotype, but expression levels increase as modulation nears the contractile phenotype (Figure 4).

Caldesmon is a protein involved in regulating thin filament activity such as actin with a possible role in the assembly and stabilization of thick and thin filaments [130]. Caldesmon is present in two isoforms: l-caldesmon and h-caldesmon. The h-caldesmon isoform is abundant in differentiated SMCs while l-caldesmon is found in synthetic SMCs. Thus, changes in ratios of h- and l- caldesmon are sometimes used to indicate a synthetic phenotype[11]. Nonetheless, from Figure 4, markers for h-caldesmon alone can be used to indicate later SMC modulation/differentiation [20]. The use of fluorescent tags only gives a qualitative visualization of the expressed proteins. More detailed investigation into expression levels would be needed to quantify and determine where on the phenotype continuum the SMCs on the various surfaces lie. This could be done using Western Blot analysis.

After 4 days in culture SMCs on unmodified and modified elastomer films (Figure 43) all expressed the contractile marker proteins suggesting that all surfaces maintained a SMC phenotype. This result is similar to that observed on the glass control. As such, the surface modifications do not interfere with phenotype. This result is in agreement with other studies. Xu *et al.* used a block copolymer of PCL/LLA (75% L-lactic acid) and

showed that phenotype was the same on the copolymer as on the TCPS control [67,131]. Nonetheless, the functionality of the phenotype can not be assessed from these images because the staining did not show distinct organized filaments. Testing of contractility against various stimuli would be needed to conclusively assess the functionality of the seeded SMCs.

The current work only focused on a short time period (7 days) while synthesis of a sufficient amount of ECM can take up to 7 weeks in culture. Identification and quantification of synthesized ECM products would also be helpful to characterize how the various surfaces are influencing behaviour. Nonetheless, the visualization of contractile markers and cell proliferation studies provides an indication of how SMCs behave on the elastomer surface. Next steps should examine ECM synthesis. Kim *et al.* found that synthesis of ECM products by SMCs can be regulated by the surface chemistry. PGA scaffolds induced more elastin production while type I collagen sponges induced more collagen production [91].

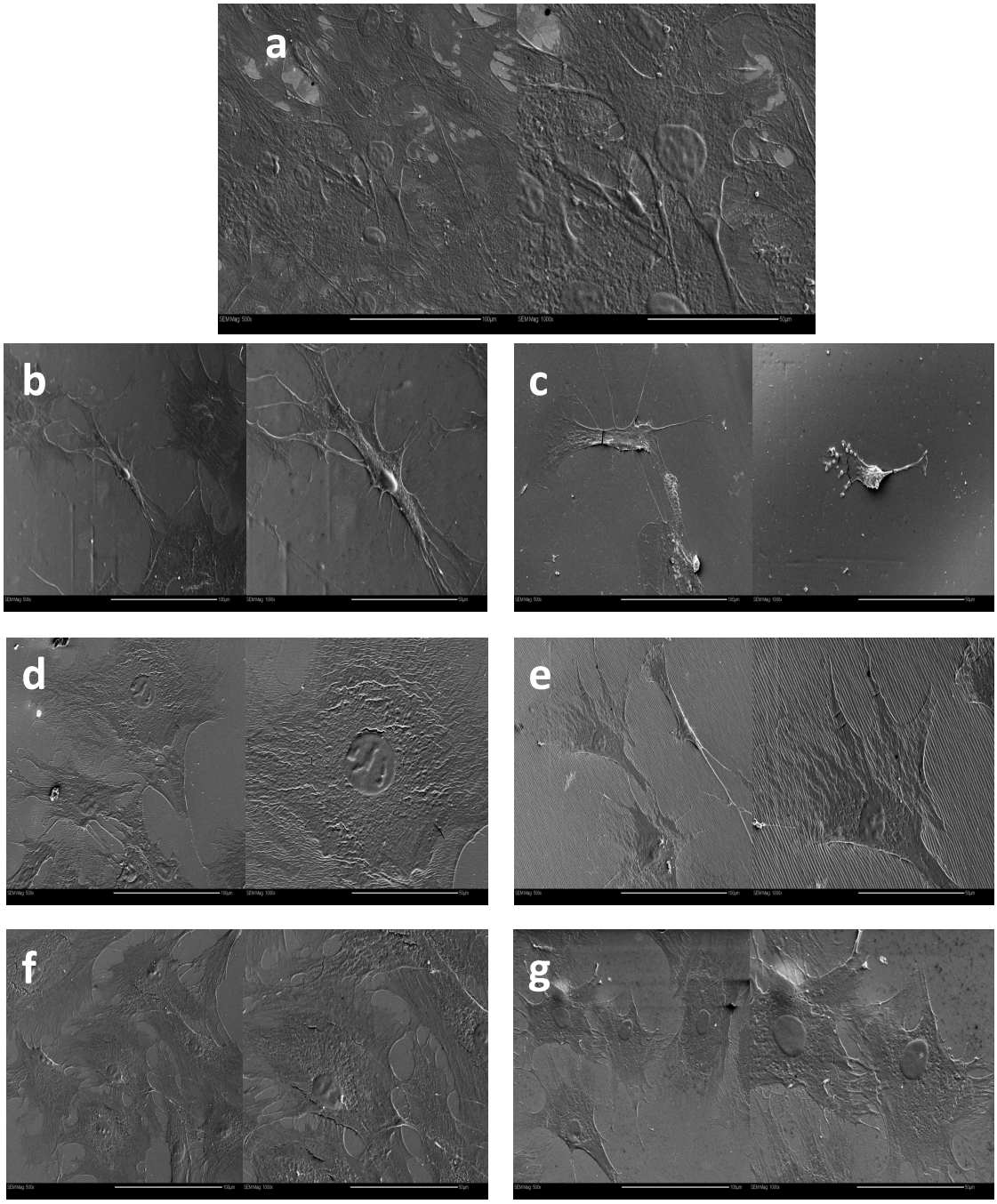

Figure 41: SEM images of SMCs on various surfaces of ELAS 1800 after 1 day in culture. a – glass control, b – unmodified ELAS 1800, c – base etched, d – GRGDS, e – RPDS, f – PEG spacer + GRGDS, g – PEG spacer + RPDS. Scale bar left = 100 μm, right = 50 μm

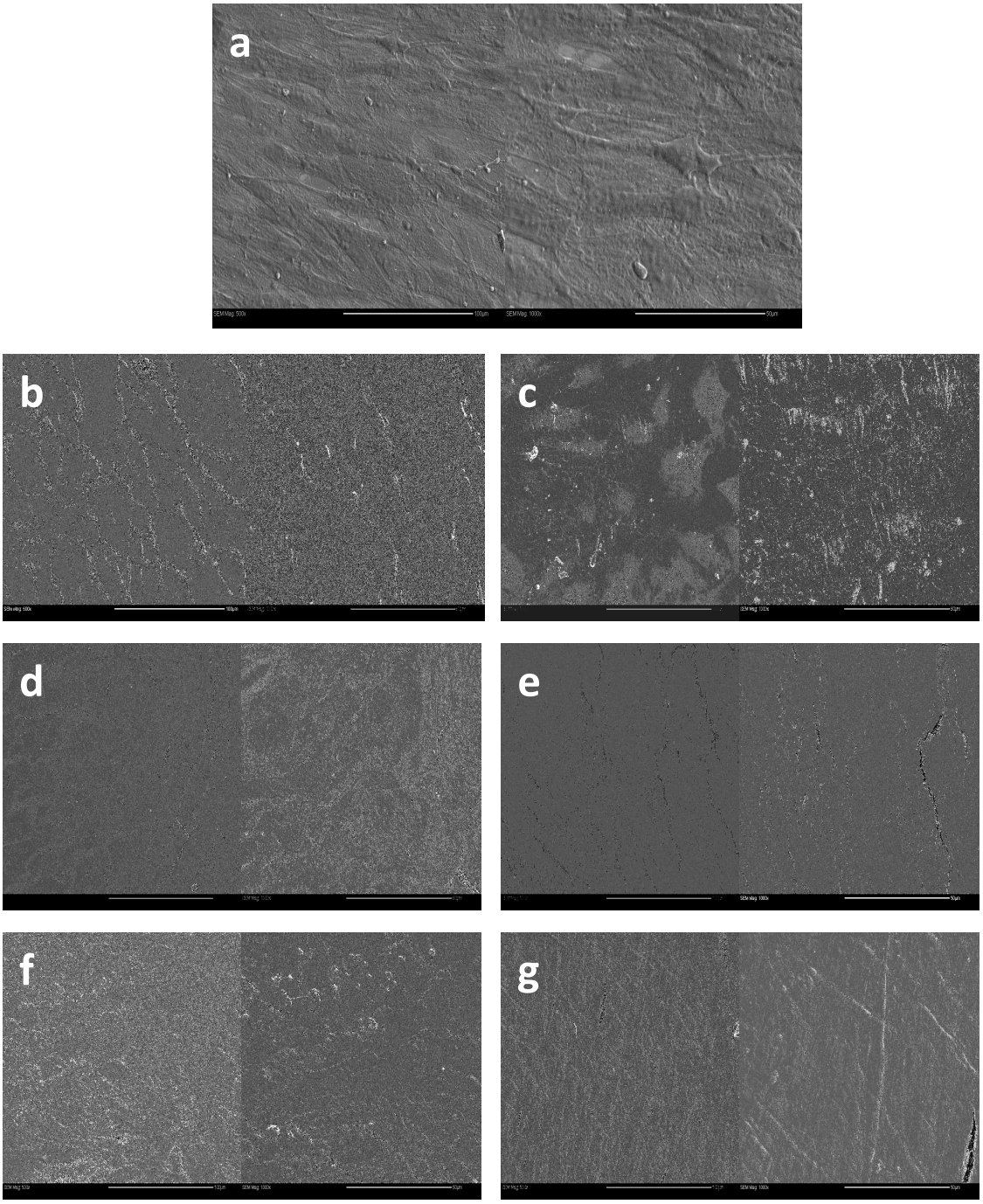

Figure 42: SEM images of SMCs on various surfaces of ELAS 1800 after 7 days in culture. a – glass control, b – unmodified ELAS 1800, c – base etched, d – GRGDS, e – RPDS, f – PEG spacer + GRGDS, g – PEG spacer + RPDS Scale bar left = 100 μm, right = 50 μm

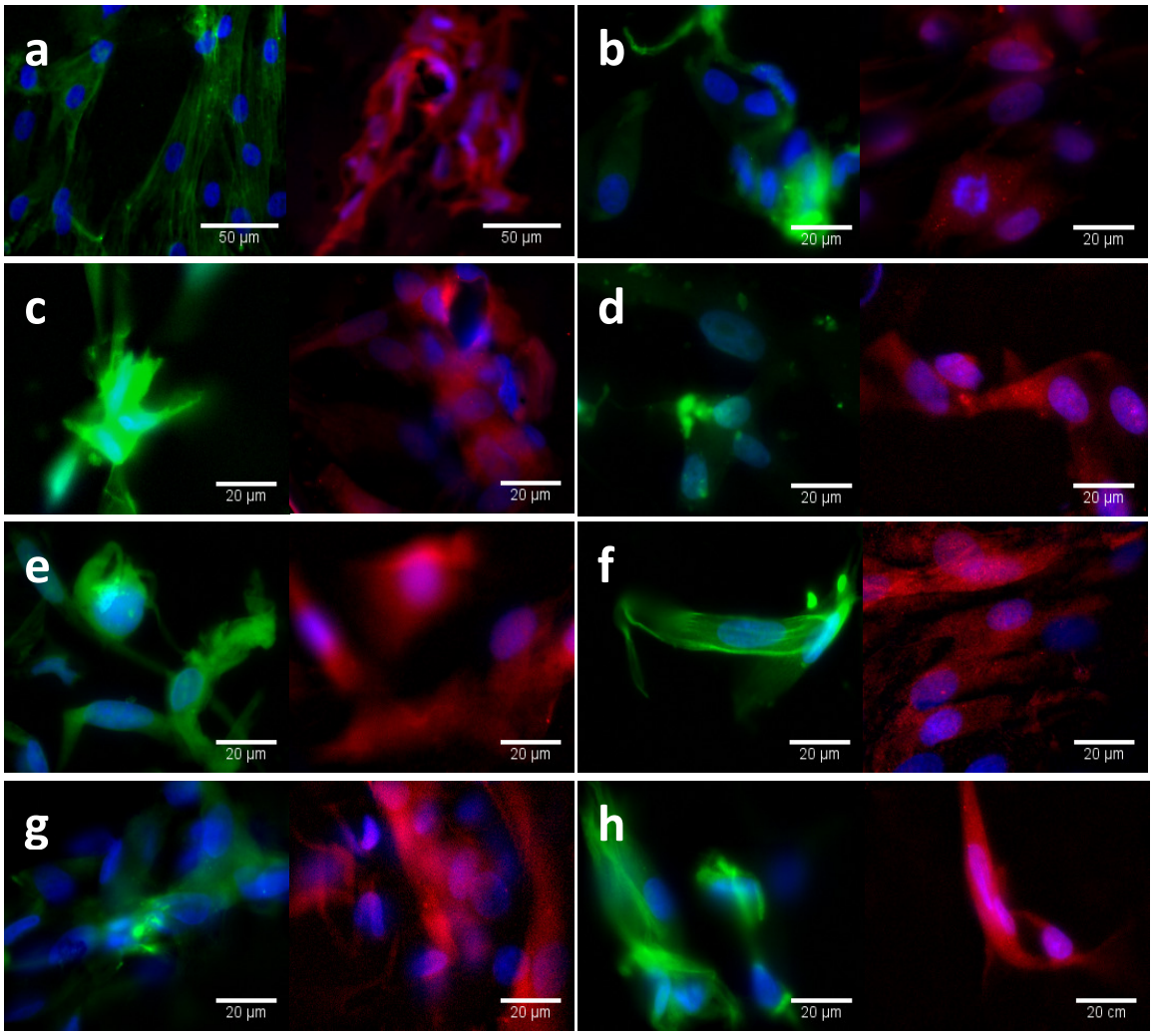

Figure 43: Immunofluorescence for SM α – actin (green) and h – caldesmon (red) expression by SMCs on various surfaces. Nuclei have been stained with DAPI (blue). All modified surfaces were films of ELAS 1800. a – glass, b – ELAS 4500, c – ELAS 1800, d – base etched, e – GRGDS, f – RPDS, g – PEG spacer + GRGDS, h – PEG spacer + RPDS.

ECM product type and rate are critical parameters that must be considered. As the scaffold degrades, it is assumed that the SMC synthesized ECM will begin to take on the role of vessel integrity and function. The biosynthesis of elastin, one of the key component of the blood vessel wall, has been lacking in previous tissue engineered scaffolds[132]. When SMCs were seeded and allowed to mature *in vitro* on collagen scaffolds no elastin was detected [33,38]. Synthetic scaffolds have had better results. Kim and Mooney observed a large amount of elastin deposition on PLA bonded scaffold surfaces over 7 weeks. It is interesting to note that cell attachment to this scaffold was relatively poor compared to a PGA scaffold, however, the latter only had an elastin content of 17% [133]. Thus, scaffold properties such as degradation rate greatly affect elastin synthesis. There is little literature concerning this area of study and as such the effect of elastomer based scaffolds on elastin production is unknown. It is speculated that elastomeric scaffolds would promote elastin synthesis since cells would be exposed to similar mechanical properties and stresses as native blood vessels.

7.4 Seeded Scaffolds

SMCs were seeded on ELAS 1800 scaffolds with various surface modifications (base etched, GRGDS, PEG spacer + GRGDS) to investigate the influence of the 3D structure on cell behaviour. SMCs were seeded by simply pipeting the cell solution over the scaffold and incubating under static conditions. It has been shown that dynamic seeding conditions improve seeding density [134]. Thus, the results provided may not be the best representation. Nonetheless, if this scaffold is to be use in the *in vivo* paradigm as described above and the scaffold is to be placed in the vasculature without any conditioning, the seeding method used in this work may provide some clues as to how SMCs would migrate from peripheral vessels or SMPs from the blood stream at a low density.

From Figure 44, SMCs on all scaffolds were attached to the contours of the pores and on the peripheral edge of the scaffold, not within the internal pores. After 7 days there is slow migration into the interior of the scaffold. This may only be a product of the seeding method. Nevertheless, similar to the thin films, the seeded SMCs expressed α – actin and h – caldesmon regardless of surface (Figure 45). Thus, these results would suggest that the 3D configuration does not influence phenotype. Kim *et al.* also observed this result; ECM synthesis was similar on thin films and scaffolds on both collagen I and PGA [91]. Thus, ASCP elastomeric films may be used in the future to do other surface chemistry studies and those results will be valid in the 3-D scaffold situation.

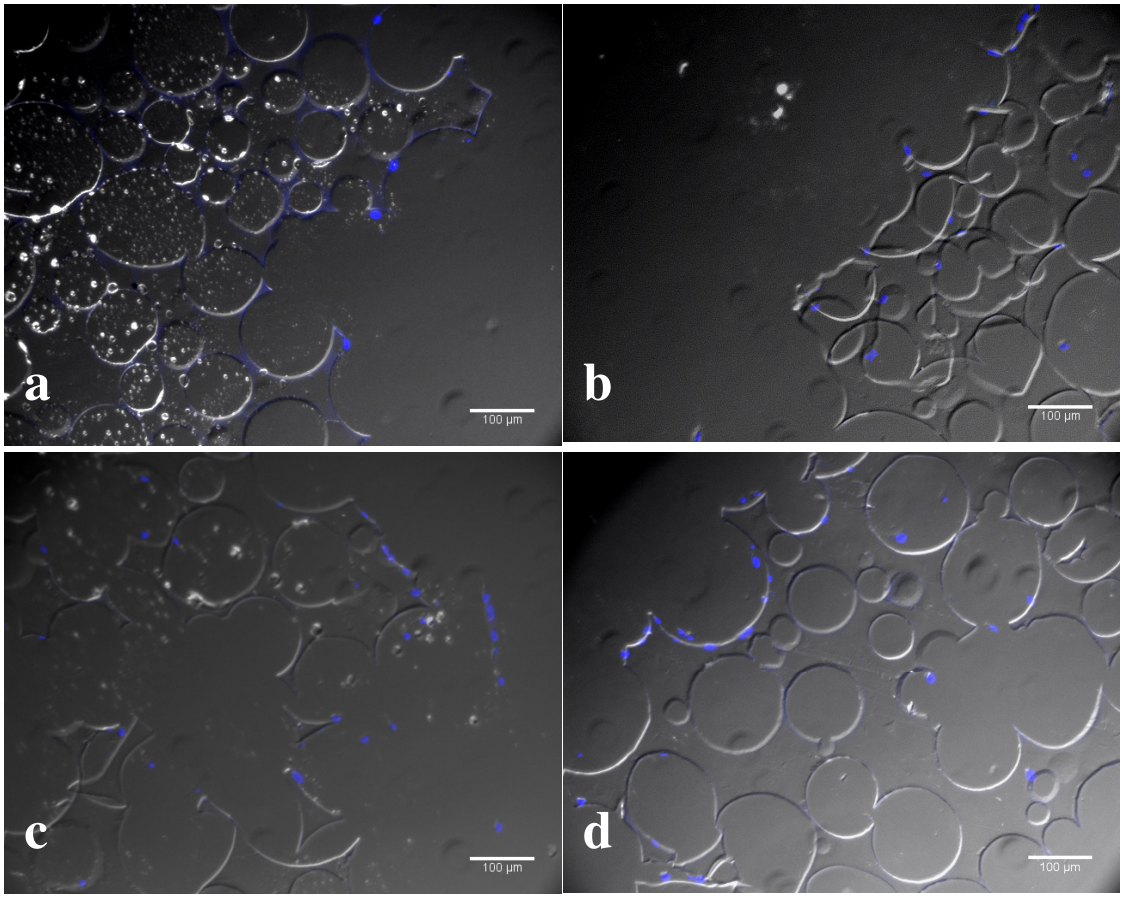

Figure 44: Location of SMCs in ELAS 1800 scaffolds after 7 days in culture. (a) is unmodified, (b) is base etched, (c) is GRGDS and (d) is PEG spacer with GRGDS surface. Cell nuclei have been stained with DAPI (blue).

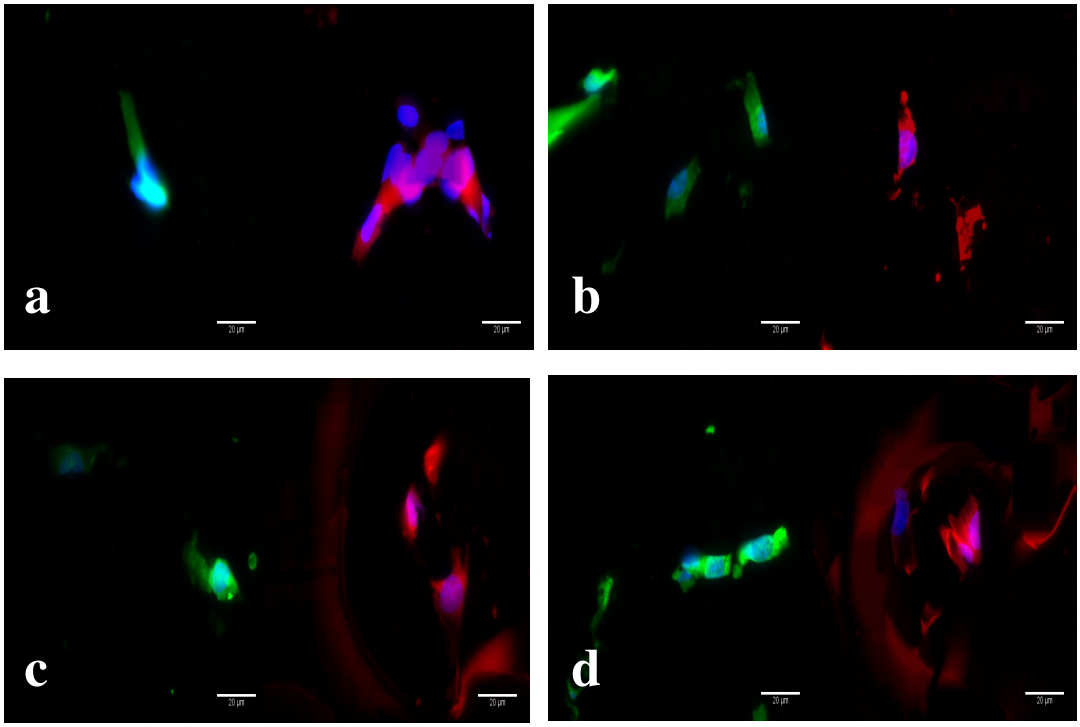

Figure 45: Phenotype of SMCs present in scaffolds after 7 days in culture. (a) is unmodified, (b) is base etched, (c) is GRGDS and (d) is PEG spacer with GRGDS surface. Cell nuclei have been stained with DAPI (blue), SM α – actin (green) and h – caldesmon (red).

Chapter 8
Results and Discussion - Biomimetic Design

The developed scaffold presented in this work has been optimized to match the mechanical properties of the coronary artery. Adding GRGDS to the surface improved SMC attachment to ASCP as well as proliferation, and this modification did not compromising SMC phenotype. Keeping in mind the suggested use of this scaffold in an *in vivo* approach, the next step was to incorporate the ASCP scaffold in a biomimetic design.

The lumen has direct contact with the blood stream and it is assumed that because of its hydrophobic nature, the elastomers will induce thrombus formation once in contact with blood. As explained in the introduction, in native arteries, a monolayer of endothelial cells (ECs) prevents thrombosis. To simulate this function in the proposed scaffold design, a nonthrombogenic layer of PEG was crosslinked on top of the elastomer scaffold. PEG hydrogels are considered nonthrombogenic because they resist protein adsorption. The lack of protein adsorption is due to the high water content, thus making it highly hydrophilic [135]. Although, out of the scope of this work, in the future, it would be beneficial to add RGD to the surface to attract endothelial cells and create a natural nonthrombotic layer. Moreover, ECs also regulate SMC behaviour [19,20].

8.1 Acrylation of PEG 4000

PEG 4000 was successfully acrylated into poly(ethylene glycol) diacrylate (PEGDA) as shown in Figure 46. The degree of acrylation was 73.8% with a sol content of 6.08 ± 0.94%. The degree of acrylation was calculated using the NMR end group analysis. In

this case the acrylate endgroup (6.0 ppm) was compared to the hydroxyl end group (2.1 ppm).

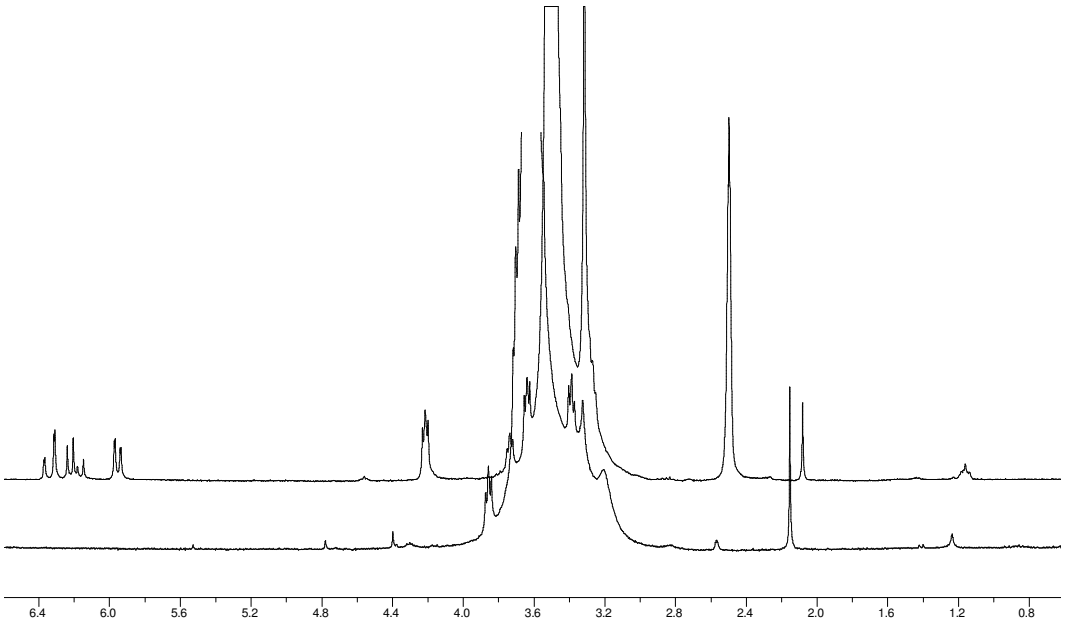

Figure 46: ^{1}H NMR spectra of PEG 4000 before (bottom) and after acrylation (top). Acrylate groups are clearly present (6.0 – 6.4 ppm). Measurements were done in $CDCl_3$.

8.2 PEGDA/ASCP construct

The PEGDA was added to the ASCP prepolymer after 30 seconds of UV exposure and then the whole construct exposed to UV for an additional 10 minutes. The ASCP prepolymer was crosslinked for 30 sec to prevent the PEGDA from mixing with the ASCP. After 30 sec, there was enough elastomer formed such that the PEGDA would be contained to the top. Nevertheless, there were enough end groups available to crosslink with the PEGDA. The sol content of the 30 second elastomer was 48.68 ± 3.18%. This procedure provided sufficient crosslinking between the PEGDA layer and ASCP in both film and porous form (Figure 47). In both cases a distinct PEGDA layer was observed. The PEGDA layer was not removed when washed with water or during the THF removal

of paraffin. The sol content of the PEGDA layer was 5.57 ± 2.04 % when solely washed with water. When the PEGDA/ASCP construct was washed with THF, the sol content of the construct was 9.17 ± 3.55 %. The mechanical properties of the hydrated nonporous PEGDA/ASCP construct were similar to the unmodified, nonporous ELAS 4500 (Table 7) with a tensile modulus of 1.35 ± 0.09 MPa. Moreover, this biomimetic design can be easily translated into tubular form which is the intended configuration (Figure 48).

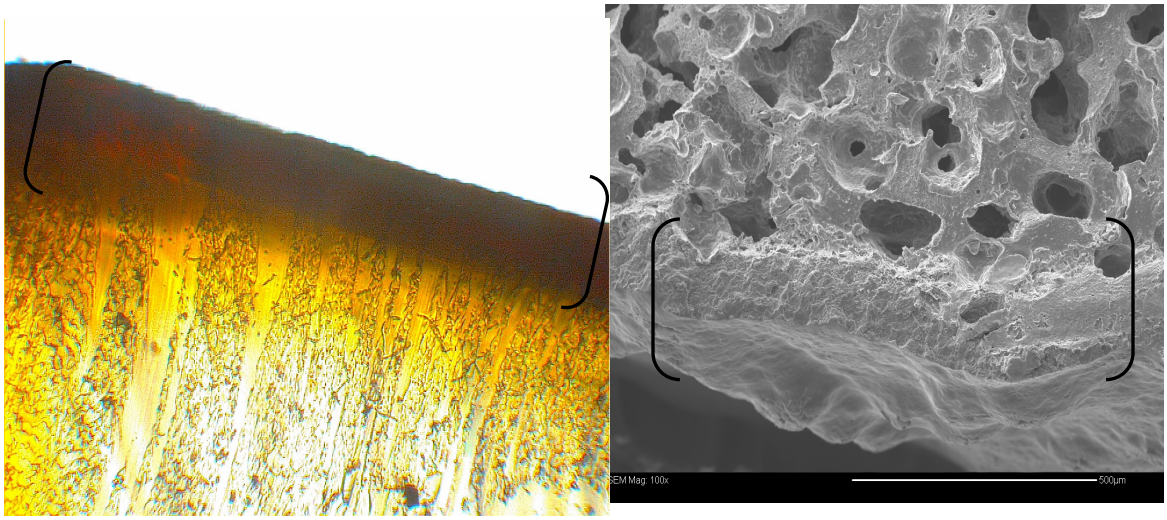

Figure 47: Light microscope image of PEGDA/ELAS thin film construct (left) using barium chloride/iodine to stain PEGDA, SEM image of PEGDA/ELAS porous (with emulsion) construct (right). ELAS 4500 was used in both cases. Parenthesis indicate PEGDA layer. SEM scale bar = 500 µm.

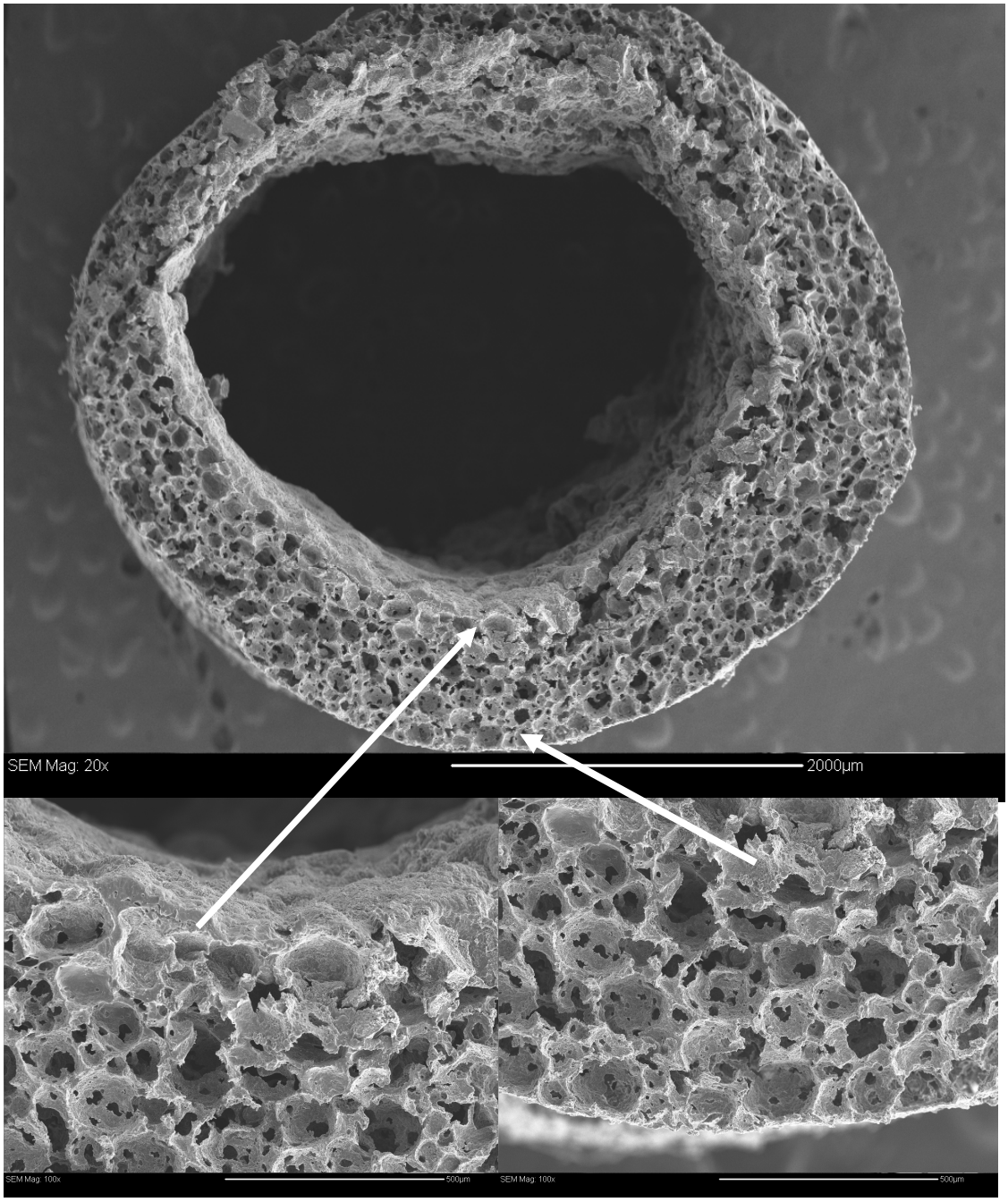

Figure 48: PEGDA/ELAS 4500 biomimetic design in tubular form. Scale bar = 2000 µm. Arrows indicate top portion with PEGDA layer and bottom portion without PEGDA. Scale bar for higher magnification images = 500 µm.

Chapter 9
Conclusions

There is a profound need to find an alternative to the autologous saphenous vein for vascular graft applications. Nonetheless, the blood vessel is a complex structure both physically and biochemically. As advances in vascular biology increase the knowledge into the intricate nature of blood vessels, so do insights into using this knowledge for tissue engineering of blood vessels. The work presented herein, provides results that can be used with knowledge of SMC biology and the mechanical nature of blood vessels, to create materials that can be tailored to match mechanical properties and promote cell proliferation without compromising cell function. In particular, the elastomer tested in this work has proven to be a potential scaffolding material for the media in the tissue engineering of vascular graft applications.

Elastomers composed of ASCP were successfully fabricated into a porous scaffold using paraffin microbeads. A porosity of 90% can be achieved using a combination of paraffin microbeads and a water/ASCP emulsion. This relatively simple procedure was able to produce pore diameters in the 100 μm range which has been previously shown to be suitable for blood vessel tissue engineering.

Mechanical properties can be manipulated by varying the ASCP prepolymer M_n resulting in varying degrees of crosslink density. Scaffolds using ELAS 1800 had mechanical properties that matched those of native arteries. Porous and nonporous scaffolds both degrade by bulk hydrolysis. The rate of degradation does not significantly change, although porous scaffolds may degrade more slowly than nonporous

counterparts. After 8 weeks, there was a significant decrease in tensile modulus and tensile strength, but only a slight decrease in ultimate strain.

The surface of the elastomers was easily modified by incorporating peptide sequences into the crosslink network. The tested base etching conditions were also effective in hydrolyzing the surface. Only surfaces with peptide sequences and a PEG spacer on ELAS 1800 increased cell attachment and cell proliferation. There also appears to be a crosslink density influence on cell proliferation. The difference in cell proliferation between surfaces may be attributed to differences in SMC phenotype as observed by cell morphology. Modified elastomer surfaces with peptide sequences provide a well tolerated surface and SMCs were well spread suggesting strong attachment and possibly a synthetic phenotype. By 7 days, SMCs on all surfaces expressed SM α – actin and h – caldesmon at 4 days, confirming SMCs phenotype expression. These cell markers are specific to SMCs modulated towards the contractile phenotype and were present regardless of configuration (thin film or 3D scaffold). However confirmation of phenotype could not be made and needs further investigation. Under the tested cell culture conditions, the improvement in cell attachment and proliferation using a peptide sequence was not specifically based on peptide activity and may be due to increased deposition of soluble cell adhesive serum proteins.

It has been demonstrated that the developed elastomer scaffold can be used in a biomimetic design and act as the pseudo media in conjunction with a nonthrombogenic layer of PEGDA that can act as the pseudo intima. The scaffold can be effortlessly manufactured into a tubular form with the PEGDA layer. Overall, the construction of blood vessel scaffold based on ASCP is relatively easy and quick. Surface modification

with peptide sequences and addition of the PEGDA layer can all be done simultaneously during the ASCP crosslinking step photoinitiated by UV light.

All objectives proposed at the beginning of this work were successfully accomplished. Thus, these results suggest that elastomers based on ASCP are promising scaffolding materials for small diameter blood vessel tissue engineering. Although, far from commercial realization, these results provide evidence that an ideal tissue engineered vascular graft is within reach.

Chapter 10
Recommendations

The work presented is only a first step in realizing a robust tissue engineering approach to small diameter blood vessel replacement. Further work needs to be done to assess the usability and detailed influence ASCP has on SMCs.

In particular, compliance, burst pressure, and suture strength need to be tested. Compliance is the real mechanical property of interest as it relates pressure change with volume. Also viscoelastic testing is needed to assess if failure will occur due to creep or stress relaxation. Burst pressure and suture strength are tests for usability by surgeons during implantation.

Peptide concentrations need to be optimized. In this study, concentrations were taken from previous studies. There may be material influences that make those concentrations not optimal.

Further investigation should be done into the phenotype of the SMCs attached to the ASCP surface. This would include quantifying and identifying the ECM components synthesized. A dynamic system examining how SMCs behave during degradation as well as under mechanical stimulation would provide valuable insights into in vivo behaviour.

Research into the pseudo intimal portion of the biomimetic design should be continued. This could include modifying the PEGDA surface layer to increase cell attachment of EC. Once this is done, studies between the interactions of ECs and SMCs

can be investigated. Lastly, implantation of the tubular construct in animal studies would test if the *in vivo* tissue engineering paradigm is valid.

References

1. World Health Organization. Leading Causes of Death in 2001, WHO World Health Report 2002. http://ucatlas.ucsc.edu/cause.php;September 2006.

2. Heart and Stroke Foundation. http://ww2.heartandstroke.ca; September 2006.

3. Michaels AD, Chatterjee K. Angioplasty Versus Bypass Surgery for Coronary Artery Disease. Circulation 2002;106:e187-190.

4. American Heart Association. Heart Disease and Stroke Statistics - 2006 Update. www.americanheart.org; September 2006.

5. Piccone V. Alternative techniques in coronary artery reconstruction. In: Sawyer PN, editor. Modern Vascular GraftsNew York: McGraw-Hill, 1987. 253-260.

6. Langer R, Vacanti J. Tissue engineering. Science 1993;260:920-926.

7. Rabkin E, Schoen F. Cardiovascular tissue engineering. Cardiovascular Pathology 2002;11:305-317.

8. Lévy BI, Tedgui A. Biology of the arterial wall. Dordrecht ; Boston: Kluwer Academic Publishers., 1999.

9. Humphrey JD. Blood vessels, mechanical and physical properties of. In: Buschow K, Cahn RW, editors. Encyclopedia of Materials: Science and Technology New York: Elsevier, 2001. p. 748-751.

10. Owens G. Molecular regulation of vascular smooth muscle cell differentiation in development and disease. Physiological reviews 2004;84:767.

11. Rensen SSM, Doevendans PAFM, van Eys GJJM. Regulation and characteristics of vascular smooth muscle cell phenotypic diversity. Neth Heart J 2007;15:100-108.

12. Sarkar S, Sales KM, Hamilton G, Seifalian AM. Addressing thrombogenicity in vascular graft construction. Journal of Biomedical Materials Research Part B: Applied Biomaterials 2007;82B:100-108.

13. Dobrin PB. Physiology and pathophysiology of blood vessels. In: Sidawy AN, Sumpio BE, DePalma RG, editors. The Basic Science of Vascular DiseaseArmonk, NY: Futura Publishing Company, Inc., 1997. p. 69-106.

14. Salmasi A, Iskandrian AS. Cardiac output and regional flow in health and disease. Dordrecht ; Boston: Kluwer Academic Publishers, 1993.

15. Cox RH. Passive mechanics and connective tissue composition of canine arteries. Am J Physiol Heart Circ Physiol 1978;234:H533-541.

16. Dobrin PB, Baker WH, Gley WC. Elastolytic and collagenolytic studies of arteries. Implications for the mechanical properties of aneurysms. Arch Surg 1984;119:405-409.

17. Li JK. Arterial System Dynamics. New York: New York University Press, 1987.

18. Davis G, Senger D. Endothelial Extracellular Matrix: Biosynthesis, Remodeling, and Functions During Vascular Morphogenesis and Neovessel Stabilization. Circ Res 2005;97:1093-1107.

19. Chamley-Campbell J. The smooth muscle cell in culture. Physiological reviews 1979;59:1.

20. Owens GK. Regulation of differentiation of vascular smooth muscle cells. Physiol Rev 1995;75:487-517.

21. Chamley JH, Campbell GR, McConnell JD, GrÃschel-Stewart U. Comparison of vascular smooth muscle cells from adult human, monkey and rabbit in primary culture and in subculture. Cell Tissue Res 1977;177:503-522.

22. Voorhees AB, Jr, Jaretzki A, 3rd, Blakemore AH. The use of tubes constructed from vinyon "N" cloth in bridging arterial defects. Ann Surg 1952;135:332-336.

23. Kakisis JD, Liapis CD, Breuer C, Sumpio BE. Artificial blood vessel: The Holy Grail of peripheral vascular surgery. J Vasc Surg 2005;41:349-354.

24. Dalman RL, Taylor LM. Basic data related to infrainguinal revascularization procedures. Ann Vasc Surg 1990;4:309-312.

25. Hoenig MR, Campbell GR, Rolfe BE, Campbell JH. Tissue-Engineered Blood Vessels - Alternative to Autologous Grafts? Arterioscler Thromb Vasc Biol 2005;25:1128-1134.

26. Berglund JD, Galis ZS. Designer blood vessels and therapeutic revascularization. Br J Pharmacol 2003;140:627-636.

27. Kannan RY, Salacinski HJ, Butler PE, Hamilton G, Seifalian AM. Current status of prosthetic bypass grafts: A review. Journal of Biomedical Materials Research Part B: Applied Biomaterials 2005;74B:570-581.

28. Valenta J. Clinical aspects of biomedicine. In: Jaroslav V, editor. BiomechanicsAmsterdam: Elsevier Science, 1993. p. 142-179.

29. Horbett T. Chapter 13 Principles underlying the role of adsorbed plasma proteins in blood interactions with foreign materials. Cardiovascular Pathology 1993;2:137-148.

30. Mitchell SL, Niklason LE. Requirements for growing tissue-engineered vascular grafts. Cardiovascular Pathology 2003;12:59-64.

31. Sabik J, Lytle B, Blackstone E, Houghtaling P, Cosgrove D. Comparison of Saphenous Vein and Internal Thoracic Artery Graft Patency by Coronary System. The Annals of Thoracic Surgery 2005;79:544-551.

32. Baird R, Abbott W. Pulsatile blood-flow in arterial grafts. The Lancet 1976;308:948-950.

33. Weinberg C, Bell E. A blood vessel model constructed from collagen and cultured vascular cells. Science 1986;231:397-400.

34. Cummings C, Gawlitta D, Nerem R, Stegemann J. Properties of engineered vascular constructs made from collagen, fibrin, and collagen–fibrin mixtures. Biomaterials 2004;25:3699-3706.

35. Seliktar D, Black R, Vito R, Nerem R. Dynamic Mechanical Conditioning of Collagen-Gel Blood Vessel Constructs Induces Remodeling In Vitro. Ann Biomed Eng 2000;28:351-362.

36. Huynh T, Abraham G, Murray J, Brockbank K, Hagen P, Sullivan S. Remodeling of an acellular collagen graft into a physiologically responsive neovessel. Nat Biotech 1999;17:1083-1086.

37. Daniel J, Abe K, McFetridge PS. Development of the Human Umbilical Vein Scaffold for Cardiovascular Tissue Engineering Applications. ASAIO Journal 2005;51:252-261.

38. L'heureux N, Paquet S, Labbe R, Germain L, Auger F. A completely biological tissue-engineered human blood vessel. FASEB J 1998;12:47-56.

39. Schmidt C, Baier J. Acellular vascular tissues: natural biomaterials for tissue repair and tissue engineering. Biomaterials 2000;21:2215-2231.

40. Isenberg BC, Williams C, Tranquillo RT. Small-Diameter Artificial Arteries Engineered In Vitro. Circ Res 2006;98:25-35.

41. Yang S, Leong K, Du Z, Chua C. The Design of Scaffolds for Use in Tissue Engineering. Part I. Traditional Factors. Tissue Engineering 2001;7:679.

42. Gunatillake, P A Adhikari,R. Biodegradable synthetic polymers for tissue engineering. European cells materials 2003;5:1.

43. Remuzzi A, Mantero S, Colombo M, Morigi M, Binda E, Camozzi D, Imberti B. Vascular Smooth Muscle Cells on Hyaluronic Acid: Culture and Mechanical Characterization of an Engineered Vascular Construct. Tissue Eng 2004;10:699-710.

44. Gao J, Niklason L, Langer R. Surface hydrolysis of poly(glycolic acid) meshes increases the seeding density of vascular smooth muscle cells. J Biomed Mater Res 1998;42:417-424.

45. Higgins SP, Solan AK, Niklason LE. Effects of polyglycolic acid on porcine smooth muscle cell growth and differentiation. Journal of Biomedical Materials Research Part A 2003;67A:295-302.

46. Shum-Tim D, Stock U, Hrkach J, Shinoka T, Lien J, Moses M, Stamp A, Taylor G, Moran A, Landis W, Langer R, Vacanti J, Mayer J,Jr. Tissue engineering of autologous aorta using a new biodegradable polymer. Ann Thorac Surg 1999;68:2298-2304.

47. Mooney DJ, Mazzoni CL, Breuer C, McNamara K, Hern D, Vacanti JP, Langer R. Stabilized polyglycolic acid fibre-based tubes for tissue engineering. Biomaterials 1996;17:115-124.

48. Sung In Jeong, Soo Hyun Kim, Young Ha Kim, Youngmee Jung, Jae Hyun Kwon, Byung-Soo Kim, Young Moo Lee. Manufacture of elastic biodegradable PLCL scaffolds for mechano-active vascular tissue engineering. Journal of Biomaterials Science -- Polymer Edition 2004;15:645-660.

49. Guan J, Fujimoto K, Sacks M, Wagner W. Preparation and characterization of highly porous, biodegradable polyurethane scaffolds for soft tissue applications. Biomaterials 2005;26:3961-3971.

50. Boccafoschi F, Rajan N, Habermehl J, Mantovani D. Preparation and Characterization of a Scaffold for Vascular Tissue Engineering by Direct-Assembling of Collagen and Cells in a Cylindrical Geometry. Macromolecular Bioscience 2007;7:719-726.

51. Inoguchi H, Kwon I, Inoue E, Takamizawa K, Maehara Y, Matsuda T. Mechanical responses of a compliant electrospun poly(l-lactide-*co*-epsilon-caprolactone) small-diameter vascular graft. Biomaterials 2006;27:1470-1478.

52. Zhang L, Ao Q, Wang A, Lu G, Kong L, Gong Y, Zhao N, Zhang X. A sandwich tubular scaffold derived from chitosan for blood vessel tissue engineering. Journal of Biomedical Materials Research Part A 2006;77A:277-284.

53. Yang J, Motlagh D, Webb AR, Ameer GA. Novel Biphasic Elastomeric Scaffold for Small-Diameter Blood Vessel Tissue Engineering. Tissue Engineering 2005;11:1876.

54. Stankus J, Guan J, Fujimoto K, Wagner W. Microintegrating smooth muscle cells into a biodegradable, elastomeric fiber matrix. Biomaterials 2006;27:735-744.

55. Nerem RM. Tissue Engineering of Blood Vessels. Wiley Encyclopedia of Biomedical Engineering 2006.

56. Yow KH, Ingram J, Korossis SA, Ingham E, Homer-Vanniasinkam S. Tissue engineering of vascular conduits. Br J Surg 2006;93:652-661.

57. Matsumura G, Hibino N, Ikada Y, Kurosawa H, Shin'oka T. Successful application of tissue engineered vascular autografts: clinical experience. Biomaterials 2003;24:2303-2308.

58. Nerem RM. Critical issues in vascular tissue engineering. Int Con Ser 2004;1262:122-125.

59. Dzau V, Gnecchi M, Pachori A, Morello F, Melo L. Therapeutic Potential of Endothelial Progenitor Cells in Cardiovascular Diseases. Hypertension 2005;46:7-18.

60. Simper D, Stalboerger P, Panetta C, Wang S, Caplice N. Smooth Muscle Progenitor Cells in Human Blood. Circulation 2002;106:1199-1204.

61. Levenberg S, Golub J, Amit M, Itskovitz-Eldor J, Langer R. Endothelial cells derived from human embryonic stem cells. Proceedings of the National Academy of Sciences 2002.

62. Zhang Z, Wang Z, Liu S, Kodama M. Pore size, tissue ingrowth, and endothelialization of small-diameter microporous polyurethane vascular prostheses. Biomaterials 2004;25:177-187.

63. Doi K, Matsuda T. Significance of porosity and compliance of microporous, polyurethane-based microarterial vessel on neoarterial wall regeneration. J Biomed Mater Res 1997;37:573-584.

64. Contreras MA, Quist WC, Logerfo FW. Effect of porosity on small-diameter vascular graft healing. Microsurgery 2000;20:15-21.

65. Wong P, Hopkins S, Vincente D, Williams K, Macri N, Berguer R. Differences in Neointima Formation between Impervious and Porous Polytetrafluoroethylene Vascular Patch Material. Ann Vasc Surg 2002;16:407-412.

66. Freed LE, Vunjak-Novakovic G, Biron RJ, Eagles DB, Lesnoy DC, Barlow SK, Langer R. Biodegradable Polymer Scaffolds for Tissue Engineering. Nat Biotech ;12:689-693.

67. Xu C, Inai R, Kotaki M, Ramakrishna S. Electrospun Nanofiber Fabrication as Synthetic Extracellular Matrix and Its Potential for Vascular Tissue Engineering. Tiss Eng 2004;10:1160-1168.

68. Curtis A, Riehle M. Tissue engineering: the biophysical background. Phys Med Biol 2001;46:R47-R65.

69. KeunKwon I, Kidoaki S, Matsuda T. Electrospun nano- to microfiber fabrics made of biodegradable copolyesters: structural characteristics, mechanical properties and cell adhesion potential. Biomaterials 2005;26:3929-3939.

70. Karande TS, Ong JL, Agrawal CM. Diffusion in Musculoskeletal Tissue Engineering Scaffolds: Design Issues Related to Porosity, Permeability, Architecture, and Nutrient Mixing. Ann Biomed Eng 2004;32:1728.

71. Ma PX, Choi J. Biodegradable Polymer Scaffolds with Well-Defined Interconnected Spherical Pore Network. Tissue Engineering 2001;7:23.

72. Thomson R, Yaszemski M, Powers J, Mikos A. Hydroxyapatite fiber reinforced poly(α-hydroxy ester) foams for bone regeneration. Biomaterials 1998;19:1935-1943.

73. Zhang R, Ma PX. Synthetic nano-fibrillar extracellular matrices with predesigned macroporous architectures. J Biomed Mater Res 2000;52:430-438.

74. Dobrin PB. Mechanical properties of arterises. Physiol Rev 1978;58:397-460.

75. Bezuidenhout D, Davies N, Zilla P. Effect of Well Defined Dodecahedral Porosity on Inflammation and Angiogenesis. ASAIO Journal 2002;48:465-471.

76. Matsuda T, Nakayama Y. Surface microarchitectural design in biomedical applications: *In vitro* transmural endothelialization on microporous segmented polyurethane films fabricated using an excimer laser. J Biomed Mater Res 1996;31:235-242.

77. Zhang J, Wu L, Jing D, Ding J. A comparative study of porous scaffolds with cubic and spherical macropores. Polymer 2005;46:4979-4985.

78. Draghi L, Resta S, Pirozzolo M, Tanzi M. Microspheres leaching for scaffold porosity control. J Mater Sci Mater Med 2005;16:1093-1097.

79. Fournier N, Doillon C. Biological molecule-impregnated polyester: an in vivo angiogenesis study. Biomaterials 1996;17:1659-1665.

80. Kohler, T R Stratton, J R Kirkman, T R Johansen, K H Zierler, B K Clowes,A W. Conventional versus high-porosity polytetrafluoroethylene grafts: clinical evaluation. Surgery 1992;112:901.

81. Deutsch M, Meinhart J, Fischlein T, Preiss P, Zilla P. Clinical autologous in vitro endothelialization of infrainguinal ePTFE grafts in 100 patients: A 9-year experience. Surgery 1999;126:847-855.

82. Chu PK, Chen JY, Wang LP, Huang N. Plasma-surface modification of biomaterials. Materials Science and Engineering: R: Reports 2002;36:143-206.

83. Thapa A, Miller D, Webster T, Haberstroh K. Nano-structured polymers enhance bladder smooth muscle cell function. Biomaterials 2003;24:2915-2926.

84. Kidane A, Salacinski H, Punshon G, Ramesh B, Srai K, Seifalian A. Synthesis and evaluation of amphiphilic RGD derivatives: Uses for solvent casting in polymers and tissue engineering applications. Medical and Biological Engineering and Computing 2003;41:740-745.

85. Hersel U, Dahmen C, Kessler H. RGD modified polymers: biomaterials for stimulated cell adhesion and beyond. Biomaterials 2003;24:4385-4415.

86. Hubbell JA, Massia SP, Desai NP, Drumheller PD. Endothelial Cell-Selective Materials for Tissue Engineering in the Vascular Graft Via a New Receptor. Nat Biotech 1991;9:568-572.

87. Stein, P D Walburn, F J Blick,E F. Damping effect of distensible tubes on turbulent flow: implications in the cardiovascular system. Biorheology 1980;17:275.

88. Bowald, S Busch, C Eriksson,I. Arterial regeneration following polyglactin 910 suture mesh grafting. Surgery 1979;86:722.

89. Tiwari A, Salacinski H, Seifalian AM, Hamilton G. New prostheses for use in bypass grafts with special emphasis on polyurethanes. Cardio Sur 2002;10:191-197.

90. Gozna, E R Mason, W F Marble, A E Winter, D A Dolan,F G. Necessity for elastic properties in synthetic arterial grafts. Canadian journal of surgery 1974;17:176.

91. Kim B, Nikolovski J, Bonadio J, Smiley E, Mooney D. Engineered Smooth Muscle Tissues: Regulating Cell Phenotype with the Scaffold. Experimental Cell Research 1999;251:318-328.

92. Sonoda H, Takamizawa K, Nakayama Y, Yasui H, Matsuda T. Small-diameter compliant arterial graft prosthesis: Design concept of coaxial double tubular graft and its fabrication. J Biomed Mater Res 2001;55:266-276.

93. Jun H-, Taite LJ, West JL. Nitric Oxide-Producing Polyurethanes. Biomacromolecules 2005;6:838-844.

94. Zilla PP, Bezuidenhout DD, Jacobus PT. US Patent No. US 7,022,135 B2, 2006 04 04.

95. Salzman EW. Nonthrombogenic Surfaces: Critical Review. Blood 1971;38:509-523.

96. Amsden BG, Misra G, Gu F, Younes HM. Synthesis and Characterization of A Photo-Cross-Linked Biodegradable Elastomer. Biomacromolecules 2004;5:2479-2486.

97. Chapanian R, Tse MY, Pang SC, Amsden BG. *In Vivo* Degradation Mechanism of, and Tissue Response to, Photo-Cross-Linked Elastomers Prepared from Star Shaped Prepolymers of Poly(e-Caprolactone-co-D,L-Lactide). Biomaterials submitted September 2007.

98. Bugarski B, Amsden B, Neufeld RJ, Poncelet D, Goosen MF. Effect of Electrode Geometry and Charge on the Production of Polymer Microbeads by Electrostatics. Can J Chem Eng 1994;72:517-521.

99. DuBois M, Gilles KA, Hamilton JK, Rebers PA, Smith F. Colorimetric Method for Determination of Sugars and Related Substances. Anal Chem 1956;28:350-356.

100. Hern D. Incorporation of adhesion peptides into nonadhesive hydrogels useful for tissue resurfacing. Journal of biomedical materials research 1998;39:266.

101. Kurfürst M. Detection and molecular weight determination of polyethylene glycol-modified hirudin by staining after sodium dodecyl sulfate-polyacrylamide gel electrophoresis. Analytical Biochemistry 1992;200:244-248.

102. Usov AI. Alginic acids and alginates: analytical methods used for their estimation and characterisation of composition and primary structure. Russian chemical reviews 1999;68:957-966.

103. Strand BL, Garing, seroslash, d O, Kulseng B, Espevik T, Skjaring, k-Braelig, k G. Alginate-polylysine-alginate microcapsules: effect of size reduction on capsule properties. Journal of Microencapsulation 2002;19:615.

104. Poncelet D, Lencki R, Beaulieu C, Halle JP, Neufeld RJ, Fournier A. Production of alginate beads by emulsification/internal gelation. I. Methodology. Appl Microbiol Biotechnol 1992;38:39-45.

105. Takeuchi H, Yasuji T, Yamamoto H, Kawashima Y. Spray-Dried Lactose Composite Particles Containing an Ion Complex of Alginate-Chitosan for Designing a Dry-Coated Tablet Having a Time-Controlled Releasing Function. Pharm Res 2000;17:94-99.

106. Amsden BG, Goosen MFA. An examination of factors affecting the size, distribution and release characteristics of polymer microbeads made using electrostatics. Journal of Controlled Release 1997;43:183-196.

107. Busby W, Cameron NR, Jahoda CAB. Tissue engineering matrixes by emulsion templating. Polym Int 2002;51:871-881.

108. Butler R, Hopkinson I, Cooper AI. Synthesis of Porous Emulsion-Templated Polymers Using High Internal Phase CO_2-in-Water Emulsions. J Am Chem Soc 2003;125:14473-14481.

109. Busby W, Cameron NR, Jahoda CAB. Emulsion-Derived Foams (PolyHIPEs) Containing Poly(ε-caprolactone) as Matrixes for Tissue Engineering. Biomacromolecules 2001;2:154-164.

110. Gibson LJ, Ashby MF. The mechanics of foam: Basic results. Cellular Solids: Structure and PropertiesToronto: Pergamon Press, 1988.,120-127.

111. Gow B, Hadfield C. The elasticity of canine and human coronary arteries with reference to postmortem changes. Circ Res 1979;45:588-594.

112. Amsden BG, Tse MY, Turner ND, Knight DK, Pang SC. In Vivo Degradation Behavior of Photo-Cross-Linked *star*-Poly(-caprolactone-*co*-D,L-lactide) Elastomers. Biomacromolecules 2006;7:365-372.

113. Sperling LH. Introduction to physical polymer science. 2nd ed. New York: John Wiley & Sons, Inc., 1992.

114. Grizzi I, Garreau H, Li S, Vert M. Hydrolytic degradation of devices based on poly(-lactic acid) size-dependence. Biomaterials 1995;16:305-311.

115. Wu L, Ding J. In vitro degradation of three-dimensional porous poly(,-lactide-co-glycolide) scaffolds for tissue engineering. Biomaterials 2004;25:5821-5830.

116. Sidouni F-, Nurdin N, Chabrecek P, Lohmann D, Vogt J, Xanthopoulos N, Mathieu HJ, Francois P, Vaudaux P, Descouts P. Surface properties of a specifically modified high-grade medical polyurethane. Surface Science 2001;491:355-369.

117. Miller D, Thapa A, Haberstroh K, Webster T. Endothelial and vascular smooth muscle cell function on poly(lactic-co-glycolic acid) with nano-structured surface features. Biomaterials 2004;25:53-61.

118. Beer J, Springer K, Coller B. Immobilized Arg-Gly-Asp (RGD) peptides of varying lengths as structural probes of the platelet glycoprotein IIb/IIIa receptor. Blood 1992;79:117-128.

119. Massia S, Hubbell J. An RGD spacing of 440 nm is sufficient for integrin alpha V beta 3-mediated fibroblast spreading and 140 nm for focal contact and stress fiber formation. J Cell Biol 1991;114:1089-1100.

120. Lin H, García-Echeverría C, Asakura S, Sun W, Mosher D, Cooper S. Endothelial cell adhesion on polyurethanes containing covalently attached RGD-peptides. Biomaterials 1992;13:905-914.

121. Hedin U, Bottger B, Forsberg E, Johansson S, Thyberg J. Diverse effects of fibronectin and laminin on phenotypic properties of cultured arterial smooth muscle cells. J Cell Biol 1988;107:307-319.

122. Katsumi A, Orr AW, Tzima E, Schwartz M. Integrins in Mechanotransduction. J Biol Chem 2004;279:12001-12004.

123. Engler A, Bacakova L, Newman C, Hategan A, Griffin M, Discher D. Substrate Compliance versus Ligand Density in Cell on Gel Responses. Biophys J 2004;86:617-628.

124. Salloum DS, Olenych SG, Keller TCS, Schlenoff JB. Vascular Smooth Muscle Cells on Polyelectrolyte Multilayers: Hydrophobicity-Directed Adhesion and Growth. Biomacromolecules 2005;6:161-167.

125. Bearinger JP, Castner DG, Healy KE. Biomolecular modification of p AAm-co-EG/AA IPNs supports osteoblast adhesion and phenotypic expression. J Biomater Sci Polym Ed 1998;9:629-52.

126. Neff JA, Tresco PA, Caldwell KD. Surface modification for controlled studies of cell–ligand interactions. Biomaterials 1999;20:2377-2393.

127. Mann BK, West JL. Cell adhesion peptides alter smooth muscle cell adhesion, proliferation, migration, and matrix protein synthesis on modified surfaces and in polymer scaffolds. J Biomed Mater Res 2002;60:86-93.

128. Tao F, Chaudry S, Tolloczko B, Martin JG, Kelly SM. Modulation of smooth muscle phenotype in vitro by homologous cell substrate. Am J Physiol Cell Physiol 2003;284:C1531-1541.

129. Opitz F, Schenke-Layland K, Richter W, Martin DP, Degenkolbe I, Wahlers T, Stock UA. Tissue Engineering of Ovine Aortic Blood Vessel Substitutes Using Applied Shear Stress and Enzymatically Derived Vascular Smooth Muscle Cells. Ann Biomed Eng 2004;32:212-222.

130. Marston SB, Huber PAJH. Caldesmon. In: Barany M, editor. Biochemistry of Smooth Muscle Contraction San Diego, California: Academic Press, 1996. p. 77-90.

131. Xu CY, Inai R, Kotaki M, Ramakrishna S. Aligned biodegradable nanofibrous structure: a potential scaffold for blood vessel engineering. Biomaterials 2004;25:877-886.

132. Patel A, Fine B, Sandig M, Mequanint K. Elastin biosynthesis: The missing link in tissue-engineered blood vessels. Cardiovascular Research 2006;71:40-49.

133. Kim BS, Mooney DJ. Engineering smooth muscle tissue with a predefined structure. J Biomed Mater Res 1998;41:322-332.

134. Kim B, Putnam AJ, Kulik TJ, Mooney DJ. Optimizing seeding and culture methods to engineer smooth muscle tissue on biodegradable polymer matrices. Biotechnol Bioeng 1998;57:46-54.

135. Wang Y, Robertson JL, Spillman WB, Claus RO. Effects of the Chemical Structure and the Surface Properties of Polymeric Biomaterials on Their Biocompatibility. Pharm Res 2004;21:1362-1373.